Atoms and Molecules in Restricted Geometries at Low Temperatures

Hiroyuki Deguchi

1987

Osaka University
Graduate School of Engineering Science
Department of Material Physics
Toyonaka Osaka

Abstract

Zeolites and pillar intercalated montmorillonites have restricted geometries of which channel diameters and interlayer distance sizes are several Å. Properties of atoms and molecules in such restricted geometries are studied experimentally at low temperatures.

The thermal properties of H_2 are studied by heat capacity measurements at liquid He^4 temperature region. Using well known phenomena of supercooling in small cavities, we attempt to supercool liquid H_2 and to obtain superfluid H_2 in Y zeolite and pillar intercalated montmorillonite. Y zeolite has regular cavities of radius of 6 Å and interconnecting channels of diameter of 8 Å. The heat capacity of low density H_2 in the Y zeolite changes temperature dependence at about 9 K and it seems to be solid-liquid transition. In the case of high density H_2 in the Y zeolite, the heat capacity fits the Einstein model. The high density Ar and N_2 in the Y zeolite give similar heat capacities and these results are explained by using sintered particle model.

$N^+(CH_3)_4$- and Al_2O_3-montmorillonites have two-dimensional (2D) space of which interlayer distances are 4.1 and 9.0 Å, respectively. The heat capacity shows T^2 temperature dependence at low temperatures and the peak of heat capacity corresponding to solid-liquid transition is not observed in the case of H_2 and D_2 adsorbed in the $N^+(CH_3)_4$-montmorillonite. But in the case of low density H_2, λ-type heat capacity anomaly observed at 7.6 K,

which does not correspond to the superfluid transition, is interpreted as the orientational ordering of the 2D ortho-H_2 solid. In the Al_2O_3-montmorillonite, the heat capacities of low density H_2 and D_2 show humps at about 10 K corresponding to the melting transition. Thus, H_2 may be supercooled at 10 K, which is higher than the predicted superfluid transition temperature of 6.6 K for para-H_2.

As for He^4 of a typical boson particle, the thermal properties in Y zeolite and pillar intercalated montmorillonites are studied. The heat capacities of He^4 depend on restricted geometries but show similarly temperature dependences interpreted as being single-particle excited state or 2D Debye solid state. In Al_2O_3-montmorillonite, the heat capacity of He^4 shows a hump around 1.7 K, which is interpreted to be due to the superfluid transition shifting towards lower temperatures than that of bulk λ point.

Also, we studied on magnetic properties of He^3 - Fermi particle - in high silica zeolites having extremely restricted geometries. The nuclear susceptibility χ_s, spin-lattice relaxation time T_1 and spin-spin relaxation time T_2 of He^3 in the restricted geometries are measured. The susceptibility χ_s of He^3 in ZSM-5 which has 3D channels of diameter of 5.5 Å shows temperature dependence of the Fermi degeneracy. On the contrary, χ_s of He^3 in ZSM-23 which has purely 1D channel shows to obey Curie's law. In the two high silica zeolites, we obtain similar results of T_1 and T_2 of He^3. Then, it is shown experimentally that the property of the Fermi liquid He^3 are changed by the extremely restricted geometry.

CONTENTS

Chapter 1 General Introduction

There have been many studies on quantum liquids and solids using He^3, He^4 and H_2 not only in bulk state but also in restricted geometries. Vycor glass, Grafoil and metal surfaces have been used so far as substances which provide the restricted geometries.[1,2] Grafoil and metal surfaces provide two-dimensional (2D) space, and Vycor glass does 3D pore network of which diameter is several tenth of Å. In these restricted geometries, adsorbed He and H_2 show various properties differing from those in bulk state, and give some new aspects for the problems of quantum statistics. However, the space size of the restricted geometries in the substances mentioned above are still relatively large in comparison with the size of adsorbed atoms and molecules.

If He and H_2 are adsorbed in a severely restricted geometry of which size is the same order of themselves, the properties of adsorbed He and H_2 are expected to differ from those adsorbed in rather loose geometries, for example, in Vycor glass. Zeolites provide such extremely restricted geometries.[3] In general, zeolites are crystals which consist of aluminosilicate frameworks and provide regular void channels and cavities of diameter of only several Å. The geometries and adsorption potentials of voids and channels depend on each species of zeolites and the contained cations. Recently, Wada et al. measured heat capacity of He^4 adsorbed in the Na-Y zeolite which has regular void channels of diameter 8 Å and cavities of radius

6.5 Å.[4] They concluded that adsorbed He^4 behaved as the semiquantum liquid in the temperature range from 3 K to 9 K as proposed by Andreev[5] for the case of liquid under high pressure.

We will discuss some problems of He^4 and H_2 adsorbed in such a space of small restricted geometries.

From the view points of quantum statistics, it is quite interesting to examine the possibility of Bose condensation or superfluidity of the atoms and molecules in the restricted geometry. As for superfluid, not only He^4 but also H_2 can be the candidates. Because molecular hydrogen is a boson and has a large quantum mechanical parameter, liquid H_2 might be possible to be superfluid below a certain critical temperature.

Using well known phenomena of supercooling in small cavities, Tell and Maris attempted to reduce the freezing temperature of liquid H_2 in Vycor glass.[6] They succeeded to supercool the liquid H_2 in Vycor glass down to 9.9 K, which is still higher than the estimated superfluid transition temperature of 6.6 K.[7] This gives a possibility that liquid H_2 may be supercooled down to 6.6 K with the use of the highly restricted geometry such as zeolites.

In addition to superfluidity, the properties of solid or liquid state and solid-liquid transition are of very much interest in such restricted geometries. The adsorbed atoms and molecules may show considerably different phase transitions from those of bulk materials. The kinetic motion or exchange of He atoms must be limited in zeolite, which should give some new

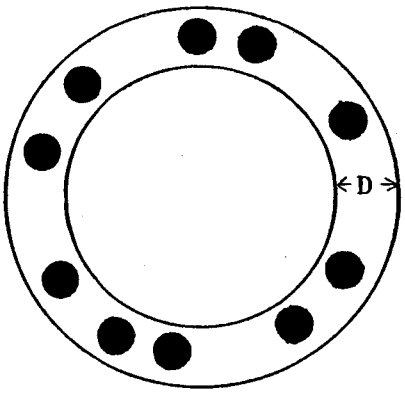

Fig. 1 He^3 atoms in a circular tube
The diameter D of the tube satisfys the condition $2r < D < 4r$, where r is the radius of He^3 atom. Therefore, He^3 atoms in the tube form an impenetrable fermions system.

aspect on quantum statistics.

On the other hand, experiments on fermions in restricted geometries give some new understandings on quantum statistic. For example, nuclear magnetism of He^3 atoms in an extremely restricted and ideally shaped geometry, which is shown in Fig. 1, would show an interesting behavior. It is assumed that He^3 atoms do not exchange their positions directly but can only change their positions in cyclic manner in the circular tube. Then, the temperature and density dependence of nuclear susceptibility of He^3 atoms in the tube would include an important aspect on the statistics. Though the restricted geometry of such a single circular tube as shown Fig. 1 cannot be provided in real materials, some restricted spaces in zeolites can be approximated to some extent the model system mentioned above. The study of the Fermi degeneracy of adsorbed He^3 in zeolites may give new informations about the theory of

the Fermi fluid.

We have mentioned about the restricted geometries of zeolites with narrow channels.

There is another interesting restricted geometry between layers in which the interlayer distance can be controlled by introducing stable cation-pillars with suitable lengths. The 2D space in the pillar intercalated montmorillonite is an example: The distance between two adjacent layers is adjustable so as to make it the same order of magnitude as the diameter of H_2 molecules.[8)]

In general, the atoms or molecules will be adsorbed weakly in such a restricted condition because they will be attracted or repelled from the adjacent layers of both sides. Therefore the interlayer space of the montmorillonite is quite different from the surfaces which Grafoil or metal particle provide.

Recently, Miyagi et al. calculated molecular attractive force acting on particles confined in very narrow space of an ideal dielectric substance.[9)] They pointed out that a molecule has lower energy in a slab shaped cavity than in the free space, even if it is not adsorbed locally on the wall of the cavity. Then, the behavior of atoms and molecules adsorbed in the interlayer 2D space is of considerable interest. We studied the possibility of the supercooling of fluid state of H_2 and the superfluidity of He^4 as well in very restricted interlayer space.

Now, we mention the experimental results briefly.

In chapter 2, the heat capacities of H_2, He^4, Ar and N_2 adsorbed in Na-Y and H-Y zeolites are given. Some remarkable

points will be summarized as follows; (i) In the case of low density, the heat capacities of H_2 in the Na-Y zeolite show T^2 (T; temperature) dependence and T^3 dependence in the H-Y zeolite below about 10 K. They do not exhibit any peak which corresponds to solid-liquid transition and show less distinct temperature dependence above 10 K. These behavior may be explained by the continuous transitions from solid to liquid as increasing temperatures. (ii) In the case of He^4 adsorbed in the Na-Y zeolite, the heat capacities C observed for several densities ,which correspond to submonolayer of He^4 in the space, fit well the following expressions

$$C = AT + BT^2 \qquad (T > T_{tr})$$

$$C = D(\frac{E}{k_B T} + 2)\exp(\frac{-E}{k_B T}) + BT^2 \qquad (T < T_{tr})$$

where T_{tr} is the temperature of inflection point. These expressions were given by Tait and Reppy for the case of submonolayer He^4 adsorbed in Vycor glass.[10] They explained theoretically that the first term in the both expression is attributed to single-particle excitation with an energy gap 2E and the second is of 2D solid of adsorbed He^4. This explanation may be applied to the He^4 in the present Na-Y zeolite. Single-particle-excited atoms are interpreted as free particles. That is, He^4 atoms with the excitation energy in the Na-Y zeolite are expected to move freely. (iii) In the case for the higher density of H_2, Ar and N_2 in the H-Y zeolite, the heat capacities fit well the Einstein model. Nishiguchi and Nakayama applied the Einstein model to explain the heat capacity of the sintered

metal particles which are similar to the particles adsorbed in the Y zeolite.[11] In this case, it is suggested that molecules in the H-Y zeolite are not adsorbed locally on the wall of the cavities. We will discuss our results on the basis of their model.

In chapter 3, the heat capacities of H_2, D_2 and He^4 adsorbed in $N^+(CH_3)_4$-and Al_2O_3-montmorillonites are investigated. The interlayer distances of $N^+(CH_3)_4$-and Al_2O_3-montmorillonites are 4.1 and 9.0 Å, respectively. The results will be summarized as follows; (i) The heat capacities of H_2 and D_2 adsorbed in the $N^+(CH_3)_4$-montmorillonite show T^2 dependence and do not show any peak which indicates the solid-liquid transition in the temperature range between 2 K and 20 K, perhaps because of too narrow space in this case. (ii) Only in the case of low density H_2 adsorbed in the $N^+(CH_3)_4$-montmorillonite, an anomalous λ-type peak is observed at 7.6 K in the virgin run of the heat capacity measurement. This result is time-dependent. Therefore the λ-anomaly might be ascribed to a 2D orientational ordering of ortho-H_2 in solid state. (iii) In the case of the Al_2O_3-montmorillonite, the heat capacities of high density H_2 and D_2 show almost T^2 dependence without any peak in the whole measuring temperature range, but those of low density H_2 and D_2 show the hump around 10 K and T^2 dependence below 9 K, which is interpreted as the process of melting from 2D solid to liquid. (iv) The heat capacities of He^4 adsorbed in $N^+(CH_3)_4$- and Al_2O_3-montmorillonites fit well the following expression given by Tait and Reppy for the case of $T > T_{tr}$

$$C = AT + BT^2 \ .$$

The first term may be attributed to single-particle excitation and the second to 2D solid of adsorbed He^4. (v) In the case of the Al_2O_3-montmorillonite, the heat capacities of adsorbed He^4 below 3 K are larger than those expected from the above expression and one of them shows a hump around 1.7 K. We will discuss the possibility of superfluidity of He^4 in this case.

We found from these experimental results, that the quantum properties of adsorbed H_2, D_2 and He^4 depend on the interlayer distance and on the density of adsorbed atoms or molecules.

In chapter 4, the quantum statiscal properties of fermion in restricted geometries are investigated. The nuclear susceptibility χ_s, spin-lattice relaxation time T_1 and spin-spin relaxation time T_2 of He^3 adsorbed in high silica zeolites and $AlPO_4$-5 are measured below 1.5 K. High silica zeolites have restricted geometries of effective 1D, 2D and 3D channel structures of diameter of several Å, where He^3 atoms are expected not to exchange their positions directly or to exchange their positions directly only in the space of the crossing of channels. The results will be summarized as follows, (i) The values of T_1 of He^3 in high silica zeolites are much shorter than that of bulk liquid He^3 and seem to depend on amount of magnetic impurities such as Fe^{3+} in crystals. (ii) We obtain similar results of T_1 and T_2 of He^3 in ZSM-5 and in ZSM-23. The former high silica zeolite (ZSM-5) has a 3D channel structure and the latter does a 1D channel structure with the similar channel diameter to that of ZSM-5. (iii) The behavior of $\chi_s(T)$

of adsorbed He^3 depends both on the diameter and structure of the channel of high silica zeolites and $AlPO_4$-5. The value of $\chi_s(T)$ becomes constant at low temperatures showing the temperature dependence like the Fermi fluid. (iv) But only in the case of He^3 adsorbed in ZSM-23, $\chi_s(T)$ of adsorbed He^3 obeys Curie's law down to about 0.1 K.

The results can be interpreted as showing some new aspects of the Fermi degeneracy of He^3 in restricted geometries.

References

1) J.G.Daunt and E.Lerner, ed. : Monolayer and Submonolayer Film, Plenum Press, New York (1973).

2) S.K.Sinha,ed. : Ordering in Two Dimensions, North Holland Press, New York (1980).

3) D.W.Breck : Zeolite Molecular Sieves, John Wily and Sons Press, New York-London (1974).

4) N.Wada, T.Ito and T.Watanabe : J. Phys. Soc. Jpn. 53 (1984) 913.

5) A.F.Andreev : Sov. Phys. JETP Lett. 28 (1978) 556.

6) J.L.Tell and H.J.Maris : Phys. Rev. B28 (1983) 5122.

7) V.L.Ginzburg and A.A.Sobyanin : Sov. Phys. JETP Lett. 15 (1972) 242.

8) R.M.Barrer : Zeolite and Clay Minerals as Sorbents and Molecular Sieves, Academic Press (1978).

9) H.Miyagi, T.Haseda and T.Nakamura : J. Phys. Soc. Jpn. 54 (1985) 1299.

10) R.H.Tait and J.D.Reppy : Phys. Rev. B20 (1979) 997.

11) N.Nishiguchi and T.Nakayama : Solid State Comm. 45 (1983) 877.

Chapter 2 Heat Capacities of H_2, He^4, Ar and N_2 Adsorbed in Na-Y and H-Y Zeolites

§ 1 Introduction

In 1972, Ginzburg and Sobyanin discussed the possibility of the appearance of superfluid-hydrogen in liquid state for the first time.[1] They stressed the fact that molecular H_2 is a boson and has the large quantum mechanical parameter. For an ideal Bose gas, the temperature $T_{\lambda 0}$ of Bose condensation is given by

$$k_B T_{\lambda 0} = 3.31 \frac{\hbar^2 n^{2/3}}{m g^{2/3}}$$

where k_B is Boltzmann's constant, m is the particle mass, n is the number density, and g is the degeneracy of each single-particle state. For para-hydrogen(para-H_2), g = 1, m = 2 amu and $n = 2.4 \times 10^{22}$ cm^{-3} at the triple point, and $T_{\lambda 0}$ is estimated to be 6.6 K. In the case of He^4, the above equation predicts a transition temperature of 3.1 K which is to be compared with the actual T_λ of 2.18 K. Thus one expects that T_λ of para-H_2 will probably be below 6.6 K.

However, the estimated value $T_{\lambda 0}$ = 6.6 K is lower than the real value of the triple point T_3 = 13.8 K. It is necessary to supercool the liquid H_2 below 6.6 K to actualize superfluid H_2. In 1983, Maris et al. discussed the supercooling of liquid H_2 in detail.[2] Tell and Maris attempted to supercool the liquid H_2 in the Vycor glass by the depressing of the freezing temperature of

liquid in porous mediums, and succeeded to supercool the liquid H_2 in the Vycor glass down to 9.9 K, which is still higher than $T_{\lambda 0}$ = 6.6 K.[3] The average pore diameter of the Vycor glass used by them was about 54 Å.

Now, we simply assume that the more severely the geometry is restricted, the further the liquid in the geometry is supercooled. Zeolites have such restricted geometries which are smaller than that of Vycor glass. We attempt to supercool the liquid H_2 not in Vycor glass but in Y zeolite. Y zeolite has regular cavities of radius of 6.5 Å and interconnecting channels of diameter of 8 Å. In such a restricted geometry as Y zeolite, the physical properties of adsorbed atoms or molecules have not been examined in detail up to now at low temperatures. So, in this report, we will give various kinds of experimental results using a variety of adsorbents such as zeolites or montmorillonites. The main aim of the present investigation is to find some general physical properties of quantum liquids in restricted geometries. As well as the possibility of superfluid H_2, some new physical properties in the restricted geometries stated above are also very interesting in comparison with those in bulk state. We study not only quantum He^4 and H_2 but also classical atom and molecule such as Ar and N_2 to make their respective properties clear.

§ 2 Experimentals

2-1 Adsorption space of restricted geometries

In general, zeolites are crystals which consist of aluminosilicate frameworks. They provide regular void channels and cavities which are located at every interconnecting points of channels. The diameters, radius, geometries and adsorption potentials in void channels and cavities depend on the species of zeolites and the contained cations therein.[4] The crystal of Y zeolite belongs to the Faujasite group.[5] Its unit cell is cubic with a cell dimension as large as 25 Å and has chemical formula of

$$Na_{56}[(AlO_2)_{56}(SiO_2)_{136}]\ 250\ H_2O\ .$$

Most of H_2O contained in zeolite crystal could be removed by heating in vacuo. In synthetic zeolites, the ratio SiO_2/Al_2O_3 can be controlled to some extent. Among various zeolites, Y zeolite has the biggest cavity with the radius of about 6 Å, which is shown in Fig. 1-(a). The cavities are linked through void channels of about 8 Å in diameter and they form a diamond-like structure. Thus Y zeolite has the restricted geometry which is regular 3D network of void channels. The cations Na^+ adsorbed in the framework are located in three possible positions as shown in Fig. 1-(b). These cations form electric dipoles with the negative charges of AlO_2^- in the framework. The total void volume which mainly comes from the cavity space is about 50 vol. % of the volume of crystal and the volume of channels is

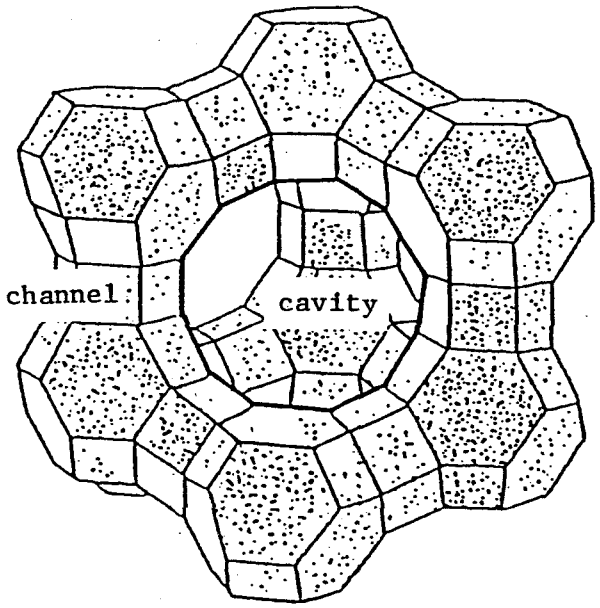

(a)

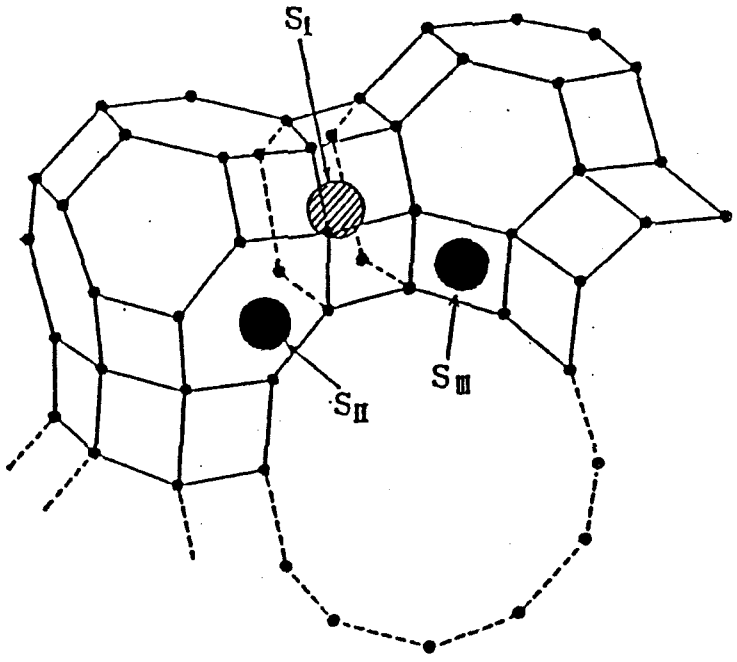

(b)

Fig. 1 (a) Structure of Y zeolite
(b) Cation Positions in Y zeolite
(Site I, Site II and Site III are shown)

negligible.

In the study, we use mostly the fine powder of the synthetic Y zeolite (TSZ-305) with Si/Al = 5, which was supplied by Tōyō Sōda Manufacturing Co. Ltd. The virgin crystals of the Y zeolite are washed by boiling in distilled water several times. Substitution of the cation Na^+ for H^+ in the zeolite is possible by keeping the powder cleaned as mentioned above, in NH_4Cl solution for a week. We call it H-Y zeolite and original one Na-Y zeolite. By this substitution, electric dipole field and the effective pore size can be changed.

2-2 Experimental apparatus and procedure

We measured heat capacities by conventional DC heat pulse method in the course of increasing temperature. The measuring system of heat capacity is shown in Fig. 2. In the upper side of Fig. 2, a generator of heat pulse dQ is shown. The dQ is obtained by the relation $dQ = IR^2dt$, where I is the current passing through the heater, R is resistance of the heater and dt is the heat pulse interval. In the lower side of Fig. 2, a temperature measuring system is shown , which is composed of carbon resistance thermometer, automatic resistance bridge (AVS-45) and X-t recorder. An Allen-Bradley carbon resister is used as the sample thermometer which is calibrated against Lake Shore Ge thermometer GR-200A-1000. The resistance of the carbon thermometer is measured by AVS-45 and the change of temperature of the sample dT by the heat pulse is determined by the calibrated R-T relation. Thus heat capacity C is obtained using

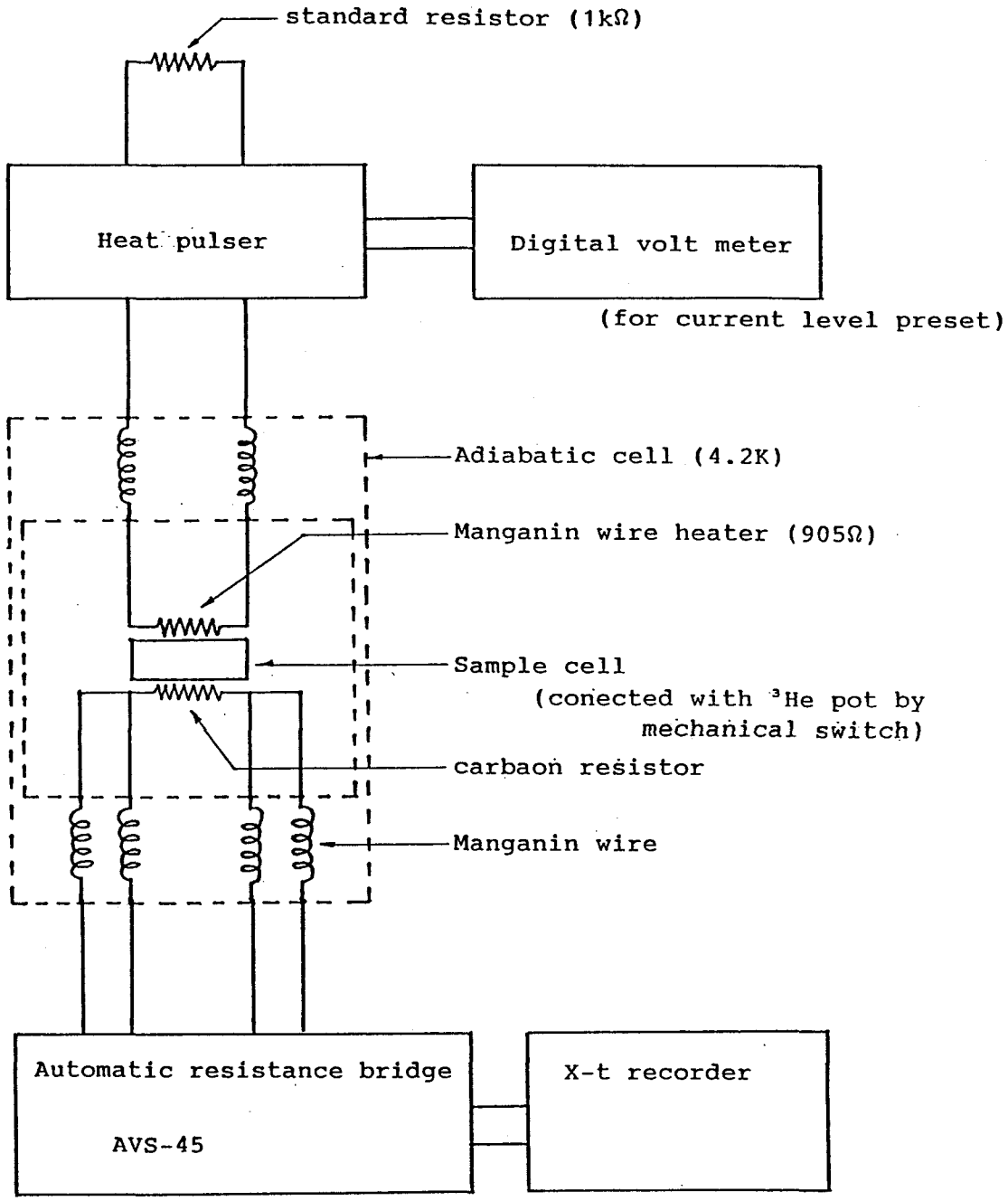

Fig. 2 Block diagram of heat capacity measuring system

the following relation,

$$C = \frac{dQ}{dT} \quad .$$

The cryostat and gas handling system are shown in Fig. 3. The sample gases of H_2, He^4 etc. are provided from the gas cylinders and are restored in the calibrated container. The molar value of the gas is calculated using the equation of gas state. The filling capillary above the adiabatic cell consists of double tubes, and we wind a manganin heater around the inner tube so as the sample gas not to be adsorbed on the wall of the inner tube.

The adiabatic cell is immersed in liquid He^4. The sample cell shown in Fig. 4 is made of copper. It can be cooled below 1 K by pumping He^4 and He^3 liquids in their respective pots. The sample cell is isolated adiabatically by disconnecting the thermal switch while measuring heat capacities. The thermometer and heater are mounted on the outer side of the sample cell.

The powdered sample of the Y zeolite is mixed with equivalent volume of copper fine powder in order to get good thermal equilibrium within the sample cell. The mixed powder is packed tightly in the sample cell. Dehydration of Na-Y or H-Y zeolite is performed by keeping the sample cell at 270°C and pumping once again to 10^{-6} torr through the capillary tube. The heat capacity of the sample cell (C) without adsorbed gas is measured at first. In the temperature range from 1 K to 20 K the results can be practically reproduced by the following expression with an accuracy of ±1 %,

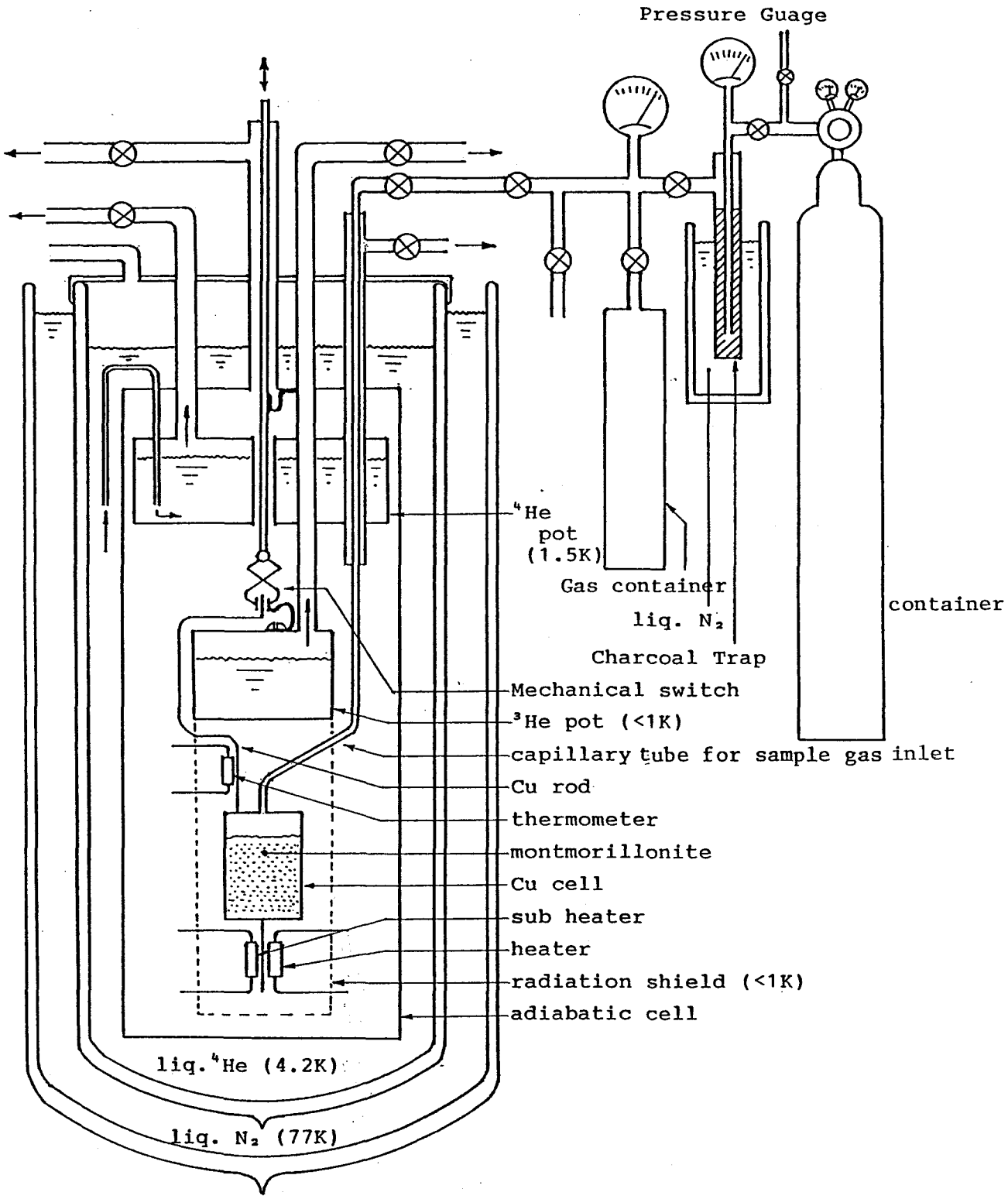

Fig. 3 Cryostat and gas handling system

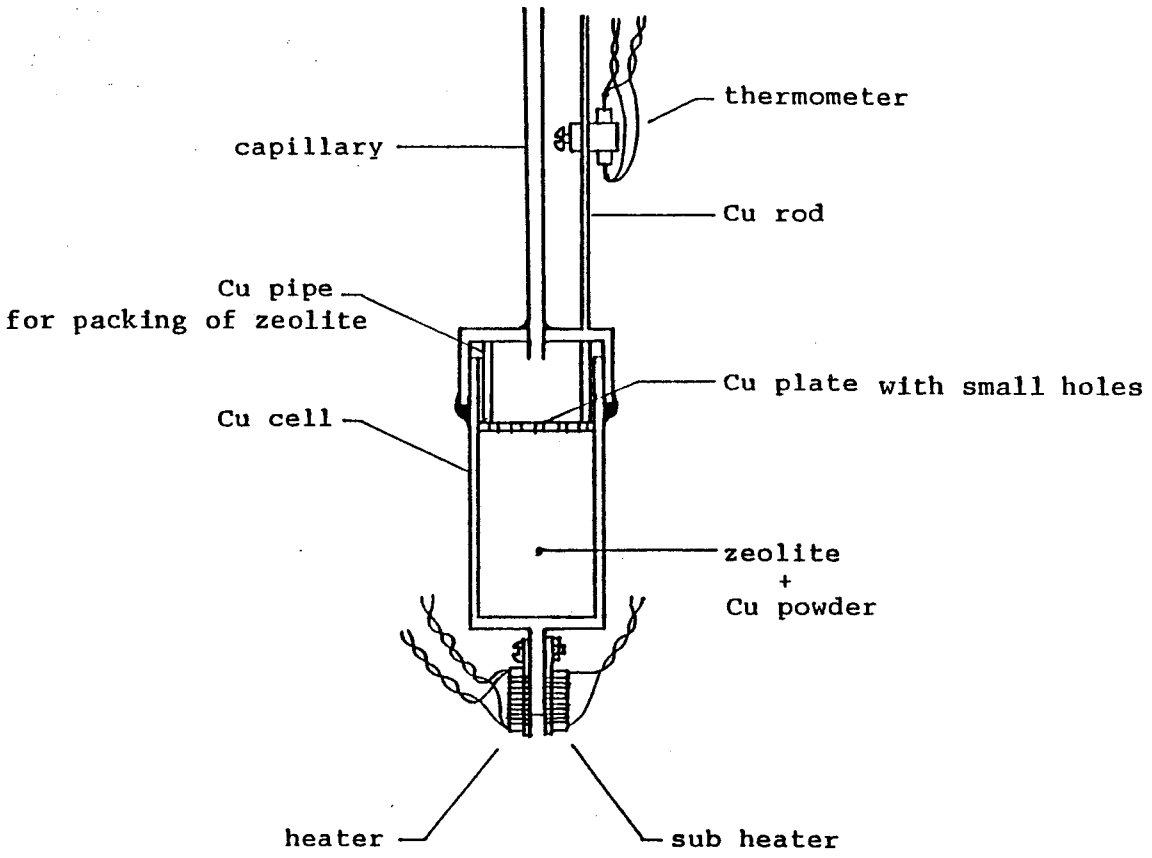

Fig. 4 Sample cell

$$C = \sum_{k=0}^{6} A_k T^k$$

where A_k's are obtained by the least square method. After dehydration, proper amount of sample gas is introduced into the cell at the liquid N_2 or He^4 temperature and cooled further down to 1 K in the cryostat dewar. Then we measure heat capacities starting from the lowest temperature. The heat capacity of the sample cell is subtracted from the total heat capacities. Thus we obtain the values of heat capacities of the adsorbed atoms or molecules.

§ 3 Experimental results

3-1 H_2 in Na-Y zeolite

Most of H_2 is expected to be adsorbed in the cavity in high density cases because the porosity ratio of 0.5 is mainly comes from the cavity space. In low density cases, the adsorbed H_2 may be possible to stay partially in the pore channels connecting the cavities and may be affected considerably by the dipole field between the Na^+ cations and the negative charges of AlO_2^- in Y zeolite. The density of H_2 of 5.0×10^{-4}mol per 1 g of Y zeolite corresponds to adsorption of one H_2 molecule in a cavity of Y zeolite.

Experimental results of the heat capacity for several densities of adsorbed H_2 in the Na-Y zeolite are shown in Fig. 5. One of the characteristics is the following fact. Comparing with the case of the bulk H_2, the bigger heat capacities are observed at low temperatures, where the bulk H_2 is already in solid state and known to obey almost Debye's T^3 law. This tendency has already been found by Tell and Maris[3]. For the case of H_2 in the Vycor glass, heat capacity shows a peak both in process of increasing and decreasing temperature, which corresponds to the melting and solidification of H_2. In our case, however, there appear no peaks but inflection points on temperature dependence. This gives a big difference from the case of several restricted geometries, especially in the 2D geometry as will be shown later in chapter 3. For the case of the Na-Y zeolite, we observe bigger heat capacities of H_2 than

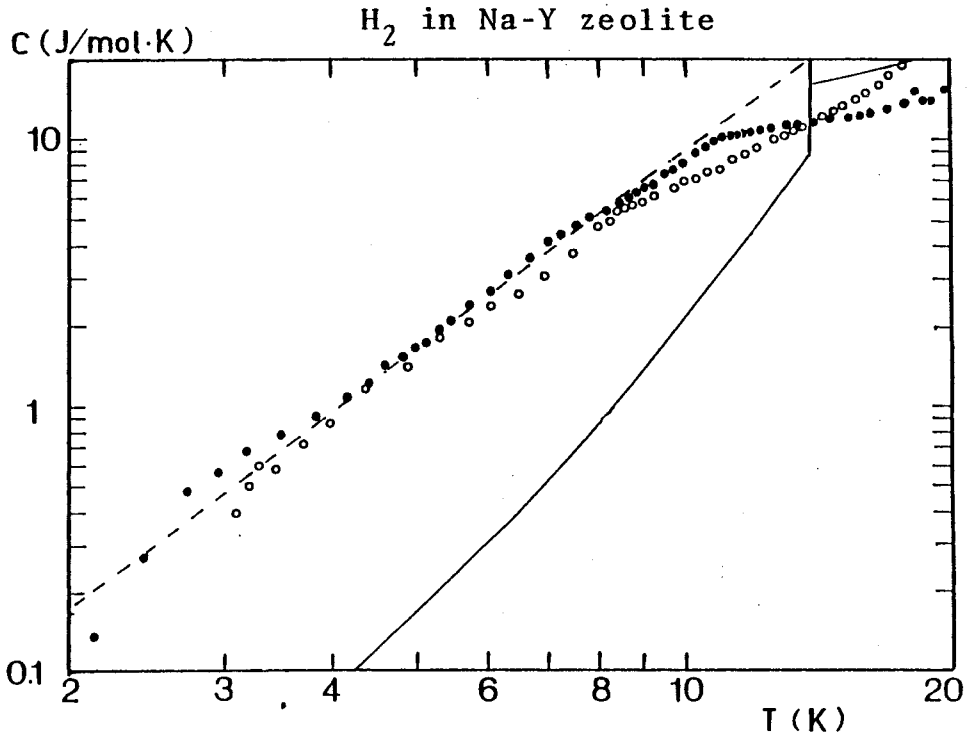

Fig. 5 Heat capacities of H_2 adsorbed in Na-Y zeolite
The density of H_2 are given by ● = 9.0×10^{-4} and o=4.5×10^{-3} mol/g, respectively. Broken line is a T^2 dependence line. Solid line shows the heat capacity of bulk H_2.

those in the H-Y zeolite over the whole temperature range. For the sample with low density of 9.0×10^{-4}mol/g in the Na-Y zeolite, the heat capacity shows almost a T^2 dependence below the inflection point around 11 K and shows almost a T^1 dependence above 11 K. For the higher density case of 4.5×10^{-3}mol/g, heat capacity shows almost a T^2 dependence below 8 K and shows almost a $T^{1.5}$ dependence above 8 K.

3-2 H_2 in H-Y zeolite

For the sample with a low density of 8.3×10^{-4}mol/g in the H-Y zeolite, the heat capacity shows a T^3 dependence below 9 K and becomes almost flat at higher temperature as shown in Fig. 6. Above 10 K, the experimental values begin to scatter because of the increasing experimental error due to outgas from

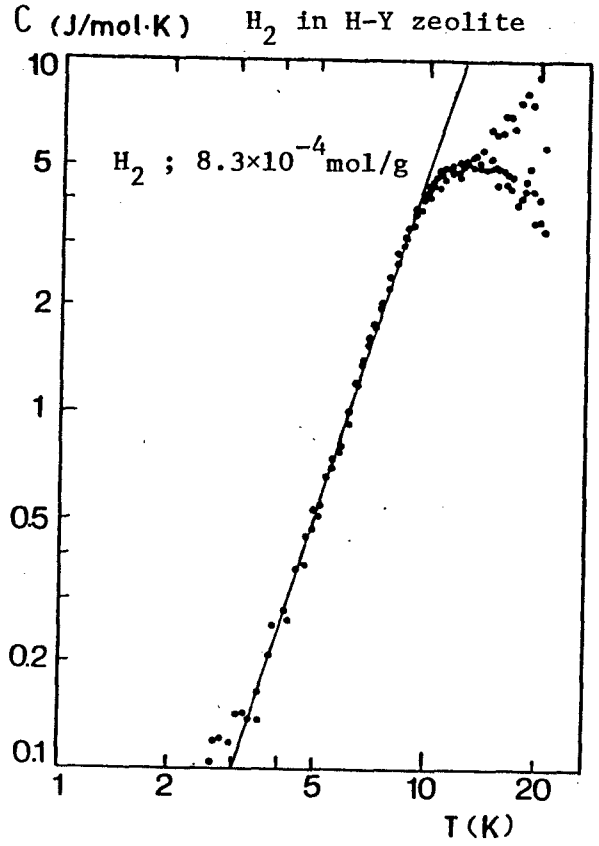

Fig. 6 Comparison of experimental values of heat capacity of H_2 in H-Y zeolite with T^3 (solid) line. The density of H_2 is 8.3×10^{-4} mol/g.

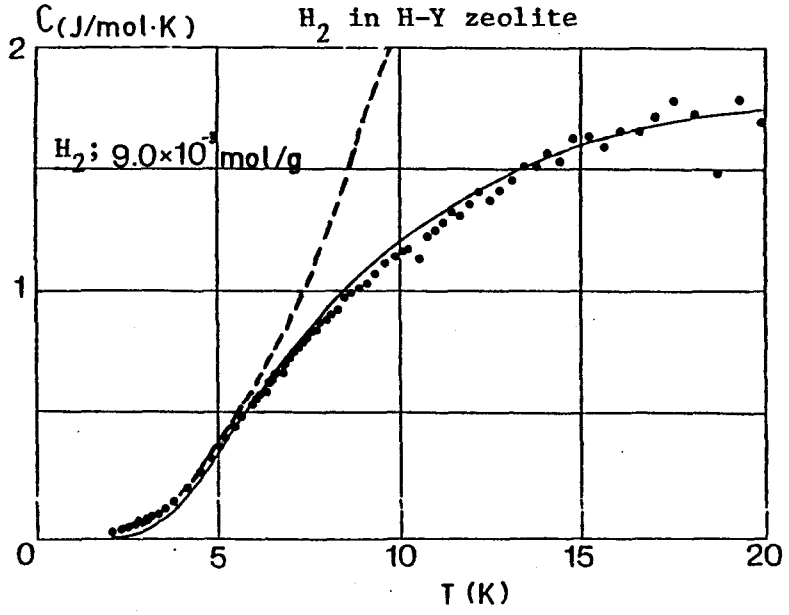

Fig. 7 Heat capacity of H_2 in H-Y zeolite. The density of H_2 is 9.0×10^{-3}mol/g. Solid and dashed lines show heat capacities calculated on the Einstein and Deby model,respectively. The characteristic temperatures are Θ_E=25 K and Θ_D=105 K. The saturation value of 2.0 J/mol·K is used in the Einstein model.

H-Y zeolite. Results for the higher density of 9.0×10^{-3}mol/g are shown in Fig. 7. The T^3 dependence is observed below 5 K, but the data rather fit the Einstein model almost over the whole temperatures with the chracteristic temperature Θ_E = 25 K and the saturation value of heat capacity C_s = 2.0 J/mol·K.

3-3 He^4 in Na-Y and H-Y zeolites

We may expect the transition to superfluidity in the case of He^4 adsorbed in Y zeolite. Wada et al. measured the heat capacity of He^4 adsorbed in Na-Y zeolite.[6] The usual λ-type peak was not detected but they found an abrupt decrease below about T_{tr} = 3 K which depended on the density of He^4. However, this anomaly at T_{tr} did not seem to be the transition to superfluidity. Above T_{tr}, the heat capacity changes linearly with temperature, which is interpreted by Wada et al. as a property of semiquantum liquid state of He^4.[7] But we take the different interpretation which will be mentioned in the discussion.

Our results for the case of He^4 in the Na-Y zeolite with He^4 density of 2.2, 4.4, 6.5 and 9.0×10^{-4}mol/g are shown in Figs. 8 - 11 plotted by C/T vs T. The data fit well the following relation above T_{tr},

$$C = AT + BT^2 \ .$$

Below T_{tr}, heat capacity decreases abruptly. The temperature dependence will be discussed later. Wada et al. did not give a T^2 dependence term of the heat capacity. The values of A, B and

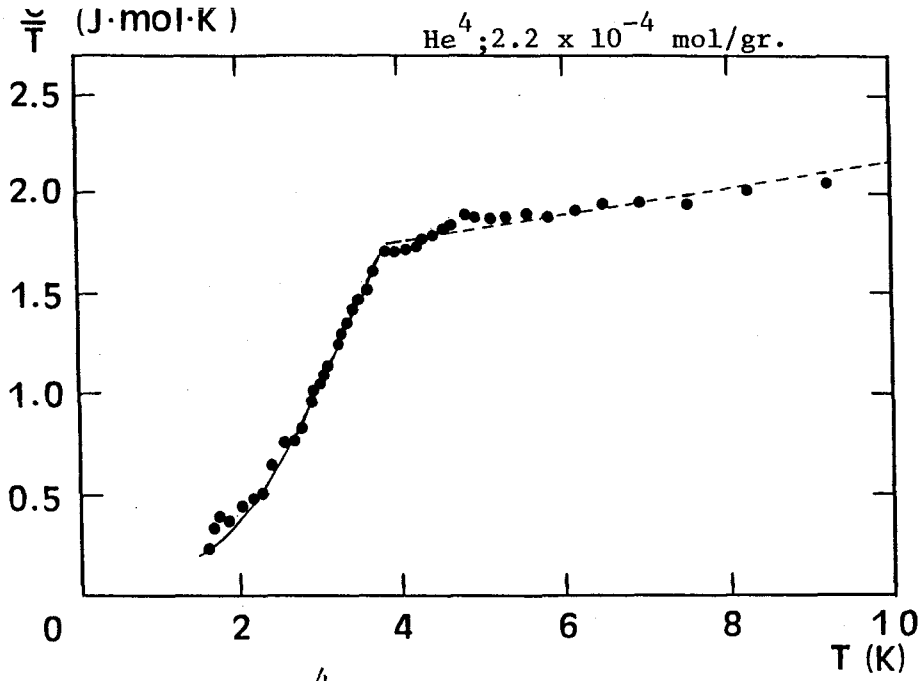

Fig. 8 Heat capacity of He^4 in Na-Y zeolite divided by temperature for He^4 density of 2.2×10^{-4} mol/gr. Solid line and broken line are fit to the data (see the text) .

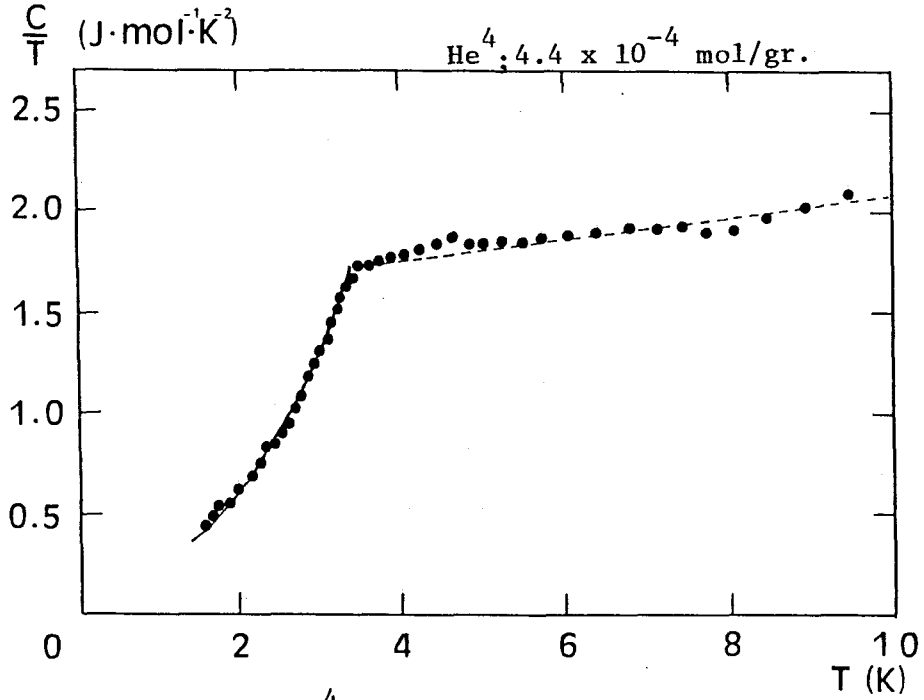

Fig. 9 Heat capacity of He^4 in Na-Y zeolite divided by temperature for He^4 density of 4.4×10^{-4} mol/gr. Solid line and broken line are fit to the data (see the text) .

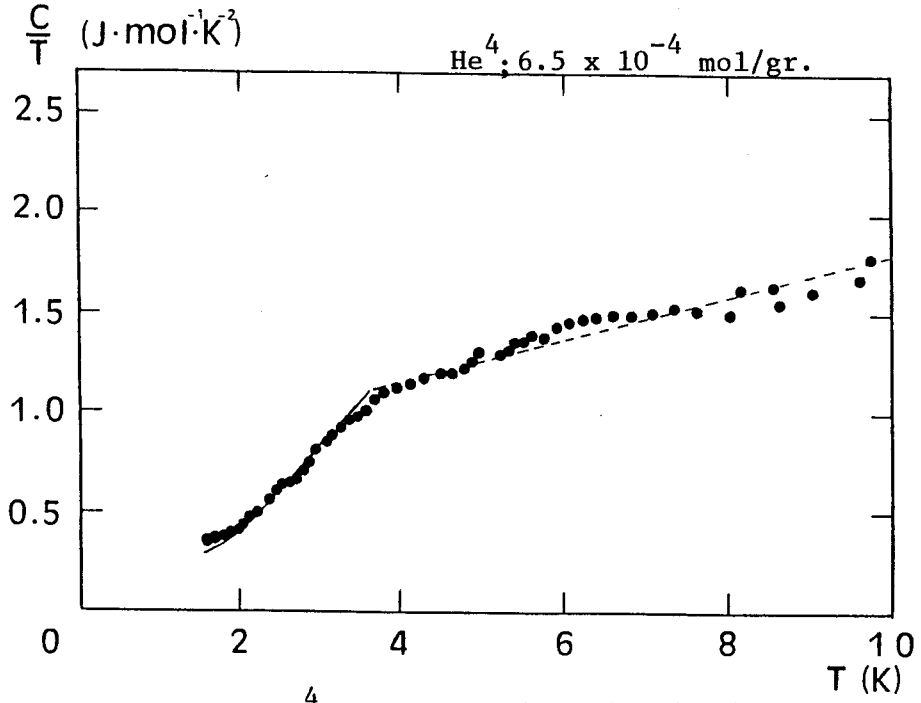

Fig. 10 Heat capacity of He^4 in Na-Y zeolite divided by temperature for He^4 density of 6.5 x 10^{-4} mol/gr. Solid line and broken line are fit to the data (see the text) .

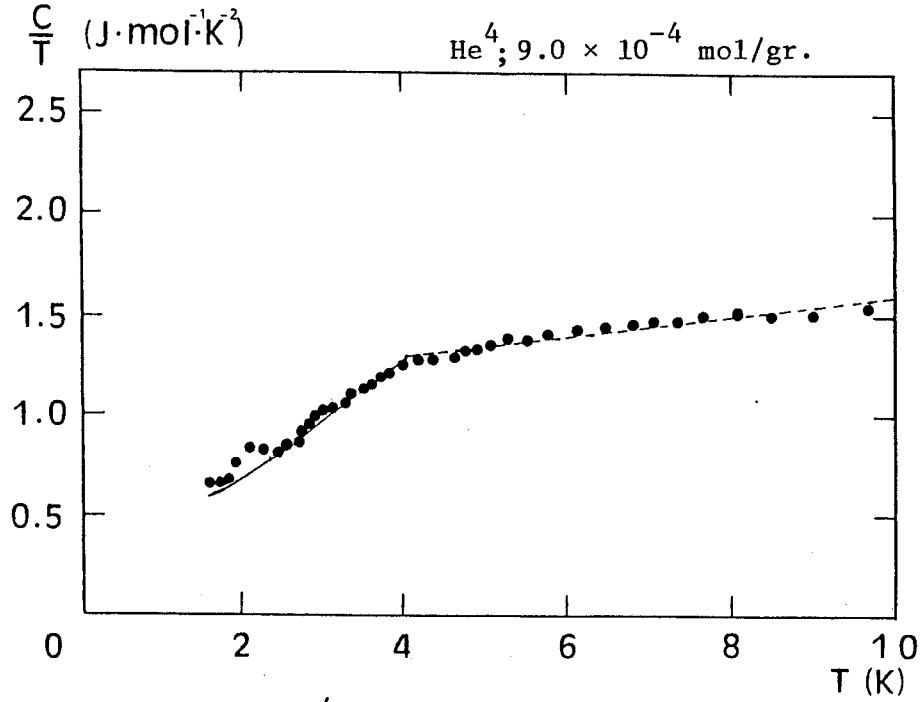

Fig. 11 Heat capacity of He^4 in Na-Y zeolite divided by temperature for He^4 density of 9.0 × 10^{-4} mol/gr. Solid line and broken line are fit to the data (see the text) .

Table 1

Heat capacities of He^4 above T_{tr} in Na-Y zeolite

$C = AT + BT^2$

n ($\times 10^{-3}$ mol/g)	A ($J \cdot mol^{-1} \cdot K^{-2}$)	B ($J \cdot mol^{-1} \cdot K^{-3}$)	T_{tr} (K)
0.22	1.50	0.070	3.8
0.44	1.54	0.056	3.4
0.65	0.74	0.106	3.8
0.90	1.10	0.050	4.1

T_{tr} in our cases are given in Table 1. With decreasing density of adsorbed He^4, the heat capacity becomes to show apparently abrupt decrease below T_{tr}. It is different from the results of H_2 in Y zeolites that the heat capacities of He^4 have T^1 dependence terms with large constant values of A.

The results for He^4 in the H-Y zeolite with densities of 4.4×10^{-4}mol/g and 10.0×10^{-3}mol/g are shown in Fig. 12 plotted by C/T vs T. In these cases, no abrupt change is observed in the present temperature range. The heat capacity of He^4 fit well BT^2 instead of $AT + BT^2$. Below 6 K, B equals to 0.29 $J/mol \cdot K^3$ for the density of 4.4×10^{-4}mol/g and equals to 0.14 $J/mol \cdot K^3$ for the density of 10.0×10^{-3} mol/g. The heat capacity at higher temperature up to 20 K is measured in the case for the density of 4.4×10^{-4} mol/g. The result are shown in Fig. 13 plotted by log C vs log T. The heat capacity shows almost a T^2 dependence

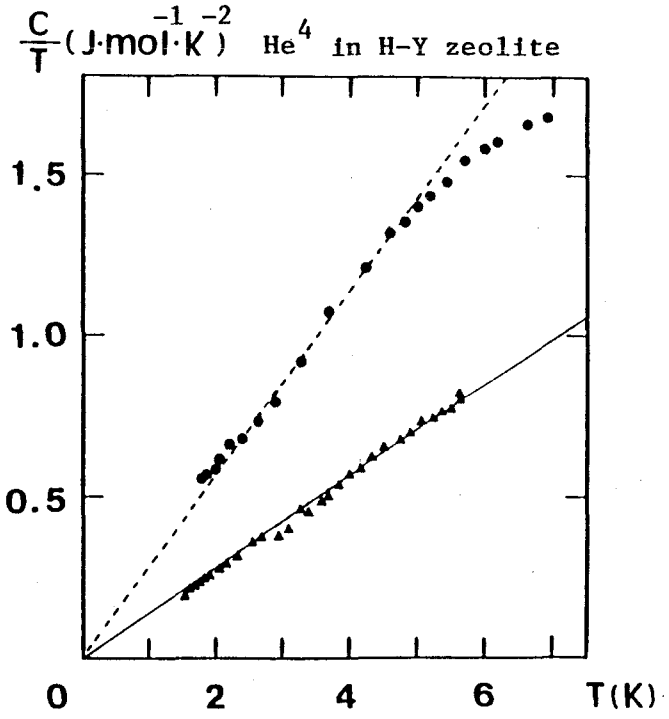

Fig. 12 Heat capacities of He^4 in H-Y zeolite divided by temperature for He^4 densities of 4.4×10^{-4} (●) and 1.0×10^{-2} (▲) mol/gr.

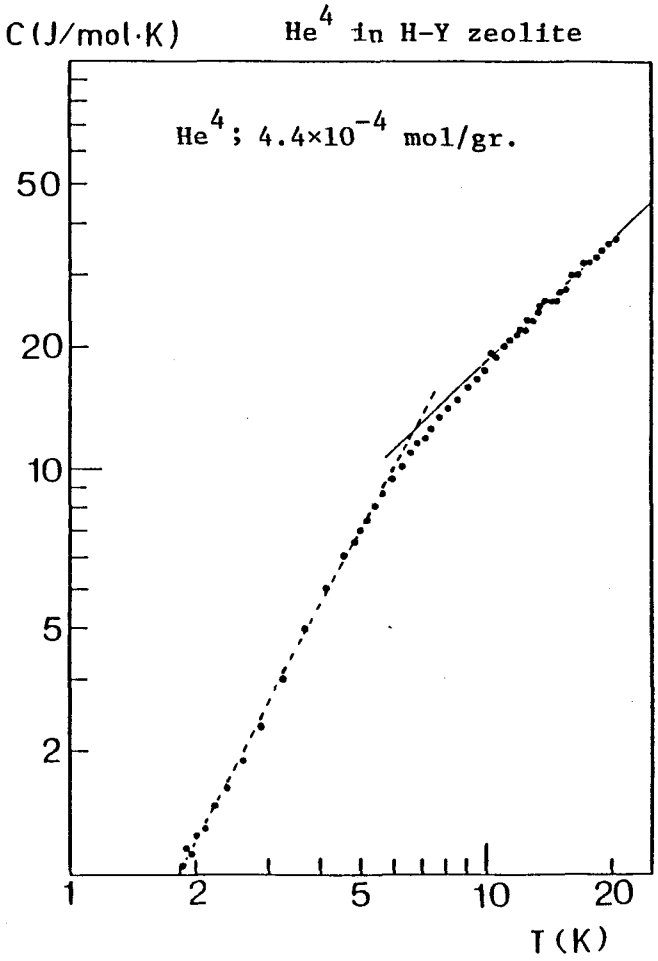

Fig. 13 Comparison of experimental values of heat capacity of He^4 in H-Y zeolite for He^4 density of 4.4×10^{-4} mol/gr. with T^1 (solid) line and T^2 (broken)line.

below 6 K and the dependence changes gradually in temperature range from 6 K to 10 K. Above 10 K, the heat capacity approaches the following value

$$C = 1.83T \text{ J/mol}\cdot\text{K} .$$

For the density of 10.0×10^{-3}mol/g, adsorbed He^4 is full in pore in the H-Y zeolite similar to the case of H_2 for the density of 9.0×10^{-3}mol/g. The heat capacity of adsorbed He^4 shows a T^2 temperature dependence and differs completely from the Einstein model in the case of high density H_2. Above 5.5 K, the heat capacity can not be measured due to outgas from zeolite.

3-4 N_2 and Ar in H-Y zeolite

Heat capacities for high density Ar and N_2 in the H-Y zeolite are also measured. The results show the similar temperature dependence with the high density case of H_2 in the H-Y zeolite, as shown in Figs. 14 and 15. The switching from the T^3 temperature dependence to the Einstein model occurs at about 7 K. The saturation values in the Einstein model for Ar and N_2 are larger than that of H_2. The values of Θ_E for Ar and N_2 are 34 K and 40 K, and the asymptotic saturation values are C_s = 12 J/mol·K and 14 J/mol·K, respectively. The Debye temperatures Θ_D of adsorbed Ar and N_2 are 59 K and 60 K which are obtained from the coefficient of the T^3 term below 7 K. The discrepancy between the Debye model with Θ_D determined above and experimental values is apparent above 7 K.

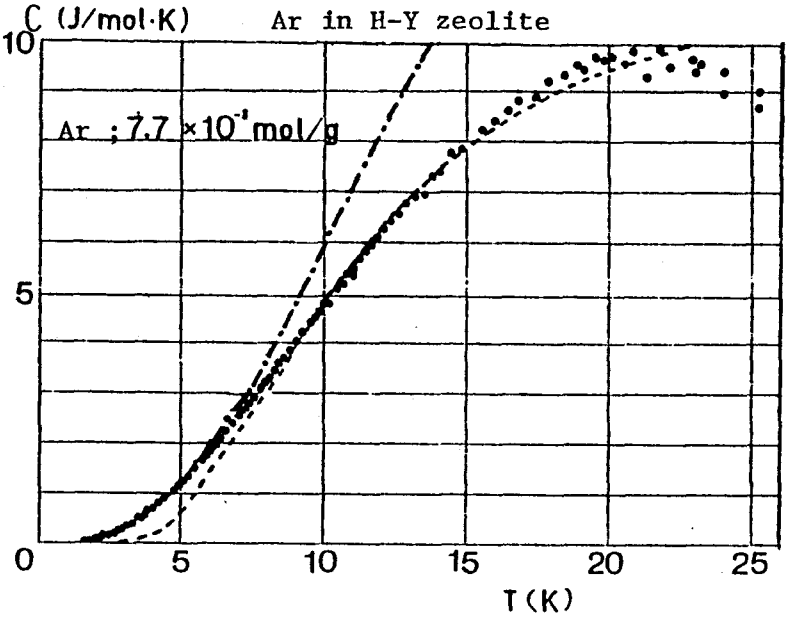

Fig. 14 Heat capacity of Ar in H-Y zeolite for Ar density of 7.7×10^{-3} mol/g. Dashed and dashed-dot lines show heat capacities calculated on the Einstein and Debye model, respectively. The characteristic temperature are Θ_E=34 K and Θ_D=58.5 K. The saturation value of 12 J/mol·K is used in the Einstein model.

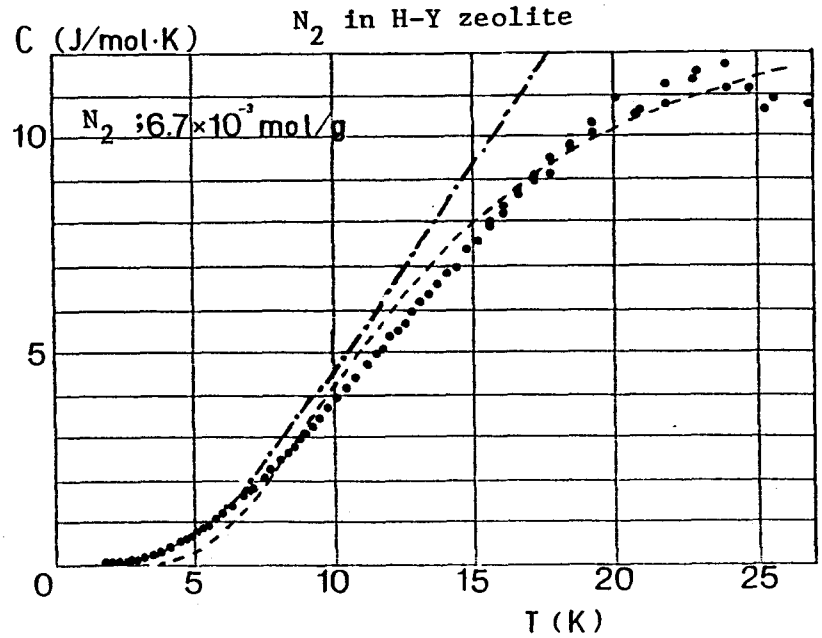

Fig. 15 Heat capacity of N_2 in H-Y zeolie for N_2 density 6.7×10^{-3} mol/g. Dashed and dashed-dot lines show heat capacities calculated on the Einstein and Debye model, respectively. The characteristic temperature are Θ_E=40 K and Θ_D=68 K. The saturation value of 14 J/mol·K is used in the Einstein model.

§ 4 Discussion

4-1 H_2 in Na-Y zeolite -- T^2 dependence

The results of heat capacity H_2 adsorbed in the Na-Y zeolite give the temperature dependence of nearly T^2 below 11 K for each value of the present densities. Moreover, the heat capacity for density of 4.5×10^{-3}mol/g has nearly the same value with that of 9.0×10^{-4}mol/g. It may be the only reason to be considered from the result that H_2 molecules in the Na-Y zeolite form the 2D solid with almost same lattice constant in these densities. At $T << \Theta_{2D}$, where Θ_{2D} is Debye temperature for the 2D solid, the heat capacity of the 2D Debye solid is given by

$$C = 240\left(\frac{T}{\Theta_{2D}}\right)^2 \text{ J/mol K.}$$

We obtain the value of Θ_{2D} = 90 K for the density of 9.0×10^{-4}mol/g regard as the 2D Debye solid. Above 11 K, the heat capacity for density of 9.0×10^{-4}mol/g shows T^1 dependence, which is similar to the case for the bulk liquid H_2. Therefore, H_2 may be solid like below 11 K and become liquid like above 11 K with continuous change. For the case of the density of 4.5×10^{-3}mol/g, the 2D solid of H_2 may become liquid partially with continuous change. Such a continuous solid-fluid transition of H_2 is observed by Stockmayer in chabazites with ellipsoidal cavities of diameter of 6.7×10 Å and interconnecting channels of diameter of 4 Å.[8] But the temperature range for the continuous transition of adsorbed H_2 in chabazite is very wide (40 K-290 K). The T^2 dependent heat capacity of H_2 in the Na-Y zeolite

will be discussed in the following section comparing with the T^3 dependent heat capacity of H_2 in the H-Y zeolite.

4-2 H_2 in H-Y zeolite -- T^3 dependence

The heat capacity of H_2 adsorbed in the H-Y zeolite for the density of 8.3×10^{-4}mol/g shows the T^3 dependence below 9 K and becomes almost flat at higher temperatures. Below 9 K, the temperature dependence suggests that H_2 behaves a 3D Debye solid. The characteristic temperature Θ_{3D} for this case is estimated to be about 90 K and is rather close to Θ_{3D} for the bulk H_2. Above 9 K, the continuous solid-liquid transition might occur similarly to the case of the Na-Y zeolite.

The difference of temperature dependence of heat capacities of H_2 adsorbed in Na-Y and H-Y zeolites may be due to the difference of the electric dipole field from the cation and AlO_2^-. This electric dipole field enhance the van der Waals force so as to localize H_2 molecules near the cations. Wada et al. measured the heat capacity and adsorption isotherm of He^4 adsorbed in Y zeolites with various kinds of cations.[9] From these data, they estimated the magnitude of the localization potential energy of each cation. In the case of He^4 adsorbed in Na-Y and H-Y zeolites, the localization potential energies W were estimated to be $W(Na^+)/k = 28$ K and $W(H^+)/k < 6$ K. Similarly, $W(Na^+)$ expected to be much larger than $W(H^+)$ also in the case of H_2 adsorbed in Y zeolites. Therefore, adsorbed H_2 molecules in the Na-Y zeolite tend to localize on the wall of the cavities and form 2D solid because of the large localization

potential energy of H_2. While H_2 in the H-Y zeolite may not be localized so strongly on the wall of the cavity but form the droplet in the cavity, because $W(H^+)/k$ is less than the solidification energy of 14 K. Then, H_2 in the H-Y zeolite shows the property expected in 3D solid at low temperature.

4-3 He^4 in Na-Y and H-Y zeolites

In the case of the Na-Y zeolite, the abrupt change of heat capacity of He^4 occurs at T_{tr}. It may be considered that the T_{tr} correspond to transition of either solid-liquid or super-normal fluid. For the case of solid-liquid transition in some restricted conditions, heat capacities almost show peaks or casps around T_c.[10,11] For example, the heat capacity of He^4 adsorbed on Grafoil is known to accompany a peak. The peak of heat capacity becomes large and T_c increases with increasing He^4 coverages.[11] In the present experiment results, it is not likely that T_{tr} is solid-liquid transition temperature, because the change of the heat capacity becomes small with increasing density of He^4 at T_{tr} and T_{tr} does not depend on the density of He^4. Nor, we do not expect T_{tr} as superfluid transition temperature, because T_{tr} is higher than the Bose-Einstein condensation temperature. And also heat capacity of He^3 adsorbed in the Na-Y zeolite is known to show similar temperature dependence to that for He^4, giving an inflection point T_{tr}.[12] Therefore, this may not be attributed to something like a superfluid transition. Kato et al. mentioned that He atoms are localized by the van der Waals potential below T_{tr} and behave

liquid-like above T_{tr} in Na-Y zeolite.[13] But they did not explain clearly about temperature dependence of heat capacity of He^4 at temperatures below T_{tr}.

Tait and Reppy obtained similar results in the case of He^4 submonolayer adsorbed in Vycor glass.[14] They analyzed the data with the following expressions

$$C = AT + BT^2 \qquad (T > T_{tr})$$

$$C = D\left(\frac{E}{k_B T} + 2\right)\exp\left(\frac{-E}{k_B T}\right) + B'T^2 \qquad (T < T_{tr}) .$$

In the first expression, the linear term arises from single-particle excitation of atoms out of islands in submonolayer into moving state with higher energy, and the quadratic term comes from pseudo-Debye 2D vibrations of the islands. Roy and Halsey discussed this model theoretically for the first time.[15] Tait and Reppy have put forward this model and shown that the energy gap 2E which is the barrier for excitation is responsible for the rapid decrease in heat capacity below T_{tr} as the single-particle excitations are rapidly frozen out. They have given the derivation of heat capacity.[14]

In the case of the Na-Y zeolite, the heat capacities of He^4 above T_{tr} fit well the first expression. Below T_{tr}, we tried to make He^4 data fit the second expression, where we put $B' = B$. Our present data below T_{tr} are reproducible with the second expression which are shown with the solid lines in Figs. 8-11. The values of the parameter D, E and B are given in Table 2. The data obtained by Tait and Reppy were explained with the two equations using B and B' ($B \neq B'$). But they did not explain

Table 2

Heat capacities of He^4 below T_{tr} in Na-Y zeolite

$$C = D\left(E/(k_B T)+2 \right)\exp\left(\frac{-E}{k_B T} \right) + BT^2$$

n ($\times 10^{-3}$ mol/g)	D ($J \cdot mol^{-1} \cdot K^{-2}$)	E/k_B (K)	B ($J \cdot mol^{-1} \cdot K^{-3}$)
0.22	28.3	12.4	0.070
0.44	24.7	10.9	0.056
0.65	7.61	9.5	0.106
0.90	7.33	7.5	0.050

well the fact that Θ_{2D} corresponding to B changed at T_{tr}. In the Na-Y zeolite case, we can take B as equal to B' and get a good agreement with the data.

In the H-Y zeolite, however, the heat capacities of He^4 differ from those in the Na-Y zeolite. Below 5 K, heat capacities of He^4 fit well $B T^2$ instead of $A T + B T^2$. From the values of B, we estimate the 2D Debye temperatures Θ_{2D} to be 28.8 K and 44.4 K for the densities 4.4×10^{-4} and 10.0×10^{-3} mol/g, respectively. The values and trend of Θ_{2D} with density are similar to the behavior of He^4 monolayer on Grafoil.[10] The temperature dependence of heat capacity of He^4 changes from T^2 to T^1 dependence above 5 K in the case of He^4 for the density 4.4×10^{-4} mol/g.

As mentioned in the discussion on H_2 in Na-Y and H-Y zeolites, the localization potential energies W were estimated

to be $W(Na^+)/k = 28$ K and $W(H^+)/k < 6$ K in the case of He^4 in Y zeolites.[9] The difference between the heat capacity of He^4 in Na-Y and H-Y zeolites may be due to the localization potential energy as that of H_2 in the same zeolites. In the case of the Na-Y zeolite, the energy gap 2E may correspond to $W(Na^+)$. The value of 2E/k, for example, is 25 K for the density of 2.2×10^{-4}mol/g and correspond to almost the same value as $W(Na^+)/k$ obtained by Wada et al. In the case of the H-Y zeolite, $W(H^+)$, corresponding to the energy gap 2E, is very small. This suffers negligible contribution from single-particle excitation and thus the heat capacities of He^4 adsorbed in the H-Y zeolite do not show the abrupt change as that in the Na-Y zeolite. In fact, the heat capacities show the temperature dependence expected in the pseudo-2D Debye solid below 6 K for the densities 4.4×10^{-4} and 10.0×10^{-3} mol/g. However, the pseudo-2D Debye solid and single-particle excitation seem to coexist in the temperature range 6 K to 10 K for the density 4.4×10^{-4} mol/g. Above 10 K, the pseudo-2D Debye solid may disappear and He^4 may be in free particle state. In the case of He^4 density of 10.0×10^{-3} mol/g, the heat capacity of adsorbed He^4 could not be measured due to outgas of He^4 from the H-Y zeolite above 5 K.

As for adsorbed H_2, the temperature dependence of heat capacities corresponding to solid like state depends on the species of cations. However, the heat capacities of He^4 in Na-Y and H-Y zeolites have T^2 temperature dependences which may be attributed to the pseudo-2D Debye solid state. This difference may be explained as the following. The van der Waals potential

energy of He^4 atoms is much smaller than that of H_2 molecules. The magnitude of localization potential energy of W is larger, even in the H-Y zeolite, than the van der Waals potential energy of He^4 atoms. Then, He^4 atoms tend to form a 2D solid on the wall of cavity both in Na-Y and H-Y zeolites and the heat capacities have a T^2 dependence in both Na-Y and H-Y zeolites. But the difference of localization potential energy seems to give influence on the 2D solid of He^4 at high temperature. For example, in the case of He^4 density of 4.4×10^{-4} mol/g, the heat capacity of He^4 in the Na-Y zeolite has a constant T^2 term from 3.4 K to 10 K, while in the case of the H-Y zeolite the T^2 term contribute little to the heat capacity at 10 K. On the basis of this result, He^4 atoms in the 2D solid in the H-Y zeolite seemed to be easy to change into single-particle excited state because of the small magnitude of localization potential energy.

4-4 High density H_2, N_2 and Ar in H-Y zeolite

The Einstein model holds well for the high density H_2, N_2 and Ar adsorbed in the H-Y zeolite, where not only the cavities but also the channels are full of atoms or molecules. Here, we present a model whose heat capacity can be approximated as an Einstein model.

We assume firstly that adsorbed atoms and molecules form small particle or cluster in each cavity and each particle oscillates with common unique frequency. The characteristic frequency f_0 has the lowest frequency expressed as,

$$f_0 = \frac{v}{2L}$$

where v is the sound velocity and L is the diameter of the particle. The characteristic frequencies f_0 are obtained using upper relation, substituting v = 2.40 Km/s (H_2)[16], 1.50 Km/s (N_2)[17] and 1.78 Km/s (Ar)[18] in bulk solid and the cavity diameter of 13 Å. The characteristic temperatures Θ_{Ecal} of H_2, N_2 and Ar are given as 7.3 K, 5.6 K, and 4.8 K, respectively. All Θ_{Ecal} are much smaller than Θ_E estimated experimentally, and the ratios of Θ_{Ecal}/Θ_E are about 0.14 - 0.30. The value of Θ_E of H_2 is the smallest, while that of Θ_{Ecal} of H_2 is the biggest of all. This model is too simple to explain whole experimental results consistently.

The pore of Y zeolite is composed of the spherical cavities and the cylindrical channels as explained in §2-1, and atoms and molecules adsorbed fully in the pore may be treated as two parts. This is similar to the model for sintered powders. Recently, Nishiguchi and Nakayama discussed thermal resistance between sintered powder and He^3 on the surface, and showed that the low energy vibrational modes are produced from the elastic deformation of the bridges connecting the particles of sintered powder.[19] They introduced the maximum angular frequency ω_E as,

$$\omega_E = \left(\frac{\pi a^2 E}{M L}\right)^{1/2}$$

where M, a, L and E denote the mass of particle, the bridge radius, the bridge length and Young's modulus of the bridge rod, respectively. And they show that the thermal properties of sintered powder are well described by the Einstein model with

the characteristic frequency ω_E below the calculated characteristic temperature $\Theta_{Ecal} = \hbar\omega_E/k_B$.

The high density H_2, N_2 and Ar are full in the H-Y zeolite, respectively and seem to form the particle in the cavity by the van der Waals potential energies which are larger than the values of W of the H-Y zeolite. Then, We applied this theory to the high density H_2, N_2 and Ar adsorbed in the H-Y zeolite. In one cavity of Y zeolite, about 20 molecules of H_2, or 8 molecules of N_2 and or 8 atoms of Ar can be contained. Thus, M of each particle of H_2, N_2 and Ar can be estimated. By substituting a = 4 Å, L = 4 Å for Y zeolite and Young's modules E for the bulk solid H_2[16], N_2[17] and Ar[18], ω_E and Θ_{Ecal} for these systems are calculated, and given in Table 3. Although this calculation is a rough estimate, the values of Θ_{Ecal} agree with that of Θ_{Ecal} better than by the model mentioned above. We can also reduce the relation, $\Theta_E(H_2) < \Theta_E(Ar) < \Theta_E(N_2)$. The difference between Θ_{Ecal} and Θ_E may mainly be due to the value E used above. The value E for such small volume of restricted geometry is probable to be different from that in bulk state. In this model, C_s of adsorbed molecules is proportional to the numbers of particles. One particle of H_2 consists of 20 molecules, while one of N_2 and Ar consists of 8 molecules. Then in the case of same adsorption value, C_s of H_2 is smaller than that of N_2. This agrees with the experimental result qualitatively. Then, this model suggests that molecules should not be adsorbed on the wall of cavities of the H-Y zeolite.

Below $T = \Theta_E/6$, heat capacities of experimental value are larger than that of the Einstein model and have a T^3 temperature

Table 3

The Einstein model of high density H_2,N_2 and Ar in H-Y zeolite

	E ($\times 10^{10}$ dyn·cm^{-3})	M ($\times 10^{-23}$ gr.)	ω_E ($\times 10^{11}$ Hz)	$\Theta_E$cal (K)	Θ_E (K)
H_2	0.214	6.67	25	19	25
Ar	2.68	53.3	31	24	34
N_2	2.08	37.3	33	25	40

dependence. Low frequency Debye's mode contributes mainly to the heat capacity at low temperature instead of Einstein's mode. The Debye temperatures Θ_D calculated from the coefficients of the T^3 term of the heat capacity H_2, N_2 and Ar are 105 K, 68 K and 59 K, respectively, while Θ_D of the bulk solid H_2, N_2 and Ar are 120 K[16], 93 K[17] and 81 K[18], respectively. The experimental values of Θ_D are smaller than those of bulk solids. In general, as decreasing the size of particle, the lattice vibrational mode becomes soft and the Debye temperature is reduced.

References

1) V.L.Ginzburg and A.A.Sobyanin : Sov. Phys. JETP Lett. 15 (1972) 242.

2) H.J.Maris, G.M.Seidal and T.E.Huber : J. Low Temp. Phys. 51 (1983) 471.

3) J.L.Tell and H.J.Maris : Phys. Rev. B28 (1983) 5122.

4) P.A.Jacobs, H.K.Beyer and J.Valyon : Zeolite 1 (1981) 161.

5) D.W.Breck : Zeolite Molecular Sieves, John wily and Sons Press, New York - London (1974).

6) N.Wada, T.Itoh and T.Watanabe : J. Phys. Soc. Jpn. 53 (1984) 913.

7) A.F.Andreev : Sov. Phys. JETP Lett. 28 (1978) 556.

8) R.Stockmeyer : Zeolite 5 (1985) 393.

9) N.Wada, Y.Yamamoto, H.Kato, T.Ito and T.Watanabe : Proceedings of 7th International Zeolite Conference (1986).

10) M.Bretz, J.G.Dash, D.C.Hickernell, E.O.McLean and O.E.Viches : Phys. Rev. A8 (1973) 1589.

11) R.L.Elgin and D.L.Goodstein : Phys. Rev. A9 (1974) 2657.

12) N.Wada, H.Kato, H.Shirataki, S.Takayanagi, T.Itoh, and T.Watanabe : Proceedings of LT-17, North Holland Press, Amsterdam (1984) 521.

13) H.Kato, N.Wada, T.Ito, S.Takayanagi and T.Watanabe : J. Phys. Soc. Jpn. 55 (1986) 246.

14) R.H.Tait and J.D.Reppy : Phys. Rev. B20 (1979) 997.

15) N.N.Roy and G.D.Halsey : J. Low Temp. Phys. 4 (1971) 231.

16) M.Nielsen : Phys. Rev. B7 (1973) 1626.

17) H.Meixner, P.Leider, P.Berberich and E.Lüscher : Phys. Lett. 40A (1972) 257.

18) P.A.Bezagly, L.M.Tarasenko and Yu.S.Ivanov : Soviet. Phys. Solid State 10 (1969) 1660.

19) N.Nishiguchi and T.Nakayama : Solid State Comm. 45 (1983) 877.

Chapter 3 Heat Capacities of H_2, D_2 and He^4 Adsorbed in Interlayer Spaces of $N^+(CH_3)_4$- and Al_2O_3-Montmorillonites

§ 1 Introduction

As mentioned in chapter 2, the heat capacities of H_2 adsorbed in Y zeolites do not show any sharp peak which corresponds to either the melting or the solidification of H_2 molecules. Though a continuous solid-liquid transition is suggested to occur at around 9 K in the H-Y zeolite, we consider that the size of void channel or pore of Y zeolite is too small to show a phase transition clearly. Then, we attempt to use the restricted geometry of which pore has the intermediate size between that of Y zeolite and that of Vycor glass, where molecular H_2 is supposed in liquid state well below the solidification temperature of H_2 in Vycor glass. The 2D space in pillar intercalated montmorillonites may be suitable substances with restricted geometries for our purpose. The intercalated space is prepared by introducing stable cation-pillars in the interlayer space of Na-montmorillonite. The interlayer distance depends on the size of introduced cation pillars. So, it is possible to control the interlayer distance by the cation-pillars. Some stable cations are used for pillars and provide the 2D space whose the interlayer separation varies from 4 Å to 20 Å.

As for the 2D restricted geometries, the surface of metal

particle and Grafoil are well known and the properties of atoms and molecules adsorbed on these surfaces have been studied by a number of workers.[1] At low temperatures, the monolayer and submonolayer of atoms or molecules on these surface tend to be localized and to behave like solid. The cation pillar-intercalated montmorillonite provides the interlayer 2D space which is different from usual surfaces as mentioned above. If the interlayer separation is the same order of magnitude with molecular sizes, the van der Waals potential of molecules may differ from those adsorbed on the surfaces mentioned above. Therefore the intercalated 2D space is expected to give some new aspects on quantum liquid.

Recently, Miyagi et al. calculated molecular attractive force acting on particles confined in an ideal dielectric substance.[2] They pointed out that a molecule has lower energy in a slab-shaped cavity or in a square tubular cavity than in the free space even if it is not adsorbed locally on the wall of the cavity. They also suggested that the potential energy must be a basic quantity in predicting features of the phase transition of condensed matter observed in pores. Then the behavior of atoms and molecules adsorbed in the interlayer 2D space is of considerable interest.

We have measured the heat capacities H_2, D_2 and He^4 adsorbed in interlayer space of $N^+(CH_3)_4$- and Al_2O_3-montmorillonites which give the interlayer separation of 4.1 Å and 9.0 Å, respectively.

§ 2 Experimentals

2-1 Adsorption space of restricted geometries in $N^+(CH_3)_4$- and Al_2O_3-montmorillonites

Among clay minerals there are some which imbibe guest molecules as prolifically as zeolites do. Generally, intercalation between the anionic siliceous sheets of these minerals makes swell rooms for atoms or molecules to be adsorbed in them. Swelling in the case of clay minerals is possible because the parallel layers in these materials are bonded to each other not covalently but by van der Waals and electrostatic forces. Electrostatic bonding arises if these are anionic charge on the sheets neutralized by interlayer cations. These cations play role of a cement which helps to hold together the anionic sheets on either side of them. When the minerals are outgassed, interlayer pore space does not usually keep room space in them; the pore space can be created only by penetration of pillar molecules and the consequent swelling with them. It is possible to open the interlayer regions permanently by the penetration and to sorb atoms or molecules like zeolites as molecular sieves.

In 1955, Barrer and McLeod showed that the silicate sheets with pillar cations of $N^+(CH_3)_4$ or $N^+(C_2H_5)_4$ were kept permanently apart providing there the intracrystalline free volume in which various non-polar as well as to polar molecules could be adsorbed.[3)] Montmorillonite is one of the minerals having the three-fold sheets found in micas as shown in

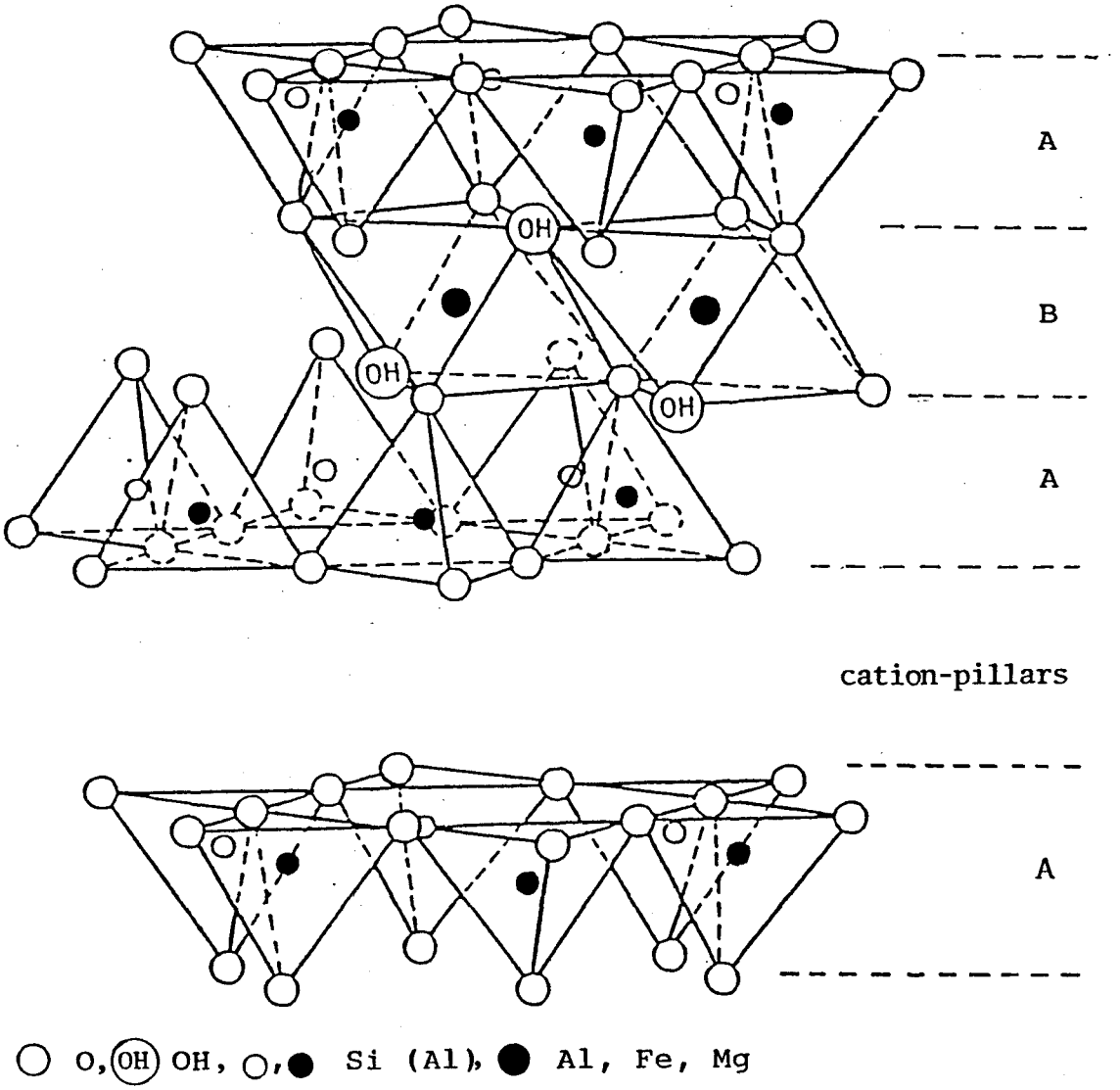

Fig. 1 Structure of the triple sheet of montmorillonite

Fig. 1[4]. The structural formula for montmorillonite is

$$Na_x(Al_{(2-x)}Mg_x)(Si_4O_{10})(OH)_2\ mH_2O\ .$$

In a typical montmorillonite, the values of x and m in the above formula are about 0.33 and 3.5, respectively. The Si_4O_{10} unit represents the composition of the tetrahedral sheets in the triple layer. The octahedral layer contains Al^{3+} or Mg^{2+} ions. The sheets are stacked in an ABA sequence to give the unit cells.

Stable $N^+(CH_3)_4$-pillars can be introduced in the interlayer space of Na-montmorillonite by ion exchange of the interlayer cations Na^+ with tetramethyl ammonium ions. The Na-montmorillonite used in this study is produced from Tsukinuno in Yamagata prefecture, Japan, with the trade name "Kunipia G" supplied by Kunimine Industrial Company. The cation exchange capacity of the clay is known to be 100 meq/ 100 g. The ion exchange is done in the following way. $N(CH_3)_4Cl$ aqueous solution is added to Na-montmorillonite which swells in distilled water. The mixture is allowed to react at 50 °C for 24 hours with occasional stirring. Then, the montmorillonite is centrifuged and washed with water several times, and dried by evacuation at 40°C. Dehydration of $N^+(CH_3)_4$-montmorillonite is performed for several hours by pumping H_2O and air out of sample at 100°C. The X-ray powder diffraction shows the basal spacing of 13.6 Å, which gives permanently the interlayer separation of 4.1 Å. The thickness of the silicate layer is 9.5 Å. Saturation capacity for interlamellar sorption which was estimated by

Barrer and Millington is 41.5 cm^3/g NTP for N_2.[5)]

Recently, a new class of solid which has large surface area has been prepared by introducing metal oxides into the interlayer spaces of swelling clays.[6)] The metal oxide acts as pillars to keep the silicate layers apart and form interlayer zeolitic cavities. Comparing montmorillonites having organic ion pillars such as $N^+(CH_3)_4$ with those having metal oxide pillars, the latters provide large surface area, large separation length and the stability up to high temperature. Al_2O_3-montmorillonite is one of the examples with metal oxide pillars.[7)] It has a basal spacing of 18.5 Å which gives the interlayer separation of 9.0 Å. Al_2O_3-montmorillonite has sorption capacity as large as Y zeolite. At the first process of the sample preparation, polymeric hydroxy-aluminum cation is introduced into the interlayer space and is replaced with the interlayer cations of montmorillonite. Then the hydroxy-aluminum cations are converted into the aluminum oxide pillars by dehydration between the layers. Therefore Al_2O_3-montmorillonite has less number of interlayer cations than Na-montmorillonite. Dehydration of Al_2O_3-montmorillonite is performed by keeping the sample at 500° C for several hours while pumping H_2O and air out of sample.

2-2 Experimental apparatus and procedure

We measure heat capacities by conventional DC heat pulse method in the course of increasing temperature. Experimental apparatus and procedure are the same as mentioned already in chapter 2.

At first, we measure the heat capacities of the sample cell which contained the $N^+(CH_3)_4$- or Al_2O_3- montmorillonite without adsorbed gas in it. In the temperature range from 1 K to 20 K, the heat capacity of the Al_2O_3-montmorillonite cell can be fitted to the same expression as that used in the case of the Y zeolite cell,

$$C = \sum_{k=0}^{6} A_k T^k$$

where A_k's are obtained by the least square method. The behavior of the heat capacity of the $N^+(CH_3)_4$-montmorillonite differs from those of Y zeolites and the Al_2O_3-montmorillonite as shown in Fig. 2. Below 2.5 K, the heat capacity shows anomaly with a broad hump around 1.5 K. Above 4 K, the heat capacity shows nearly $T^{2.5}$ dependence. The anomalous part of the heat capacity below 4 K is shown in Fig. 3, which is obtained by subtracting the heat capacity with $T^{2.5}$ dependence term from the total heat capacity. This anomalous heat capacity fits well a Schottky type heat capacity which has the maximum value at 0.8 K and reproduced by the following expression,

$$C = \frac{A(\frac{E}{k_B T})^2 \exp(\frac{E}{k_B T})}{(1 + \exp(\frac{E}{k_B T}))^2}$$

where $E/k = 1.9$ K and $A = 3.58 \times 10^{-3}$ J/g K. This Schottky type heat capacity may be due to the rotational mode of CH_3-radical in $N^+(CH_3)_4$. The rotational energy Θ_r of CH_3-radical is estimated to be $\Theta_r/k = 1$ K.

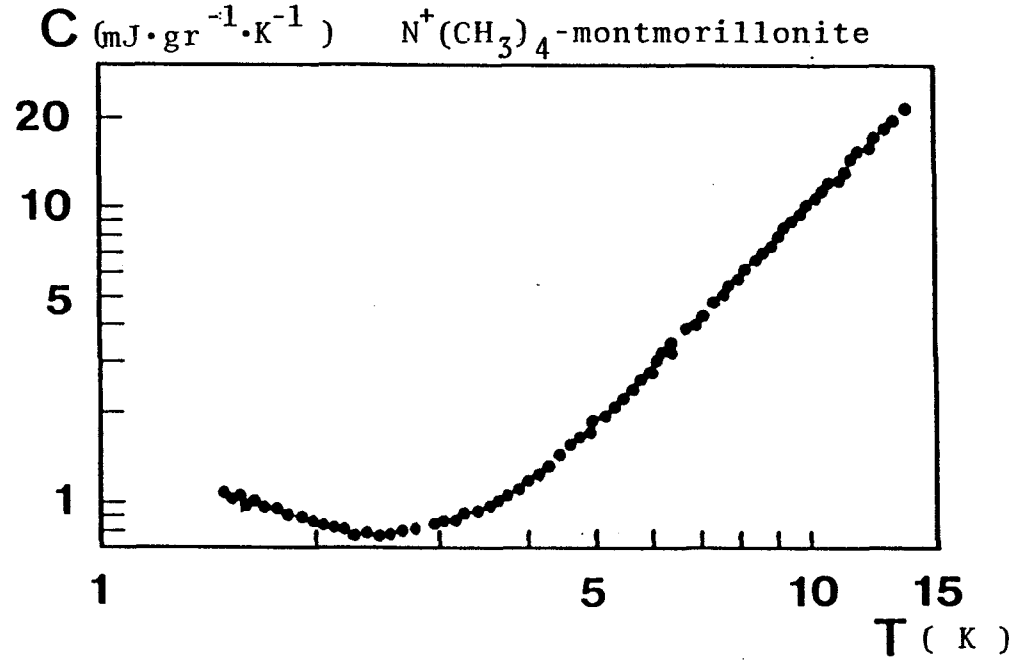

Fig. 2 Heat capacity of $N^+(CH_3)_4$-montmorillonite

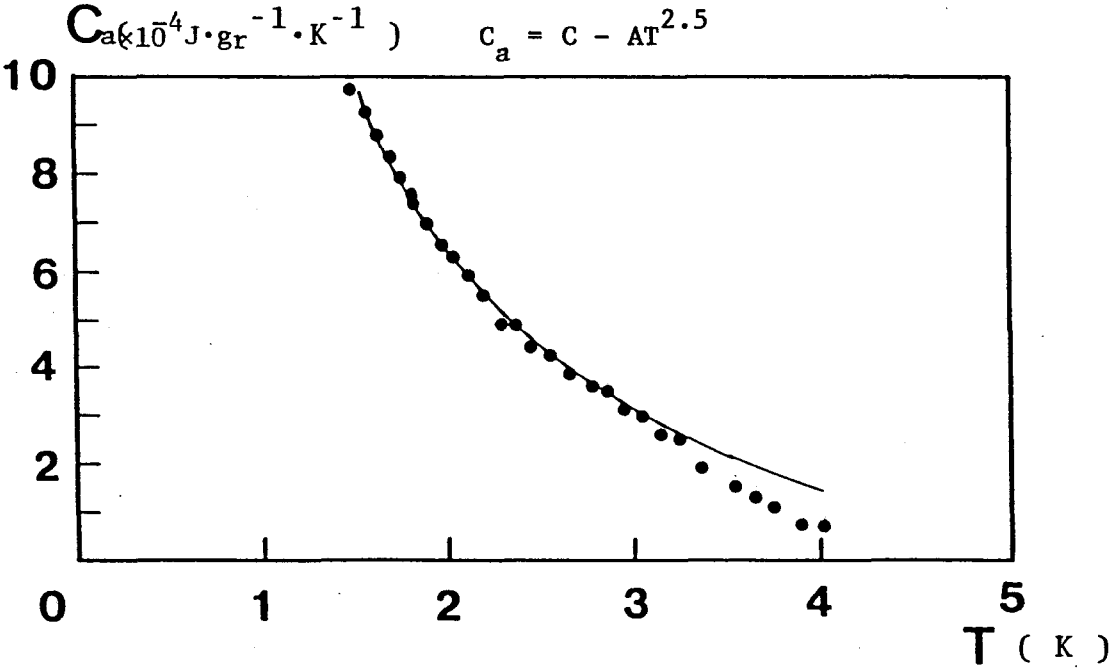

Fig. 3 Heat capacity anomaly of $N^+(CH_3)_4$-montmorillonite below 4K. The heat capacity of $T^{2.5}$ dependent term is subtracted. Solid line shows the Schottky type heat capacity (see the text).

§ 3 Experimental results

3-1 H_2, D_2 and He^4 in $N^+(CH_3)_4$-montmorillonite

Fig. 4 shows the results of several repeated measurements for the sample with H_2 of the density 5.0×10^{-4} mol/g adsorbed in the $N^+(CH_3)_4$-montmorillonite. In this case, H_2 molecules occupy about 10 % of the free volume of the interlayer space except the part of pillars. In the course of the first run of the measurement, we found a λ-type anomaly at 7.6 K. At the higher temperatures, the heat capacity shows nearly T^2 dependence up to the measured highest temperature of 20 K. However, the anomaly observed in the virgin run disappeared in the subsequent runs which were carried out after cooling again the sample down to 2 K from 20 K. Below 7.6 K, the heat capacity can be expressed by

$$C = AT^2 + B\exp(\frac{-E}{k_BT})$$

where $A = 5.45\times10^{-2}$ J/mol·K and $E/k = 45.7$ K. An independent experiment for slightly lower H_2 density than 5.0×10^{-4} mol/g has given similar results, showing the appearance and disappearance of the λ-type peak at 7.6 K in the virgin and subsequent run, respectively. Noteworthy is that the evolution of heat from the sample is detected, which is possibly due to ortho-para conversion. Considering that ortho-para ratio might be related with the appearance of the λ-type anomaly, we keep the sample with the density of 5.0×10^{-4} mol/g overnight at liquid He^4 temperature. Then, we cannot observe the anomaly at all even in

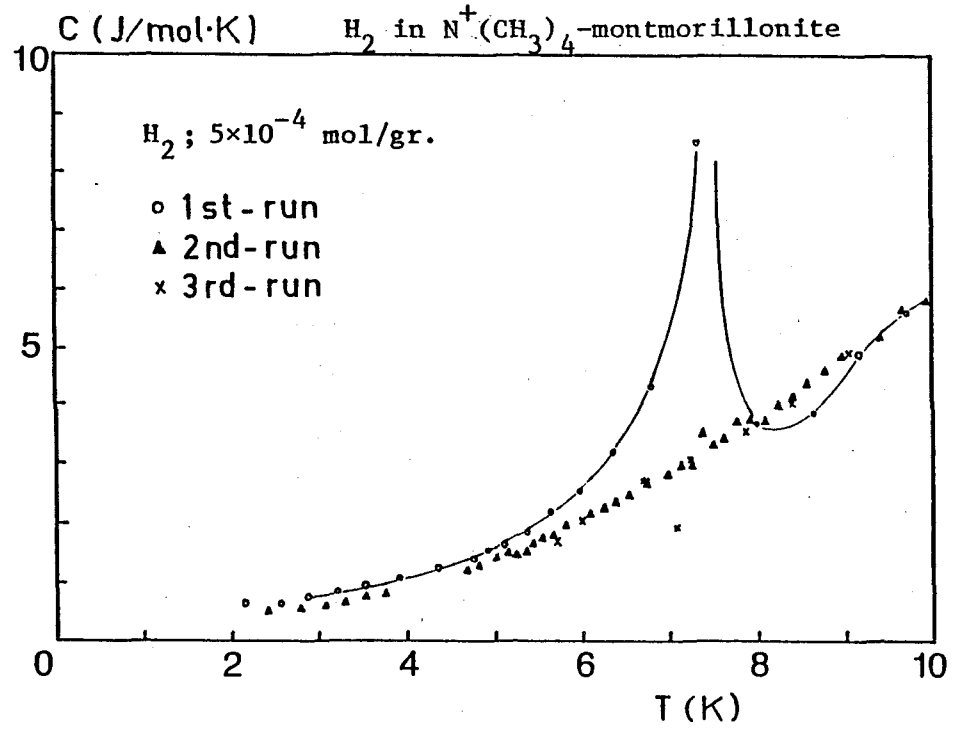

Fig. 4 Heat capacity of Hydrogen in $N^+(CH_3)_4$-montmorillonite for H_2 density of 5×10^{-4} mol/gr. ○ and ▲, × denote the virgin and subsequent run, respectively.

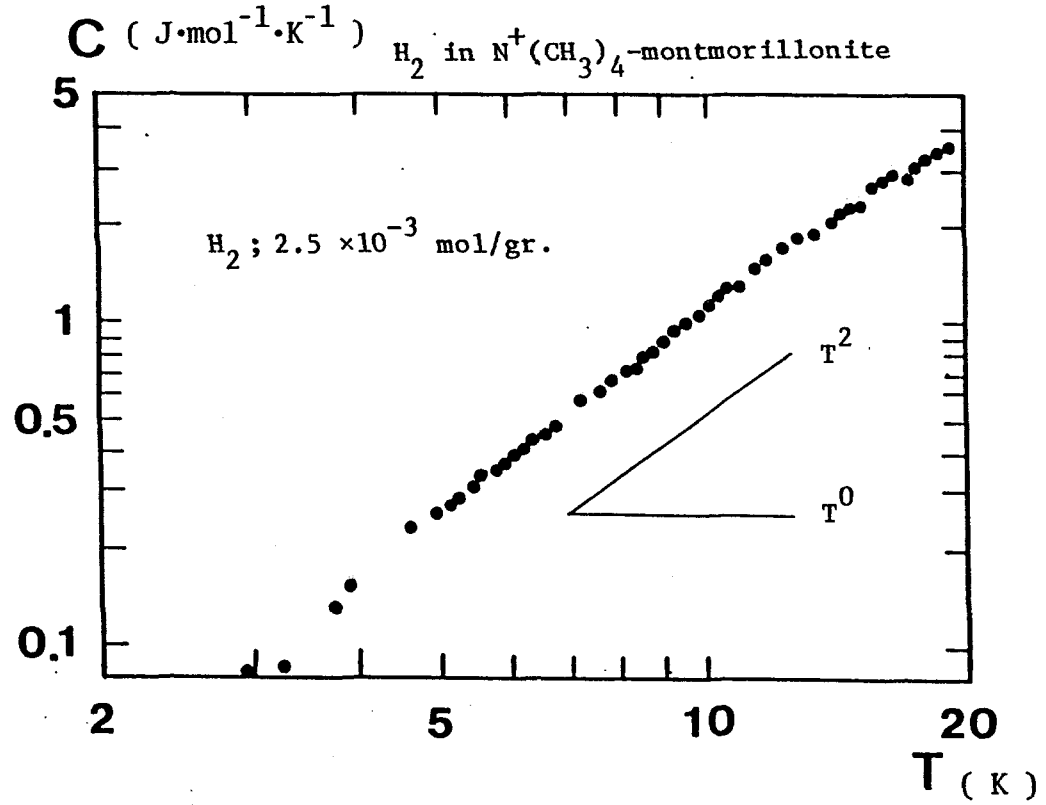

Fig. 5 Heat capacity of Hydrogen in $N^+(CH_3)_4$-montmorillonite for H_2 density of 2.5×10^{-3} mol/gr.

the virgin run.

We measure heat capacities of H_2 density of 2.5×10^{-3} mol/g. The heat capacity shows a simple T^2 dependence without any anomaly in the measured temperature region. The result is shown in Fig. 5 plotted by log C vs log T.

The heat capacity of D_2 for the density 5.0×10^{-4} mol/g adsorbed in the same substance is shown in Fig. 6. The heat capacity shows a simple T^2 dependence without any anomaly.

As for He^4 adsorbed in the $N^+(CH_3)_4$-montmorillonite, the result of the heat capacity for the density of 5.0×10^{-4} mol/g is shown in Fig. 7 plotted by C/T vs T. This result gives the similar temperature dependence to that in the case of He^4 adsorbed in the H-Y zeolite. In the temperature range 1.55 K < T < 3.2 K, the measured heat capacity fits well the following relation,

$$C = 0.1T + 0.06T^2 \quad (J/mol\cdot K) \ .$$

The temperature dependence of heat capacity changes continuously in the temperature range 3.2 K < T < 4.25 K and shows a T^1 dependence above 4.25 K.

3-2 H_2, D_2 and He^4 in Al_2O_3-montmorillonite

In the case of adsorbed H_2, we measure the heat capacities of H_2 for densities of 0.5, 1.0 and 5.0×10^{-3} mol/g. The result of H_2 for the density of 0.5×10^{-3} mol/g is shown in Fig. 8. With this density, H_2 molecules occupy about 5 % of the free volume of interlayer space excepting the part of pillars. The heat

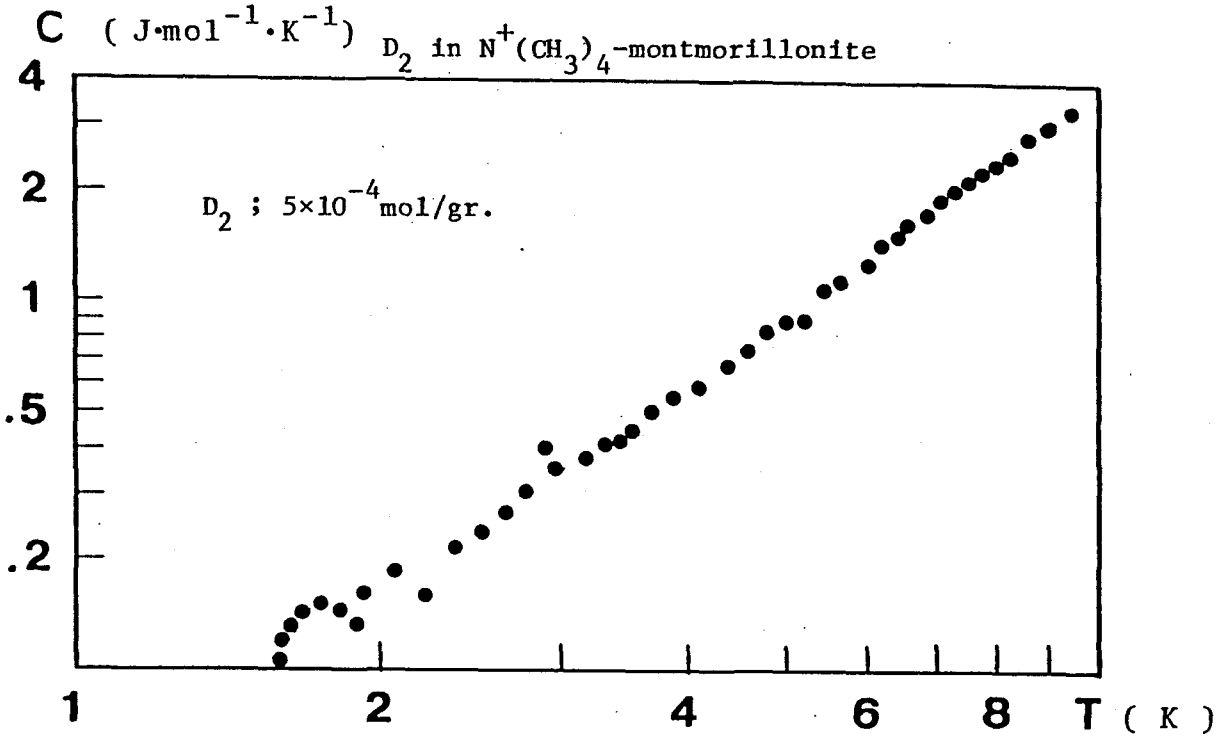

Fig. 6 Heat capacity of D_2 in $N^+(CH_3)_4$-montmorillonite for D_2 density of 5×10^{-4} mol/gr.

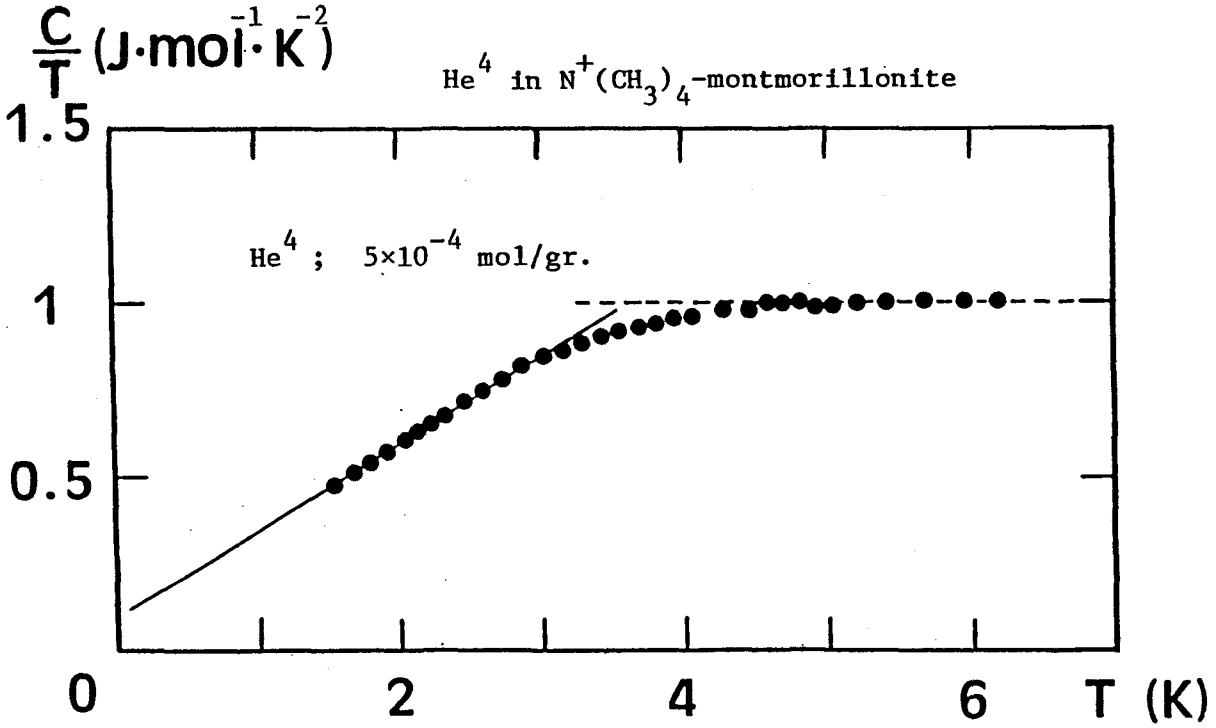

Fig. 7 Heat capacity of He^4 in $N^+(CH_3)_4$-montmorillonite divided by temperature for He^4 density of 5×10^{-4}mol/gr. Solid and broken lines are fits to the data (see the text).

capacity of H_2 has a hump around 10 K. The experiments for this density are repeated several times and the figure shows the the data superimposed. The scattering of the data points of the heat capacities above 12 K is possibly due to the outgas from the sample and also partly due to the large background heat capacity which is about 90 % of the total heat capacity. Below 6 K the heat capacity shows the temperature dependence close to T^2.

The result of H_2 for the density 1.0×10^{-3} mol/g shows in Fig. 9 plotted by log C vs log T. The heat capacity of H_2 does not have any hump around 10 K, but has a shoulder around 5 K. The data show nearly a T^2 dependence in the whole temperature range.

The similar result is obtained also in the heat capacity of H_2 with the density 5.0×10^{-3}mol/g as shown in Fig. 10. No peak in observed for this density, either. The data show a T^2 dependence in the whole temperature range.

In the case of D_2, the result of the heat capacity of the density 5.0×10^{-4} mol/g is similar to that of H_2 with the same density. The heat capacity of D_2 has a hump around 9 K as shown in Fig. 11. Below 7 K, the heat capacity shows nearly a T^2 dependence.

As for He^4 adsorbed in the Al_2O_3-montmorillonite, the heat capacities of He^4 for densities 1.0×10^{-3}, 2.1×10^{-3} and 2.0×10^{-3} mol/g are shown in Figs. 12 and 13. In the case of the density 1.0×10^{-3}mol/g, the heat capacity above 2.5 K fits well the following expression,

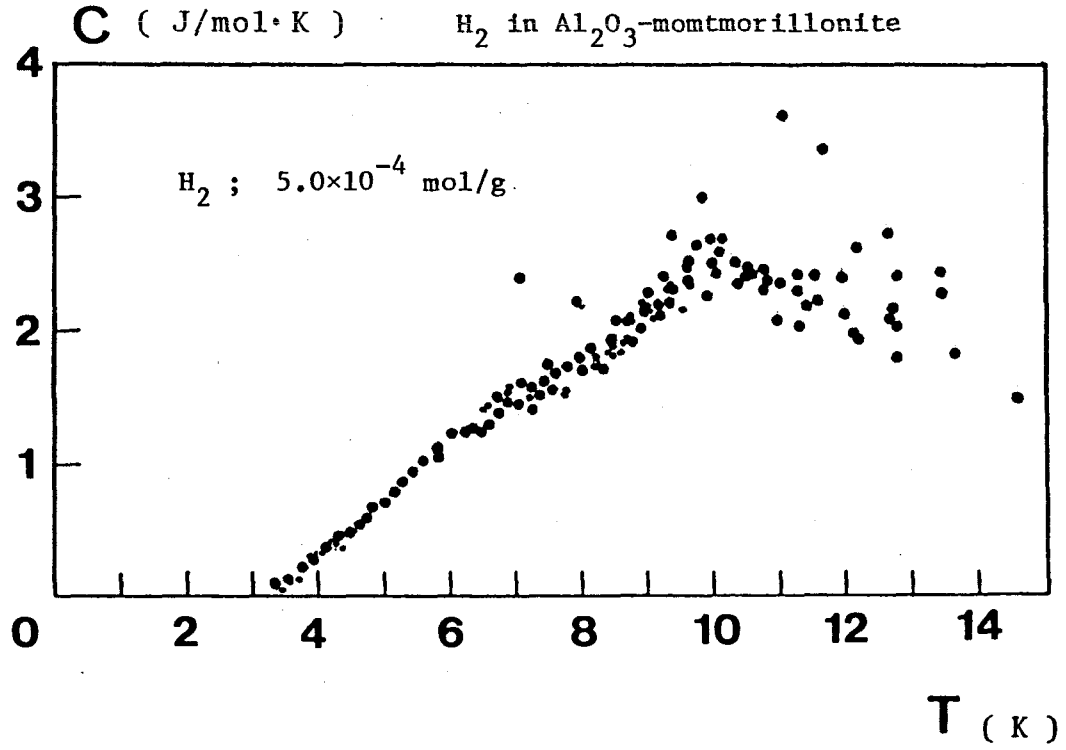

Fig. 8 Heat capacity of H_2 in Al_2O_3-montmorillonite for H_2 density of 5×10^{-4} mol/gr. Several runs are superimposed.

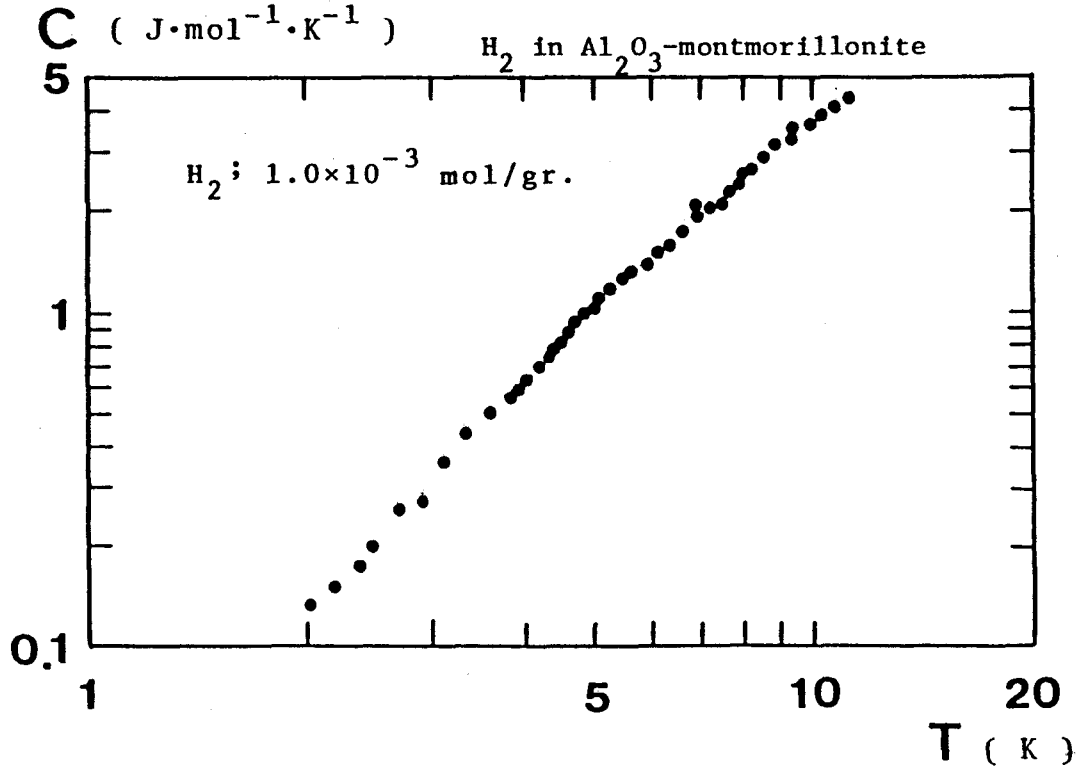

Fig. 9 Heat capacity of H_2 in Al_2O_3-montmorillonite for H_2 density of 1.0×10^{-3} mol/gr.

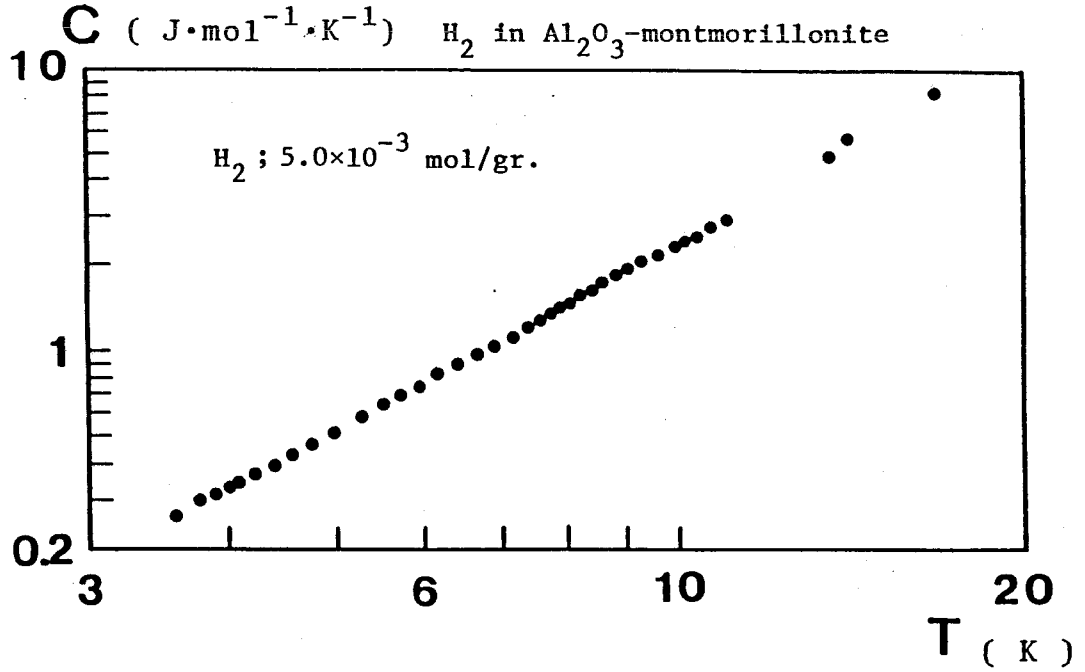

Fig. 10 Heat capacity of H_2 in Al_2O_3-montmorillonite for H_2 density of 5.0×10^{-3} mol/gr.

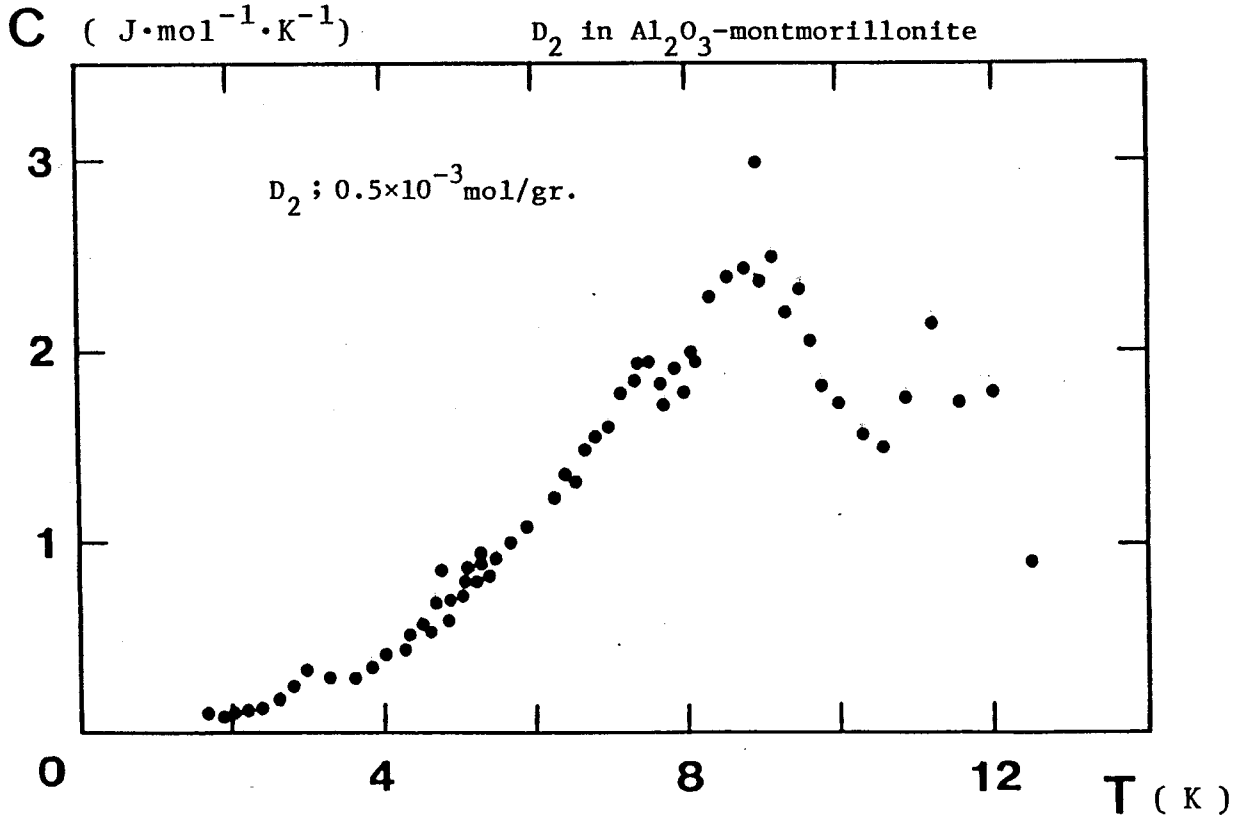

Fig. 11 Heat capacity of D_2 in Al_2O_3-montmorillonite for D_2 density of 0.5×10^{-3} mol/gr.

$$C = 0.14T + 0.26T^2 \quad (J/mol \cdot K) \ .$$

Below 2.5 K, the heat capacity is large as compared with above formula. This tendency differs from the cases for He^4 adsorbed in Y zeolites and the $N^+(CH_3)_4$-montmorillonite. In the case for the density 2.1×10^{-3} mol/g, the result is similar to that for the density 1.0×10^{-3} mol/g. Above 5 K, the heat capacity fits the following expression,

$$C = 0.3T + 0.15T^2 \quad (J/mol \cdot K) \ .$$

The heat capacity is large as compared with above relation below 5 K. This is different from the cases of Y zeolites. Below 3 K, the heat capacity for the density 2.1×10^{-3} mol/g is larger than that for 1.0×10^{-3} mol/g. The examination of the temperature dependence below 4 K gives a hump around 1.7 K for He^4 with the density 2.0×10^{-3} mol/g as shown in Fig. 13. Except the hump, the heat capacity fits well the following expression in the whole measured temperature range,

$$C = 0.45T + 0.08T^2 \quad (J/mol \cdot K) \ .$$

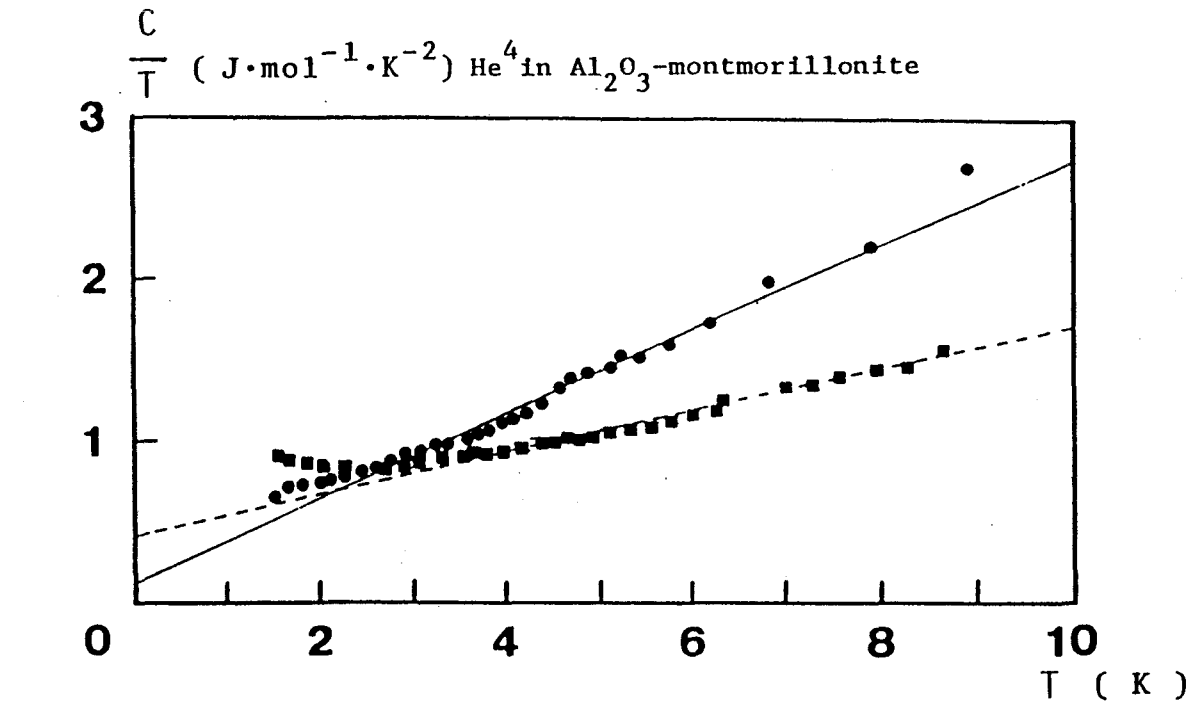

Fig. 12 Heat capacities of He^4 in Al_2O_3-montmorillonite divided by temperature for He^4 densities of 1.0×10^{-3} mol/gr.(●) and 2.1×10^{-3} mol/gr. (■). Solid line and broken line are fit to the data (see the text).

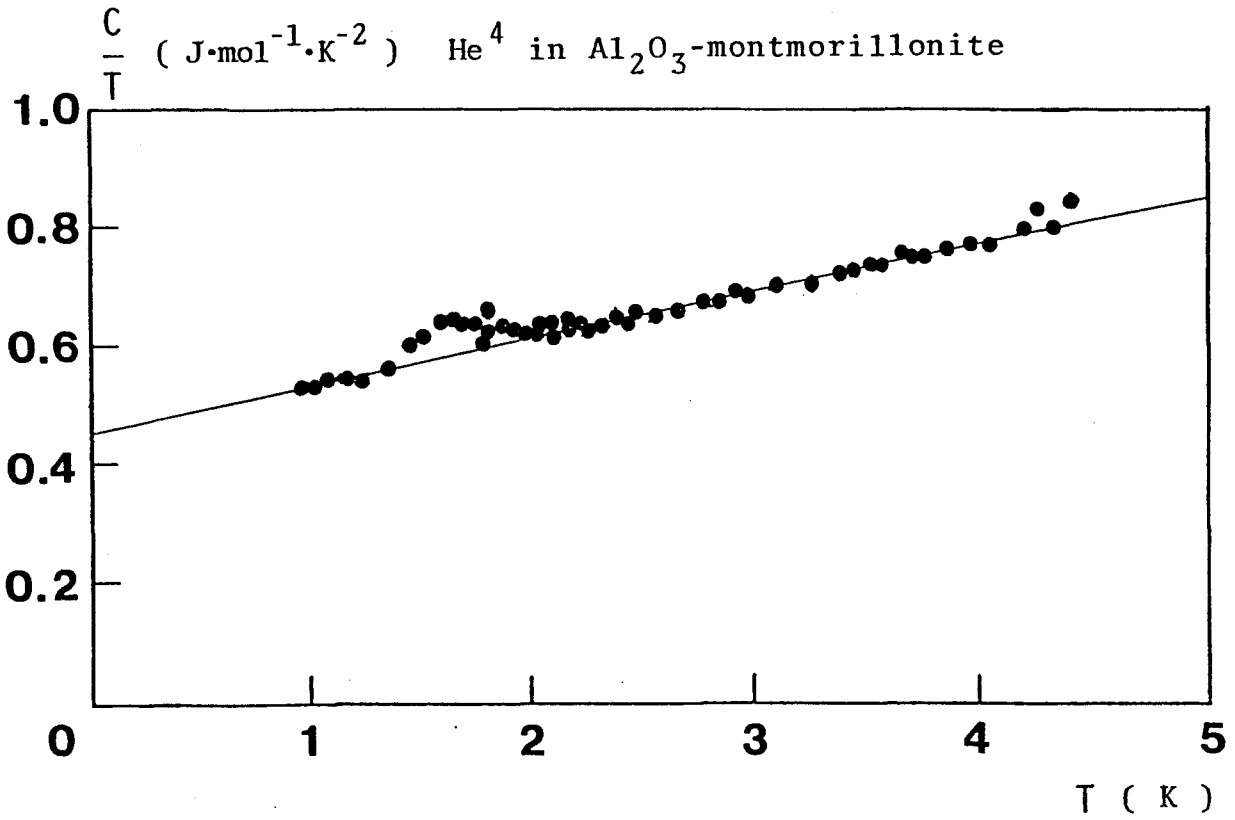

Fig. 13 Heat capacity of He^4 in Al_2O_3-montmorillonite divided by temperature for He^4 density of 2.0×10^{-3} mol/g. Solid line is fit to the deta (see the text).

§ 4 Discussion

4-1 λ-type anomaly of H_2 in $N^+(CH_3)_4$-montmorillonite

Anomalies of heat capacity of H_2 are observed in two independent experimental runs for the density of 5.0×10^{-4} mol/g. In these two experiments, we take relatively short time to cool down the sample and to measure heat capacity in the temperature range from 1.5 K to 7.6 K, comparing with the time for other runs of observations which show no capacity anomaly, too. Generation of heat from the sample is observed during cooling the sample down to 1.5 K. There are two common points on the results of the observed anomalous heat capacity. The measured heat capacity in the first run is larger than those in the second and the third run below 6 K, and has anomaly between 6 K and 7.6 K. Above 7.6 K, heat capacities of all runs have almost the same values and show the T^2 dependence.

Therefore it is not possible that the solid-liquid transition occurs at 7.6 K. Then, H_2 molecules adsorbed in the $N^+(CH_3)_4$-montmorillonite may form a 2D solid in the whole measured temperature range. Because of large heat capacity and generation of self heating of the sample in the first run at low temperatures, the anomaly may suggest the existence of ortho-H_2. The heat capacity of solid ortho-H_2 is larger than that of solid para-H_2. In bulk solid H_2, ortho-para conversion rate is 2 % per hour and the heat of the conversion is about 81 J/mol below 10 K. One of the possibility is that orientational order-disorder transition of ortho-H_2 takes place in this case. In the

bulk H_2, ortho orientational order occurs with higher ortho concentration than about 50 %. The transition temperature T_c depends on ortho concentration: 2.8 K and 1.5 K for ortho concentration of 100 % and 75 %, respectively, for example.[8] Up to now, no experimental confirmation has been obtained for the orientational ordering of ortho-H_2 in 2D solid adsorbed in restricted geometries. Transition temperatures of ortho-H_2 orientational ordering for the 2D systems were calculated by O'shea and Klein.[9] They predicted T_c = 1.5 K for 2D ortho-H_2, which is much lower than 7.6 K. But T_c depends generally on lattice constants and structure of H_2 solid strongly.

In order to investigate ortho-para conversion of adsorbed H_2, we also performed NMR study of adsorbed H_2. The ortho-para conversion rate should be detected from time dependence of NMR intensity of adsorbed H_2. The results show the ortho-para conversion rate is several % per hour at 4.2 K. Then, the ortho concentration after the first run is expected to become very low and the λ-type anomaly could not occur the second and third run.

4-2 H_2 and D_2 in $N^+(CH_3)_4$- and Al_2O_3-montmorillonites

Below 7 K, the heat capacities of H_2 and D_2 adsorbed in montmorillonites exhibit a T^2 temperature dependence, giving an indication of the 2D solid behavior. The low temperature region of the T^2 dependence are analyzed in terms of a 2D Debye model. The experimental 2D Debye temperature Θ_{2D} is found to be nearly independent of temperature up to T/Θ_{2D} = 0.07, consistent with the temperature range where the next asymptotic formula is

valid.

$$C = 240 \left(\frac{T}{\Theta_{2D}}\right)^2 \quad (J/mol \cdot K)$$

Using this formula below 7 K, Θ_{2D} of H_2 and D_2 adsorbed in $N^+(CH_3)_4$- and Al_2O_3-montmorillonites are obtained and given in Table 1. The value of Θ_{3D} of bulk solid H_2 is about 120 K and that of bulk solid D_2 is 89 K.

In Al_2O_3-montmorillonite, the heat capacities of H_2 and of D_2 for the density 5.0×10^{-4}mol/g have the hump at 10 K and 9 K, respectively, and do not show a T^2 dependence above these temperatures. Comparing with λ-anomaly of H_2 in $N^+(CH_3)_4$-montmorillonite, these humps are time-independent and the result of the subsequent run is almost the same as that of the virgin run. Therefore, the humps possibly correspond to the process of melting from 2D solid to liquid.

Nielsen et al. obtained the phase diagrams of adsorbed monolayers of D_2 and H_2 on Grafoil.[10] In the 2D layers adsorbed on Grafoil, the melting temperature of H_2 is almost the same as that of D_2. In submonolayer, the melting temperature increases from 10 K to 20 K by increasing the amount of adsorbed H_2 or D_2. In this case, they interpreted that the phase changed from the $\sqrt{3}$-structure solid into the gas-like region.

Tell and Maris measured the heat capacity of H_2 and D_2 in Vycor glass.[11] The melting temperature of H_2 and D_2 are 11.7 K and 16.6 K, respectively. The broad peaks corresponding to the melting of H_2 and D_2 in Vycor glass resemble to those of our cases. The melting temperature 10 K of our result of H_2 is just

Table 1

Θ_{2D} of H_2 and D_2 adsorbed in montmorillonites

Kind of gas specimen	Kind of pillar between montmorillonite	Density of gas specimen ($\times 10^{-3}$ mol/g)	Θ_{2D} (K)
H_2	$N^+(CH_3)_4^-$	0.5	66
H_2	$N^+(CH_3)_4^-$	2.5	150
H_2	$Al_2O_3^-$	0.5	81
H_2	$Al_2O_3^-$	1.0	77
H_2	$Al_2O_3^-$	5.0	107
D_2	$N^+(CH_3)_4^-$	0.5	80
D_2	$Al_2O_3^-$	0.5	98

below 11.7 K.

Except for the case of low density H_2 and D_2 in the Al_2O_3-montmorillonite, the heat capacities of H_2 and D_2 in montmorillonites do not show the peak corresponding to the solid-liquid transition below 20 K. The change of temperature dependence corresponding to a continuous solid-liquid transition is not seen, either. In the interlayer 2D space, the solid-liquid transition may depend strongly on the density of adsorbed molecules and the interlayer distance in the 2D space. Therefore, behavior of H_2 and D_2 in the interlayer 2D space is different from that on Grafoil or in Vycor glass.

The behavior of adsorbed H_2 in the Al_2O_3-montmorillonite is different from that in the $N^+(CH_3)_4$-montmorillonite. If the difference is due to the interlayer distance, then the data show that free H_2 appears in the Al_2O_3-montmorillonite. Also, adsorbed molecules may tend to localize around the cation pillars and the $N^+(CH_3)_4$-montmorillonite has much more cations than the Al_2O_3-montmorillonite.

4-3 He^4 in $N^+(CH_3)_4$- and Al_2O_3-montmorillonites

In the case of He^4 adsorbed in the $N^+(CH_3)_4$-montmorillonite, the result is similar to that of He^4 for the density 4.4×10^{-4} mol/g adsorbed in H-Y zeolite. Below 3.2 K, adsorbed He^4 atoms form the 2D solid accompanying the single particle excitation of which heat capacity shows a T^1 dependence as explained in chapter 2.[12] Above 4.25 K, the 2D solid may mostly disappear and He^4 may be at free particle state

where He^4 atoms behave like gas giving a T^1 dependence of the heat capacity.

In the case of He^4 adsorbed in the Al_2O_3-montmorillonite, the results differ from those for Y zeolites and the $N^+(CH_3)_4$-montmorillonite at low temperatures. In the high temperature range, the heat capacity fits well the relation, $C = AT + BT^2$. If the T^2 term indicates the heat capacity of a 2D solid and its coefficient does not change at low temperatures, the T^1 dependent term, which corresponds to the heat capacity of single particle excitation, becomes large at low temperatures. The larger the density of He^4 is, the larger the heat capacity at low temperatures becomes. In the case of He^4 for the density 2.1×10^{-3} mol/g, the hump around 1.7 K is observed. Then, it is possible that the superfluid transition occurs in some part of adsorbed He^4, which corresponds to the T^1 dependent term.

Heat capacities of multilayers He^4 on Grafoil were measured by Bretz.[13] Thicker films display the truncated λ-type anomaly which depends on the thickness. The anomaly looks like a suppressed λ-peak of bulk He^4 and has the plateau between T_p and T (bulk λ-point). The temperature T_p depends on thickness and varies from 1.6 K to 1.9 K. This result is different from that of He^4 in the Al_2O_3-montmorillonite.

References

1) J.G.Daunt and E.Lerner, ed. : Monolayer and Submonolayer Films, Plenum Press, New York (1973).

2) H.Miyagi, T.Haseda and T.Nakamura : J. Phys. Soc. Jpn. 54 (1985) 1299.

3) R.M.Barrer and D.M.McLeod : Trans. Faraday Soc. 51 (1955) 1290.

4) R.M.Barrer : Zeolite and Clay Minerals as Sorbents and Molecular Sieves , Academic Press (1978).

5) R.M.Barrer and A.D.Millington : J. Coll. Interface Sci. 25 (1967) 359.

6) S.Yamanaka : J. Clay Sci. Soc. Jpn. 21 (1981) 78.

7) G.W.Brindley and R.E.Sempels : Clay Miner. 12 (1977) 229.

8) I.F.Silvera : Rev. Mod. Phys. 51 (1980) 393.

9) S.F.O'shea and M.L.Klein : Chem. Phys. Lett. 66 (1979) 381.

10) M.Nielsen, J.P.McTague and W.Ellenson : J. Phys. (Paris) 38 (1977) C4-10.

11) J.L.Tell and H.J.Maris : Phys. Rev. B28 (1983) 5122.

12) R.H.Tait and J.D.Reppy : Phys. Rev. B20 (1979) 997.

13) M.Bretz : Phys. Rev. Lett. 31 (1973) 1447.

Chapter 4 NMR Study of He^3 Adsorbed in High Silica Zeolites And $AlPO_4$-5

§ 1 Introduction

In recent 20 years, NMR experiments on He^3 adsorbed on a variety of substrates, such as Grafoil, Vycor glass and zeolites(3A and 13X), have been performed in order to extract both static and dynamical properties. In these restricted geometries, adsorbed He^3 atoms have revealed thermal and magnetic properties quite different from those of bulk He^3.

Some remarkable points are as follows.

(i) Grafoil provides 2D space and He^3 atoms adsorbed on its surface behave like either 2D solid, 2D liquid or 2D gas.[1-3)]

(ii) Several NMR studies on adsorbed He^3 in Vycor glass have been reported.[4-7)] The results have shown that T_1 and T_2 of adsorbed He^3 are very short comparing with those of bulk He^3 and that the nuclear susceptibility χ_s of He^3 is larger than that of bulk liquid He^3 in the temperature range down to 50 mK. The results of $\chi_s$of adsorbed He^3 can be interpreted very well with the statistical layer model which treats adsorbed He^3 as independent layers of bulk solid and of liquid.[5)]

Thus, He^3 adsorbed on Grafoil and Vycor glass have the properties of 2D solid and liquid.

(iii) The earlier NMR studies on He^3 adsorbed in zeolites were performed at temperatures above 1K by Careri et al.[8)] and Weaver.[9)] Careri et al. measured nuclear magnetization M of

He^3 adsorbed in the 13X synthetic zeolite and found M of He^3 not to follow Curie's law but to exhibit a temperature independent tendency below 2.5 K. Weaver measured T_1 and T_2 of adsorbed He^3 in 13X and 3A zeolites. The relaxation times were very short and showed different temperature dependence from those of bulk He^3.

Because these experiments mentioned above were performed at temperatures above 1 K, it is difficult to study whether these adsorbed He^3 atoms follow the Fermi statistics.

(iv) Recently Kato et al. measured heat capacity of He^3 adsorbed in the Na-Y zeolite in the temperature range between 0.1 K and 2 K.[10] Their heat capacity measurement of adsorbed He^3 has a plateau around 0.2 K. From the result, they suggested the Fermi degeneracy of He^3 adsorbed in the Na-Y zeolite.

Now, we will explain restricted geometries used in this study and mention our interests.

High silica zeolites such as ZSM-5 have the restricted geometries of which diameters are of the same order as that of He^3 atom. In general, high silica zeolites contain very few cations in the crystal and are of high purity. The sizes of diameter of channel and the channel structures, for example 1D or 2D channel system, depend on each species of zeolites. The possibility of exchanging the position of He^3 atoms must be limited in these restricted geometries resulting in the specific distribution of momentum of He^3 atoms in the system. If He^3 atoms behave like fluid at low temperatures in these restricted geometries, it is very interesting how the Fermi degeneracy works and how the properties of Fermi statistics appears.

Therefore we measure the nuclear susceptibility of He^3 adsorbed in high silica zeolites below 1.5 K. The behaviors should depend strongly on the way of exchanging of particles reflecting the apparent statistical properties in the system.

§ 2 Experimentals

2-1 Adsorption space of high silica zeolites and $AlPO_4$-5

The six specimens used as adsorbent in our experiment are given in Table 1. ZSM-5[11,12] and ZSM-23[13] are high silica zeolites in which SiO_2/Al_2O_3 ratio is greater than 30. Silicalite-1[14] and Silicalite-2[15,16] contain almost negligibly small amount of Al^{3+}. The ratio of SiO_2/Al_2O_3 in both specimens exceeds 1000. The unit cell of these high-silica zeolites and Silicalites is given by $Na_nAl_nSi_{96-n}O_{192}$, where n in the formula is about 1 in a typical silicalite and smaller than 0.1 in some Silicalites. High silica zeolite and Silicalite contain very small amount of cations, and therefore are hydrophonic. We use the high silica specimen of ferrierite of which SiO_2/Al_2O_3 ratio is 20.[17] $AlPO_4$-5 is one of the aluminophosphate molecular sieves, which was synthesized by Wilson in 1982.[18] It has similar properties with some zeolites which are used as adsorbent for molecular sieve and as catalyst or catalyst support. The chemical formula is $Al_2O_3 \cdot P_2O_5$. The neutral aluminophosphate frameworks are moderately hydrophilic because of the small difference in electronegativity between aluminum (1.5) and phosphorus(2.1).

The size and structure of channel of these specimens are given in Table 1.

ZSM-5 has the effective 3D channels constructed by the ring of 10-membered openings and narrow channels, which is shown in Fig. 1. Straight channels parallel to (010) have openings

Table 1

High silica zeolites and $AlPO_4$-5

No.	Specimen	Diameter of channel (Å)	Channel structure	Porocity	SiO_2/Al_2O_3
1	ZSM-5	5.4 × 5.6 (100) 5.1 × 5.4 (010)	3D	0.32	190
2	Silicalite-1	5.4 × 5.6 (100) 5.1 × 5.7 (010)	3D	0.32	1900
3	Silicalite-2	5.5 (100) 5.5 (010)	3D	0.3	1490
4	Ferrierite	4.3 × 5.5 (001) 3.4 × 4.8 (010)	2D	0.28	20
5	ZSM-23	5.3 × 5.6 (100)	1D	0.21	63
6	$AlPO_4$-5	8.0 (001)	1D	0.3	—

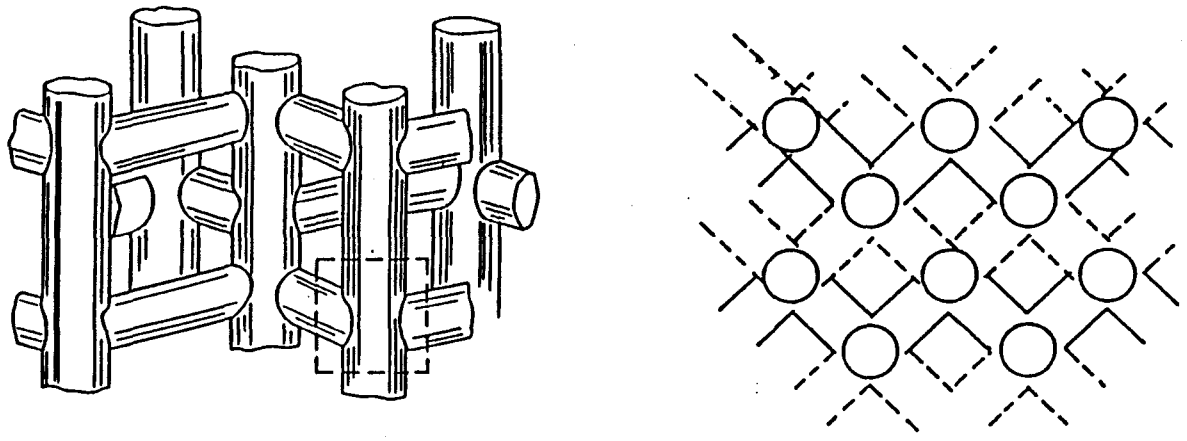

(a) (b)

Fig. 1 The channel structure in ZSM-5 (a)
C-projection of the channel structure (b)

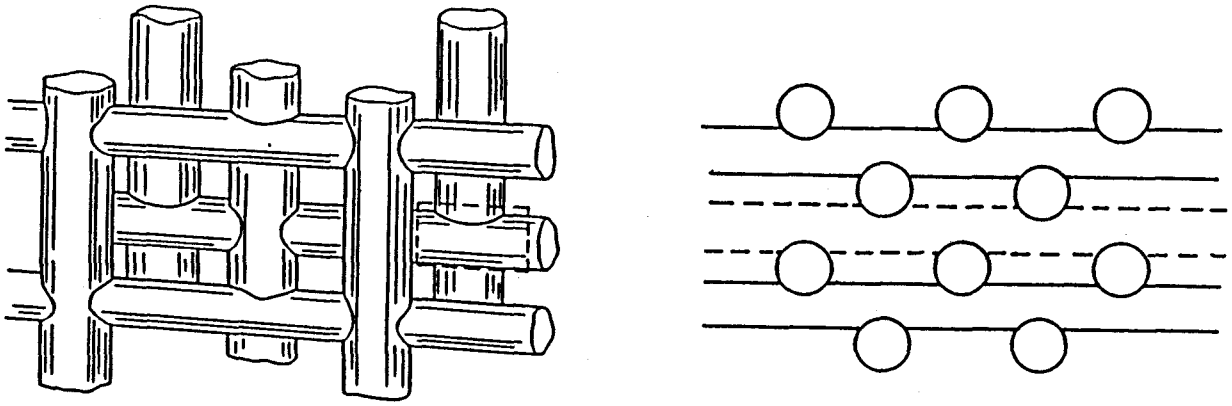

(a) (b)

Fig. 2 The channel structure in ZSM-11 (a)
C-projection of the channel structure (b)

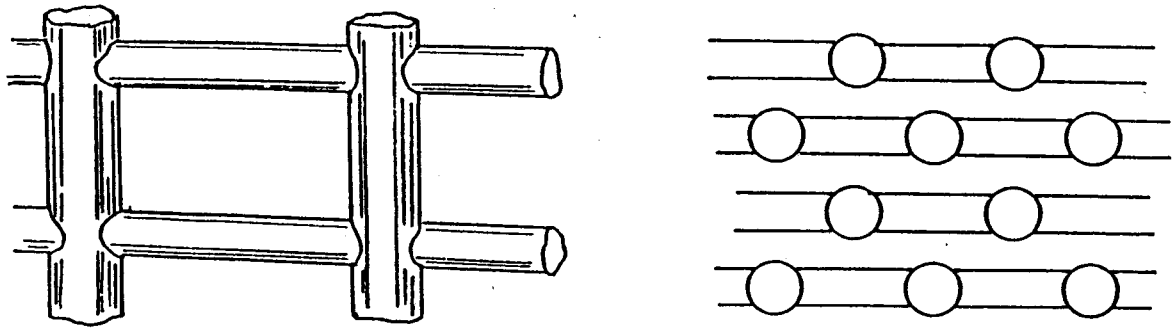

(a) (b)

Fig. 3 The channel structure in ferrierite (a)
C-projection of the channel structure (b)

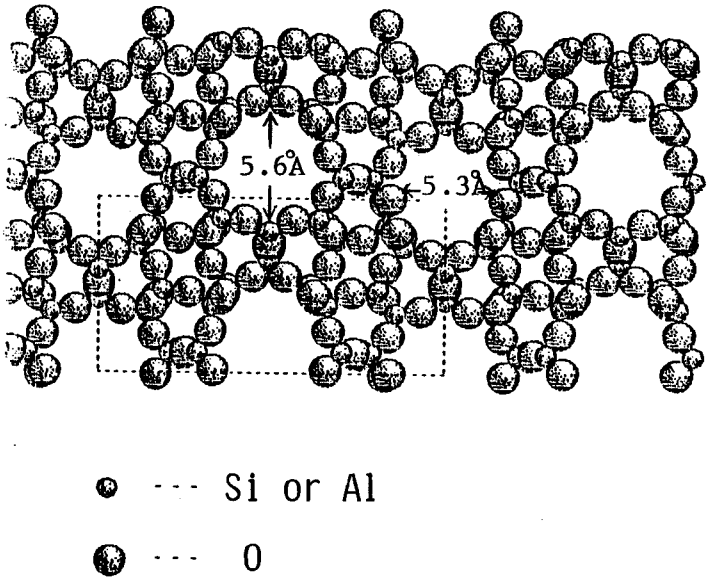

Fig. 4 The frameworks of ZSM-23 (a-projection)

constructed by 10-membered ring of size 5.4×5.6 Å. The zigzag channels along (100) with openings of the size of 5.1×5.4 Å intersect the straight channels at right angles. Diffusion in the (001) direction can take place between the intersecting channels parallel to (100) and (010). Silicalite-1 has almost the same channel sizes and channel structure as ZSM-5.

Similarly, Silicalite-2 has almost the same pore size and channel structure as ZSM-11. As in ZSM-5, the ZSM-11 framework contains two intersecting channels with 10-membered ring openings. But unlike those in ZSM-5, they are both straight and have the same openings of the size of 5.5 Å which is shown in Fig. 2.

The framework of ferrierite is shown in Fig. 3. Ferrierite has effective 2D channels system. One channel parallel to (001) has openings determined by 10-membered ring of size 4.3×5.5 Å and the other parallel to (010) has openings constructed by 8-membered ring of size 3.4×4.8 Å.

ZSM-23 has 1D channel parallel to (100) having openings constructed by 10-membered ring of size 5.6×5.3 Å, which is shown in Fig. 4.

Similarly, $AlPO_4$-5 has 1D channel oriented parallel to the c axis and bounded by 12-membered ring of size 8.0 Å composed of alternating AlO_4 and PO_4 tetrahedron.

These specimens mentioned above are selected for our study on the behavior of He^3 in very restricted geometries.

The ZSM-5 and Silicalite-1 are supplied by Dr. Ueda of Osaka University. Silicalite-2 and $AlPO_4$-5 are supplied by

Chiyoda Chemical Engineering and Construction Co. Ltd. and also ferrierite by Tōyō Sōda Manufacturing Co. Ltd. Dehydration of these samples is performed by keeping them at 500°C for several hours.

2-2 Experimental apparatus and procedure

We use He^3-He^4 dilution refrigerator as a cryostat by which samples are cooled down to 20 mK. The sample gas of He^3 is provided by the gas handling system which is explained in 2-2 in chapter 2. The filling line of He^3 is connected to the gas handling system. The sample cell is shown in Fig. 5. The cell is made of an epoxy (Stycast 1266) and powdered sample is packed in the cell with the packing factor of about 0.8. NMR detection coil is wound around sample cell. The bundle of copper wires is anchored to the mixing chamber of the He^3- He^4 dilution refrigerator. A ruthenium oxide resister is used as the thermometer which is calibrated against Lake Shore Ge thermometer. The thermometer is immersed in liquid He^3 which is also in direct contact with the high silica zeolites or $AlPO_4$-5.

The Q meter method which uses continuous-wave magnetic resonance technique (CW-NMR) is used at resonant frequency of f = 1.7 MHz.[19] The block diagram of CW-NMR system is given in Fig. 6. A small field modulation H_m (amplitude of 0.1 G at 200 Hz) and phase sensitive detection are used for measurements. By sweeping external field H in the vicinity of resonance field, the signal proportional to $d\chi''/dH$ is obtained. The integration with long time constant gives the value proportional to $\chi_s(H)$.

Fig. 5 Sample cell and copper bundle

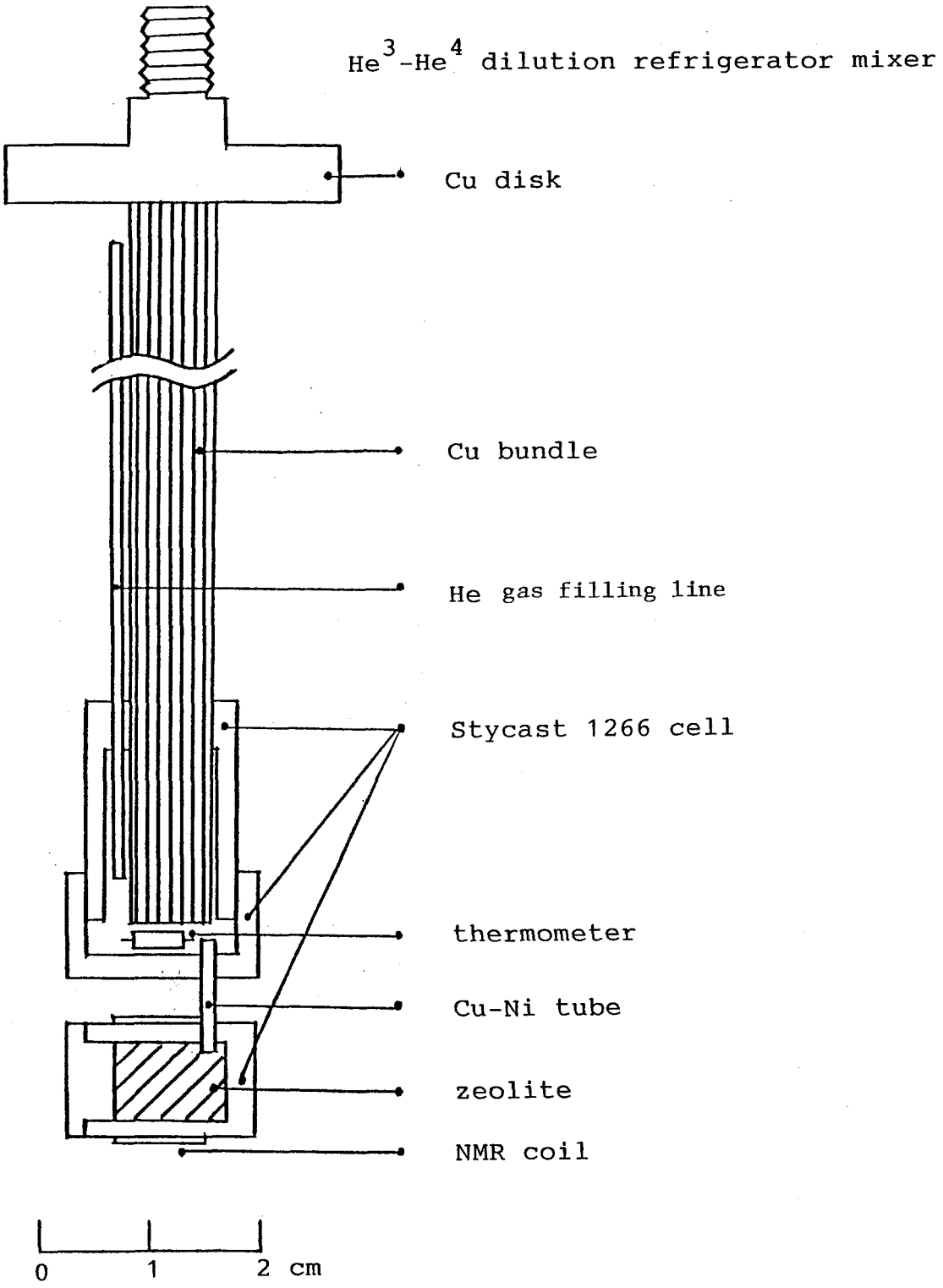

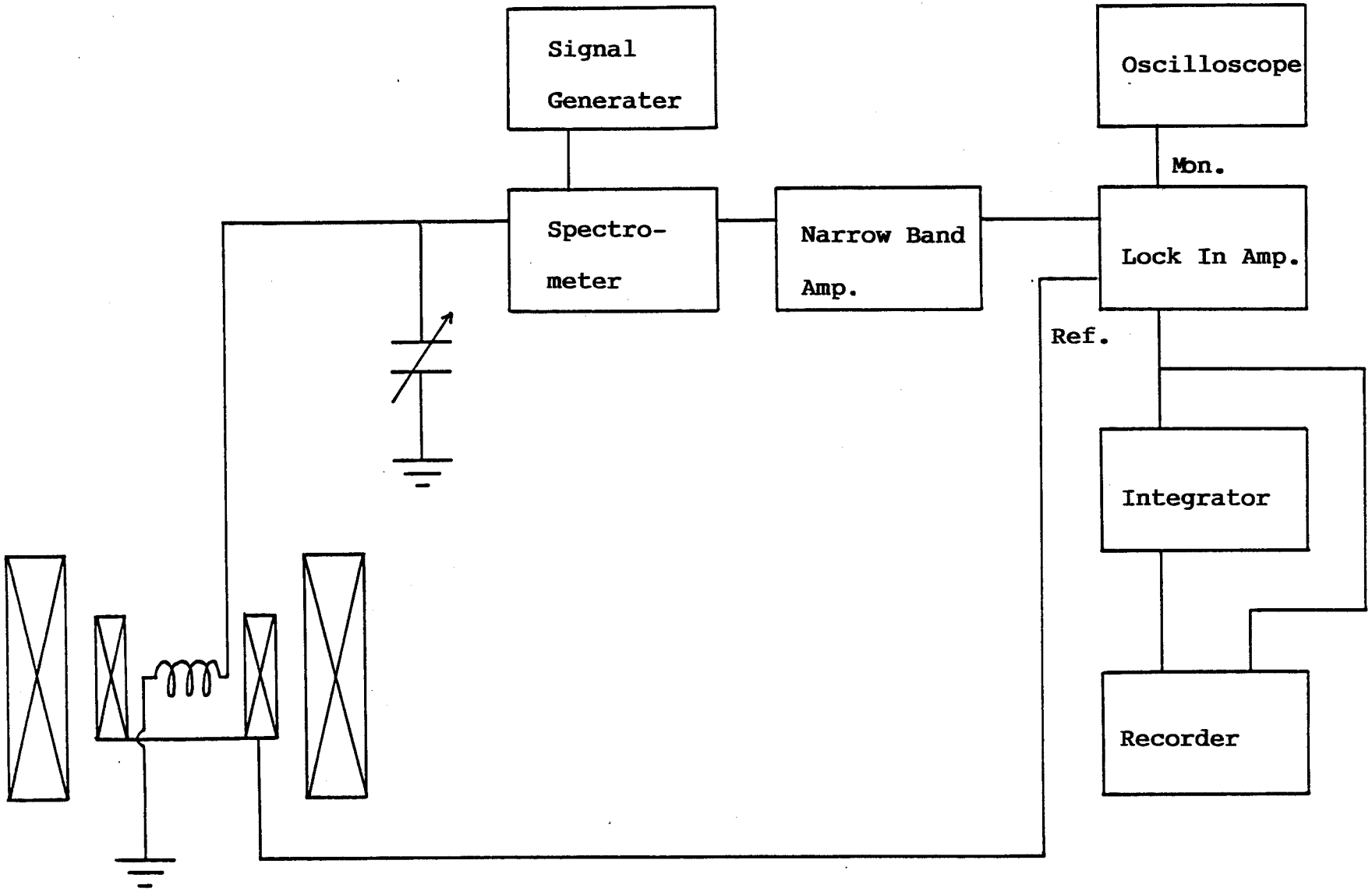

Fig. 6 Block diagram of CW-NMR measurement system

To estimate the static susceptibility χ_s, we use a relation valid for small values of the r.f. field $H_1 \sin(\omega t)$, namely

$$\chi''(H) = \frac{1}{2} \chi_s \cdot H_0 \cdot g(H)$$

where $g(H)$ is a shape function and H_0 is resonance field. In practice, $g(H)$ can be regarded as a function of the modulation field H_m. In this experiment, the broadening of the resonance arises from inhomogeneities of the magnetic field and magnetic impurities in sample. As the broading is independent of temperature, χ_s is assumed to be proportional to the maximum height of the signal $\chi''(H)$, and its variation with temperature is readily obtained.

In order to get rid of the reduction of χ'' value due to saturation, the following condition should be kept.

$$\gamma^2 H_1 T_1 T_2 \ll 1 \quad ,$$

where γ is the gyromagnetic ratio, and T_1 and T_2 are spin-lattice and spin-spin relaxation time respectively. We use pulsed NMR technique at resonant frequency of 2.0 MHz to measure T_1 and T_2. The block diagram of pulsed-NMR measuring system is given in Fig. 7. The pulsed NMR coil is the same as that used for CW-NMR. T_2 of adsorbed He^3 is obtained by the spin echo-method and T_1 by the comb pulse method. The NMR free induction signals or the spin echo signals are sampled by the signal averager and the auto digitizer(AUTINCS MODEL S121). The data are transferred to a personal computer (NEC PC-9800) through GP-IB bus and are data-processed by it. The computer is also used for the timing control of various type of pulse sequences and

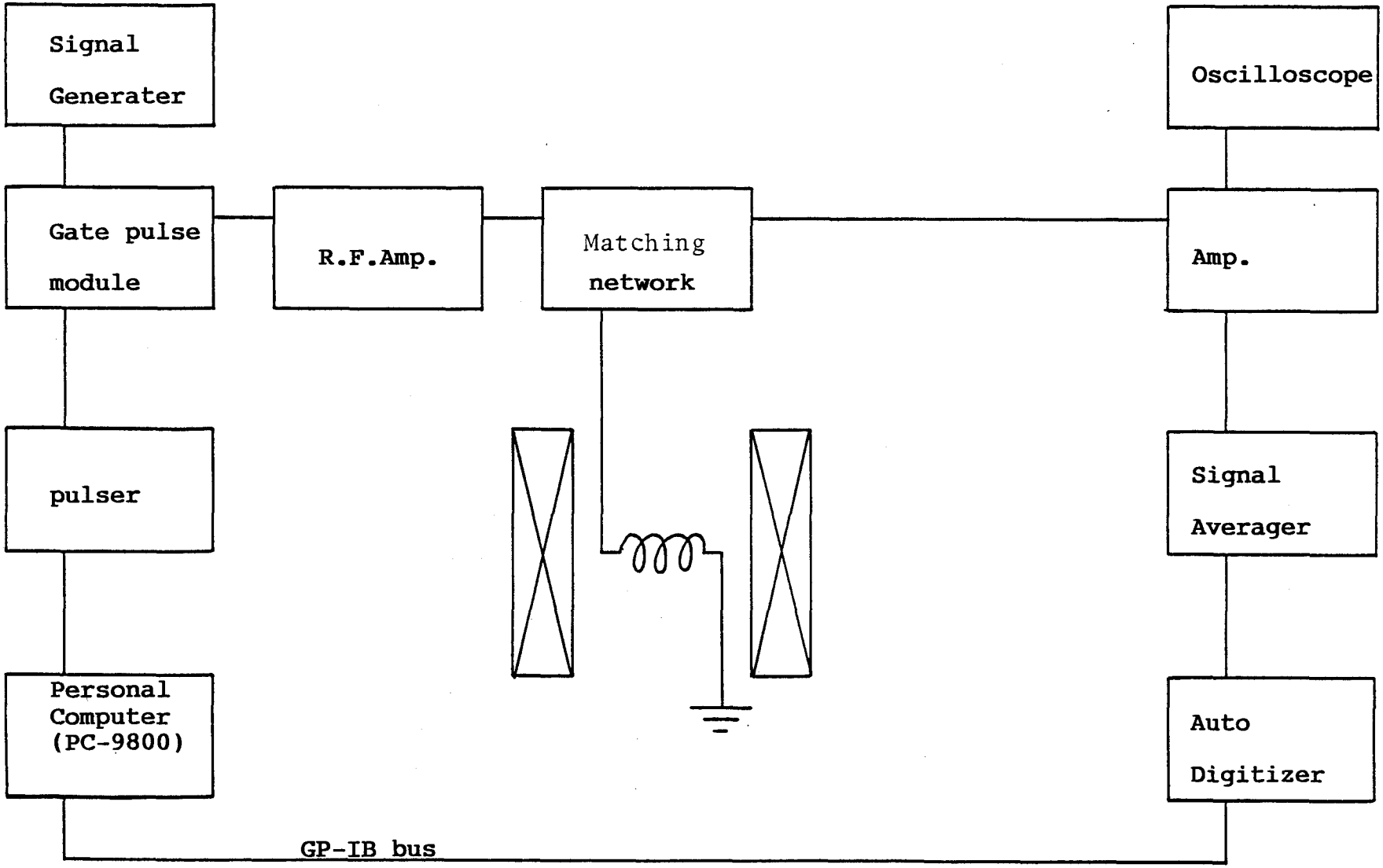

Fig. 7 Block diagram of pulsed NMR

data acquisition triggers the auto digitizer.

Experimental procedure is as the following. The sample cell is evacuated by a diffusion pump for several hours at room temperature, and then the cryostat is cooled down. He^3 gas is adsorbed through the filling line into the sample while the sample cell is cooled down from 77 K to 3 K. After He^3 is adsorbed in the sample, the small quantity of liquid He^3 is added in the sample cell. The bulk liquid is thermally in direct contact with the copper bundle. The pressure of bulk liquid He^3 is almost equal to saturation vapor pressure. The NMR signal of bulk liquid He^3 is found to cause saturation because of its long T_1 of the order of 100 sec. Then after several passage of resonance point, only the NMR signal of adsorbed He^3 with T_1 shorter than that of bulk liquid He^3 is observed. The NMR signal is measured while the temperature of sample cell decreases from 2 K to 0.04 K.

As for Silicalite-1, we measure not only χ_s of pure He^3 but also χ_s of He^3 diluted with He^4. In the case of experiments of dilute He^3 in the adsorbed mixture, He^3 is adsorbed in Silicalite-1 and then the sample cell is immersed in liquid He^4 in order to avoid selective adsorption of He^4. The concentration of adsorbed He^3 may be higher than that of prescribed concentration.

§ 3 Experimental results

3-1 T_1 and T_2 of He^3 adsorbed in high silica zeolites

T_1 of He^3 adsorbed in ZSM-5, Silicalite-1, Silicalite-2 and ZSM-23 are measured.

(i) The results for ZSM-5 and Silicalite-1 are given in Table 2 and 3. It seems that T_1 of He^3 adsorbed in ZSM-5 or Silicalite-1 have little temperature dependence. There exists two kinds of time constant of spin-lattice relaxation, T_1 and T'_1, of He^3 adsorbed in Silicalite-1. These relaxation times are about 100 times longer than that of adsorbed in ZSM-5. The pore size and structure of ZSM-5 are same as those of Silicalite-1. The difference of the two specimens is the concentration of Al^{3+} and Na^+ in the framework. It has been known that T_1 of He^3 adsorbed in several materials is influenced strongly by the magnetic impurities. Al^{3+} in the framework of zeolite is easily replaced by magnetic impurities such as Fe^{3+}. So, we make chemical analysis of ZSM-5 and Silicalite-1. The result is that the concentration of Fe^{3+} is 500 ppm in ZSM-5 and 15 ppm in Silicalite-1. The difference of T_1 of adsorbed He^3 is found to be due to the magnetic impurities in substrate.

(ii) Temperature dependence of T_1 of He^3 adsorbed in Silicalite-2 and ZSM-23 are studied in more detail. The results are shown in Fig. 8 and 9. Though the values of T_1 have a little temperature dependence in both cases, it is about 0.15 - 0.35 sec in Silicalite-2 and 50 - 70 msec in ZSM-23. The values of T_1 of He^3 adsorbed in ZSM-23 are comparable with those of He^3

Table 2

T_1 of He^3 adsorbed in ZSM-5 f = 2.0 MHz

T (K)	0.92	0.30	0.11
T_1 (msec)	55	43	38

Table 3

Two kind of spin-lattice relaxation times T_1 and T_1' of He^3 adsorbed in Silicalite-1 f = 2.0 MHz

T (K)	0.76	0.33	0.14	0.071
T_1 (sec)	2.5	2.8	1.6	0.55
T_1' (sec)	7.0	13	23	17

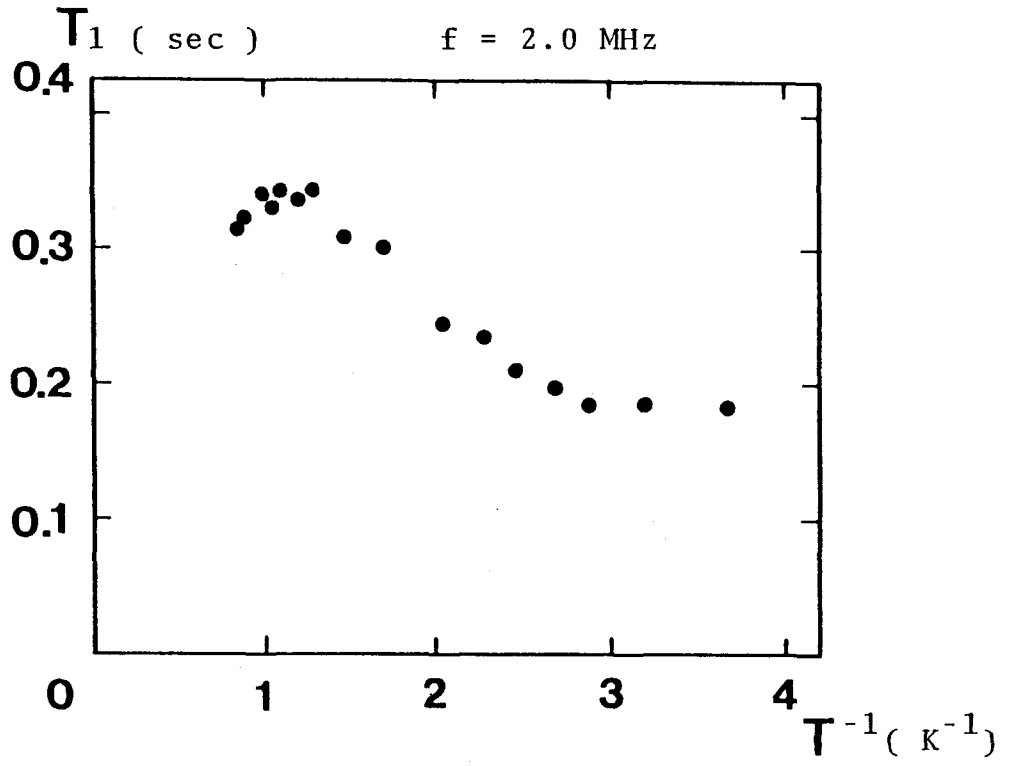

Fig. 8 T_1 of He^3 adsorbed in Slicalite-2

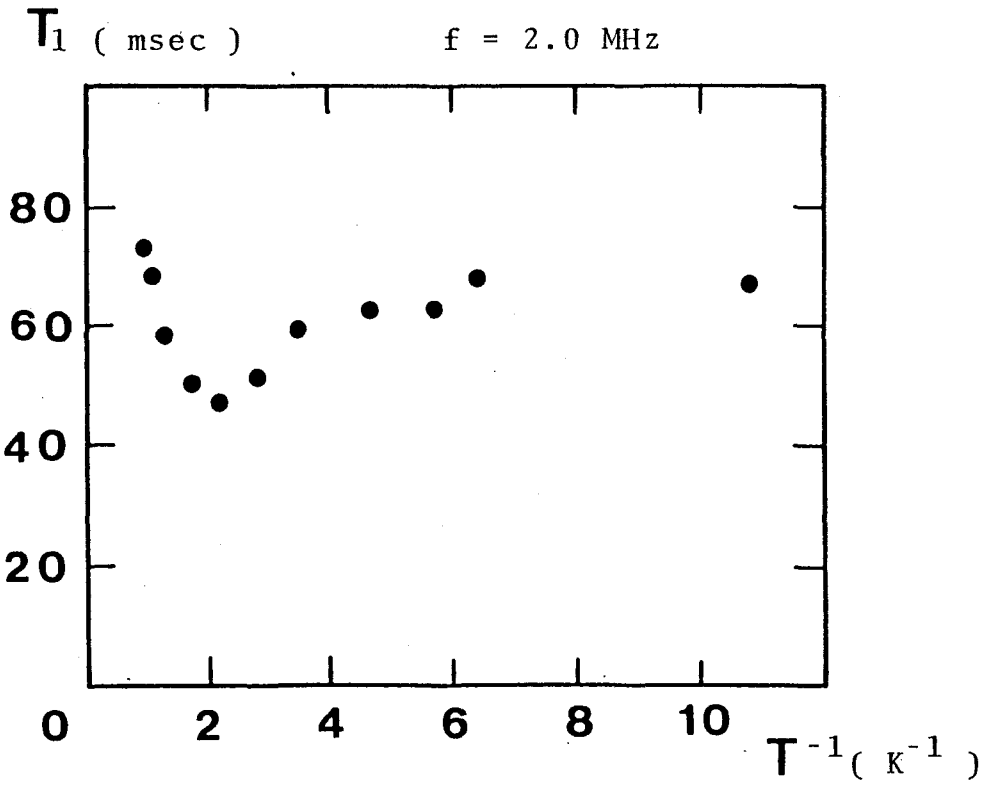

Fig. 9 T_1 of He^3 adsorbed in ZSM-23

adsorbed in ZSM-5. And the values of T_1 in Silicalite-2 are comparable with those in Silicalite-1,too. This seems to be due to the similar ratio of SiO_2/Al_2O_3 in these samples.

(iii) The measurements of T_2 of He^3 adsorbed in ZSM-5 and ZSM-23 are made. The results are shown in Fig. 10 and 11. The temperature dependence of T_2 of He^3 in ZSM-23 is similar to that in ZSM-5. In both cases, T_2 decreases with decreasing temperature above 0.3 K and has a constant value of about 0.6 msec below 0.3 K.

The values of T_1 and T_2 of He^3 adsorbed in ZSM-5 and in ZSM-23 are comparable with those of He^3 adsorbed in Vycor and zeolite 13X which was made at temperatures above 1K.[9)]

Now, we can estimate the saturation condition by substituting the typical values of T_1 = 1 sec, T_2 = 1 msec and γ of He^3 nuclear spin into the relation mentioned in 2-2. The value of H_1 is obtained in the following.

$$H_1 = \gamma^{-1}(T_1T_2)^{-1/2} = 1.5 \text{ mgauss} .$$

Then in the case of CW-NMR measurement, the non-saturation condition which is mentioned in 2 holds if H_1 is much smaller than 1.5 mgauss. In our CW-NMR measurement, H_1 is kept smaller than 1 mgauss. In fact, no saturation effect is observed in NMR signals of He^3 adsorbed in high silica zeolites. Therefore, we are sure that measured χ_s of He^3 in high silica zeolites exactly corresponds to the value at measuring temperatures.

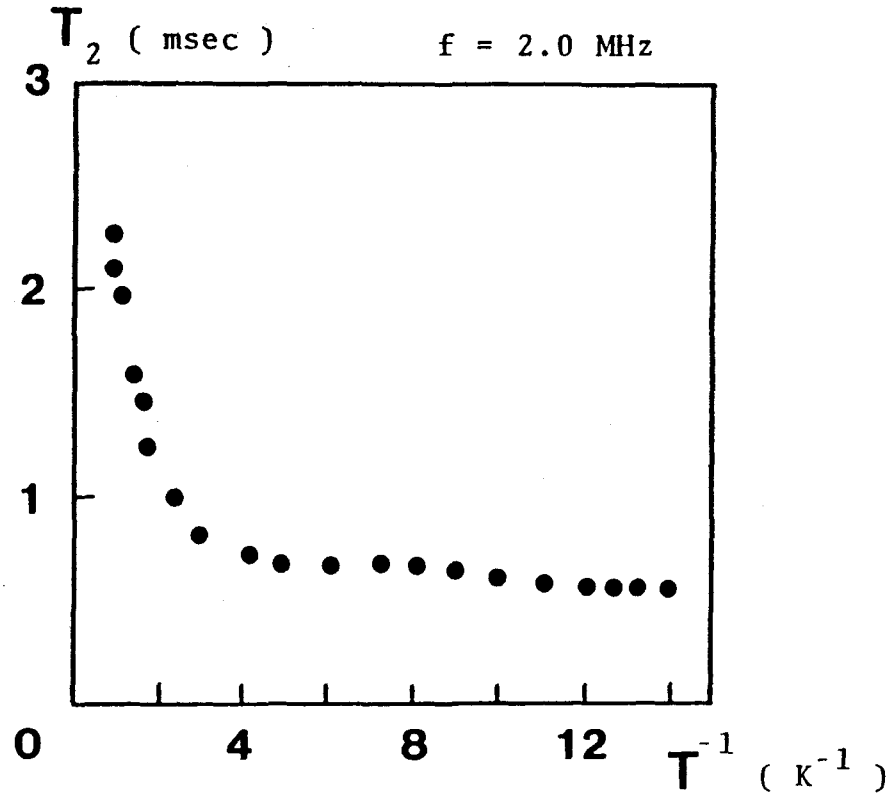

Fig. 10 T_2 of He^3 adsorbed in ZSM-5

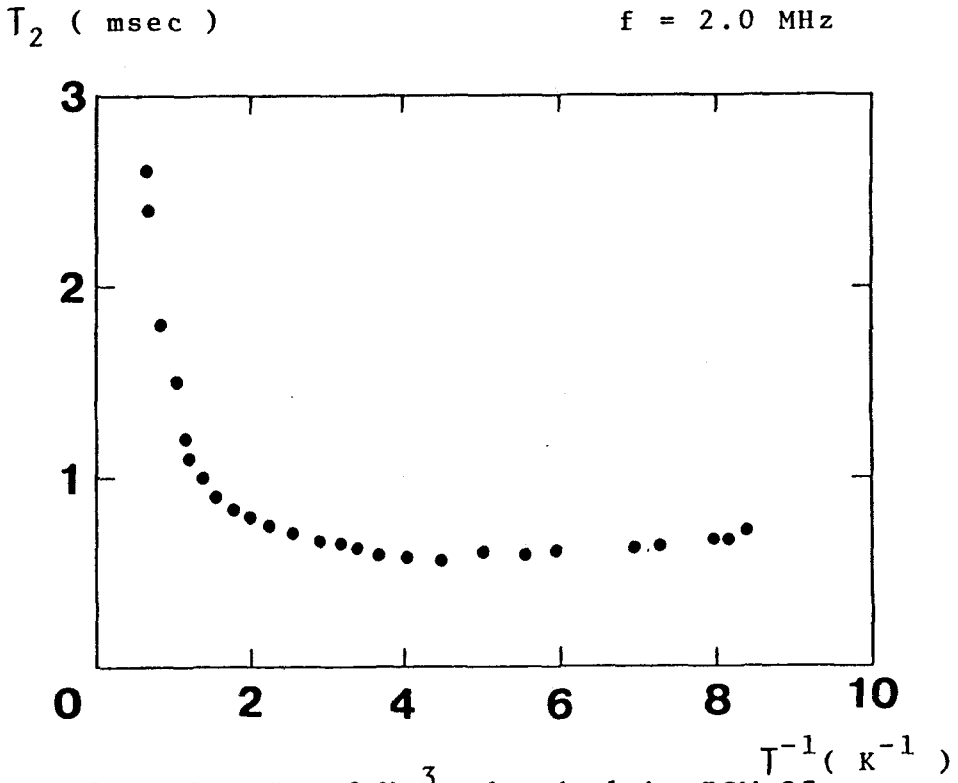

Fig. 11 T_2 of He^3 adsorbed in ZSM-23

3-2 Nuclear susceptibilities of He^3 adsorbed in high silica zeolites and $AlPO_4$-5

The magnetic susceptibilities of He^3 adsorbed in high silica zeolites and $AlPO_4$-5 are obtained. We estimated the Curie constant C in the vicinity of 1 K. The value of χ_s(1 K) is normalized as C in order to compare with the theoretical susceptibility. In bulk state, the susceptibility χ_s of liquid He^3 was calculated theoretically by L.Goldstein.[20] His theoretical model was based on a molecular field approach, and gave the numerical values of the susceptibility χ_s of He^3 in terms of Fermi temperature T_F as a parameter. The theoretical result fits well χ_s of bulk liquid He^3 in the range $T/T_F < 1$.

The experimental results are shown with the theoretical susceptibility, choosing the best value of T_F.

The value of χ_s of adsorbed He^3 in ZSM-5 and Silicalite-1, which have same size of 3D channels, are shown in Fig. 12 and 13. These data have similar temperature dependence and nearly the same T_F = 0.32 K with each other.

The value of χ_s of He^3 adsorbed in Silicalite-2, which has different 3D channels from Silicalite-1, is shown in Fig. 14. The susceptibility χ_s of He^3 adsorbed behaves similarly to that in ZSM-5 and in Silicalite-1. But the value of χ_s in low temperature limit is smaller than that in ZSM-5 and in Silicalite-1. The best value of T_F is estimated to be 0.40 K.

The value of χ_s of He^3 adsorbed in ferrierite having 2D channels is shown in Fig. 15. The result is similar to that of He^3 adsorbed in ZSM-5. But the value of χ_s in low temperature

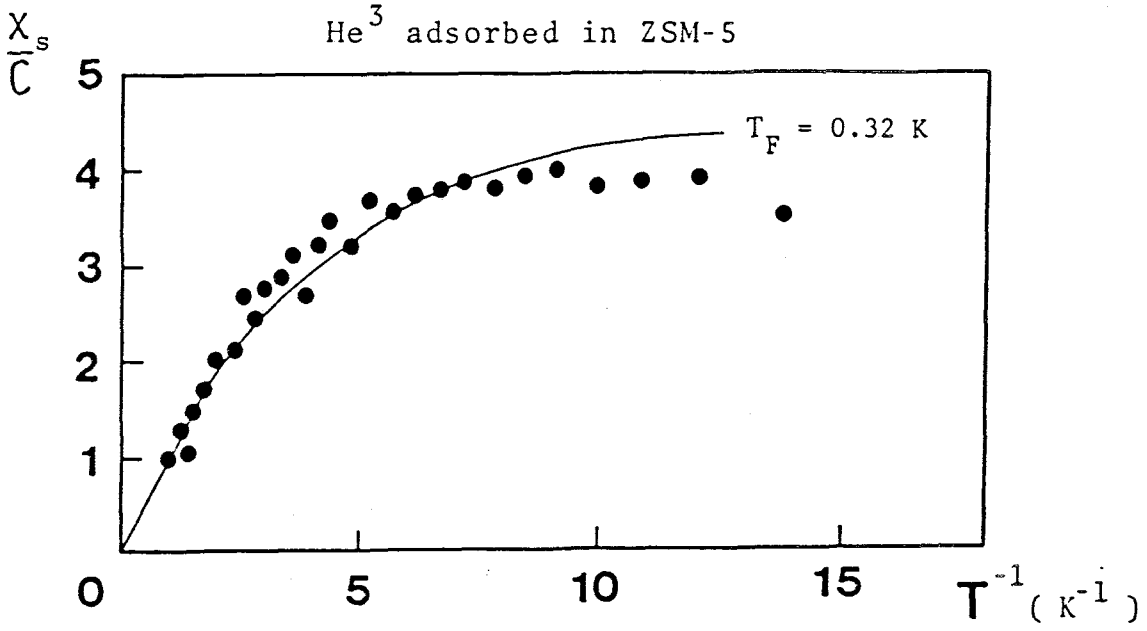

Fig. 12 Magnetic susceptibility of He^3 adsorbed in ZSM-5.
Solid curve is the theoretical susceptibility of liq. He^3 using T_F = 0.32 K.

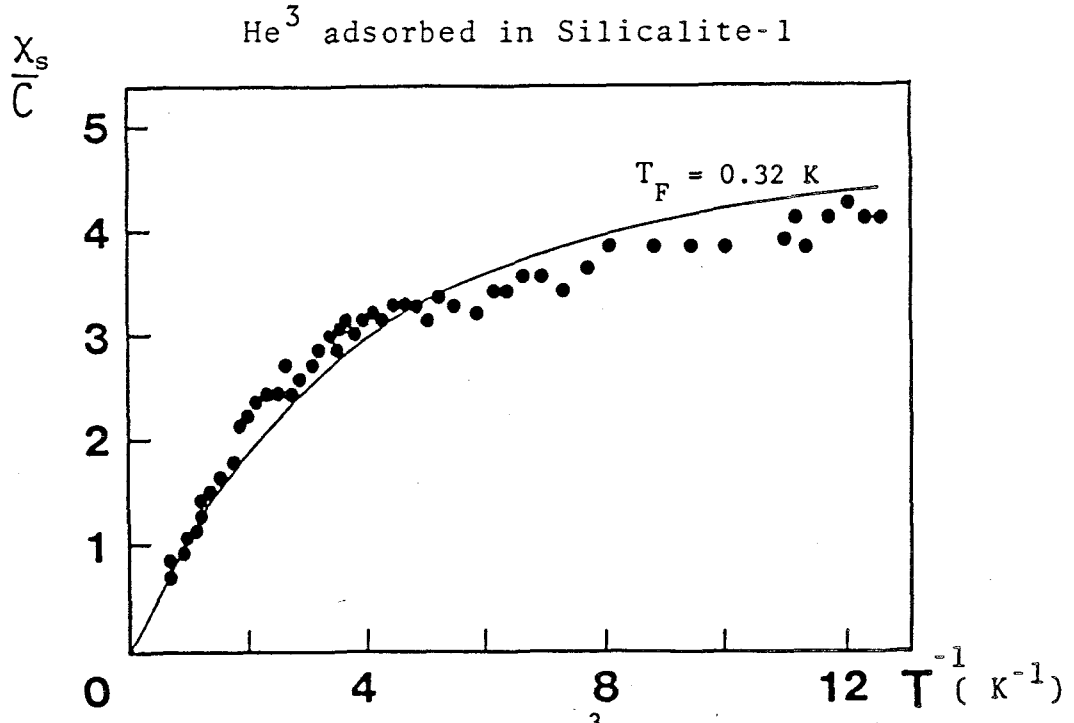

Fig. 13 Magnetic susceptibility of He^3 adsorbed in Silicalite-1
Solid curve is the theoretical susceptibility of liq. He^3 using T_F = 0.32 K.

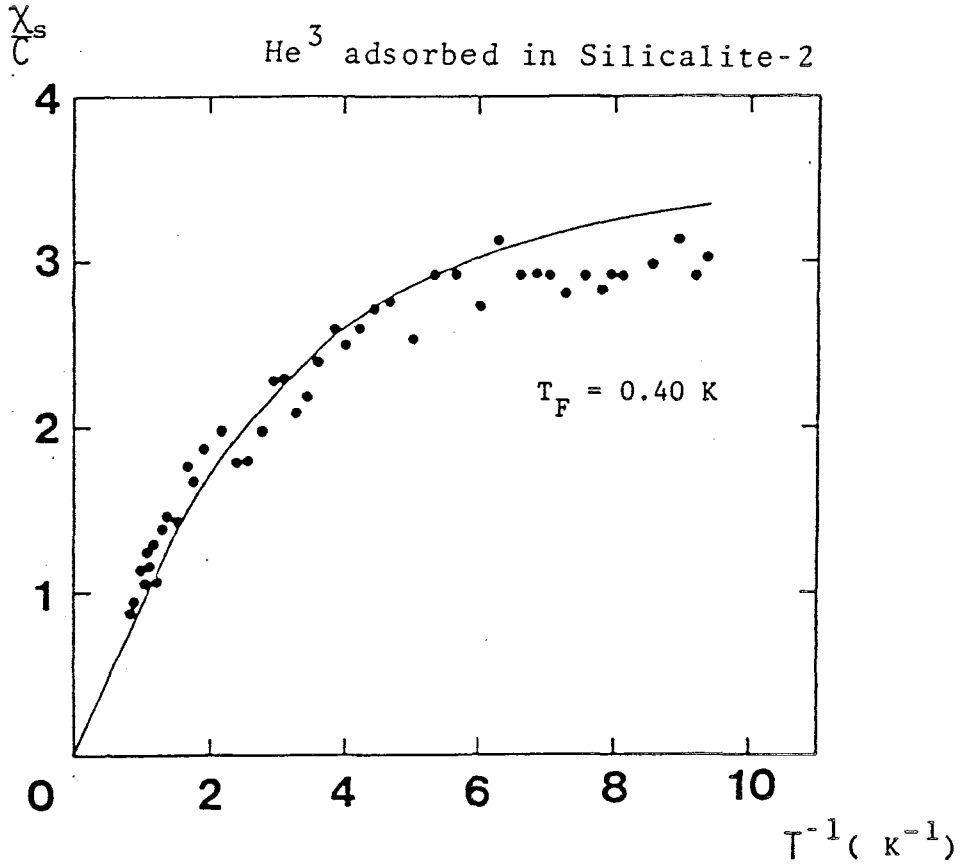

Fig. 14 Magnetic susceptibility of He^3 adsorbed in Silicalite-2. Solid curve is the theoretical susceptibility of liq. He^3 using T_F = 0.40 K.

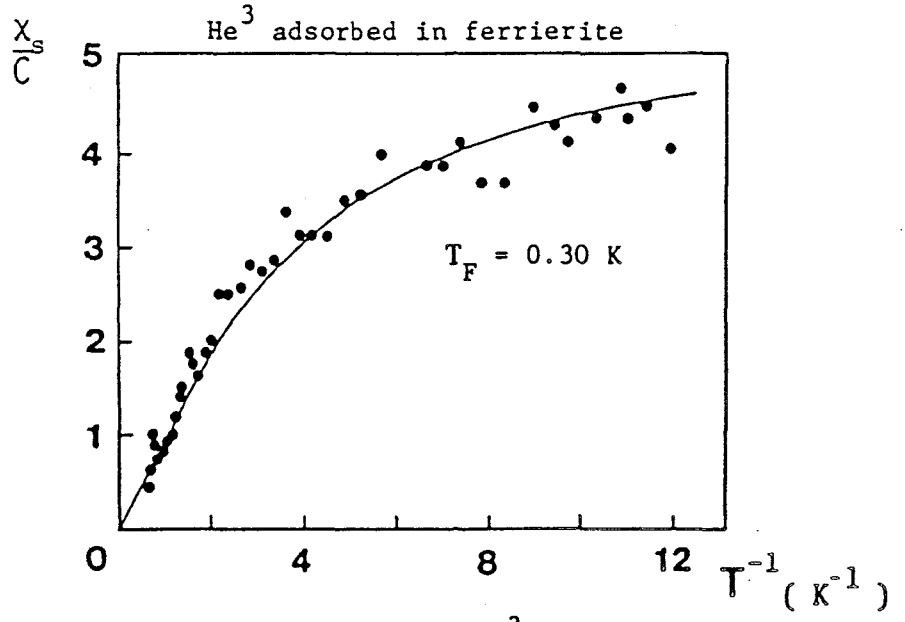

Fig. 15 Magnetic susceptibility of He^3 adsorbed in ferrierite. Solid curve is the theoretical susceptibility of liq. He^3 using T_F = 0.30 K.

limit is larger than that in ZSM-5. The value of T_F is 0.30 K in this case.

In the case of $AlPO_4$-5 having 1D channels, the result is shown in Fig. 16. The data have the similar temperature dependence with that of He^3 in Silicalite-2. The value of T_F is obtained as 0.39 K.

In the case of ZSM-23, which has 1D narrower channel than $AlPO_4$-5, the susceptibility χ_s of He^3 is very different from that mentioned above as shown Fig 17. It fits Curie's law. The Fermi degeneracy of χ_s is not observed in the temperature range measured.

In the case for Silicalite-1, we measure χ_s of He^3 diluted with He^4. The results of He^3 with the prescribed concentration 0.04 and 0.08 are shown in Figs. 18 and 19, respectively. The susceptibilities χ_s are almost proportional to 1/T above about 0.2 K and larger than that of pure He^3 in Silicalite-1 at low temperatures. The values of χ_s depend sensitively on the concentration of He^3. The values of T_F are obtained as 0.075 K and 0.22 K for the concentration 0.04 and 0.08, respectively.

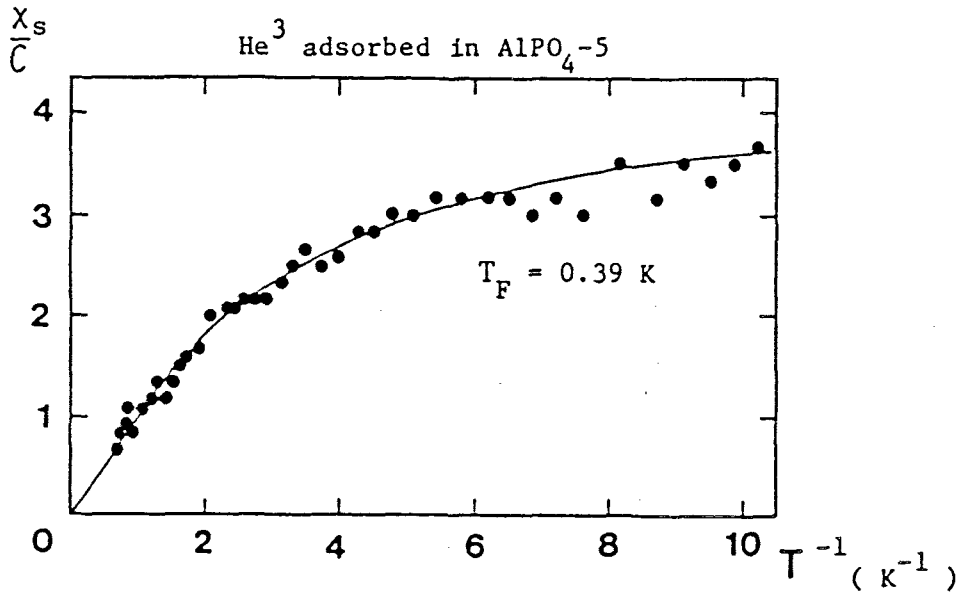

Fig. 16 Magnetic susceptibility of He^3 adsorbed in $AlPO_4$-5. Solid curve is the theoretical susceptibility of liq. He^3 using T_F = 0.39 K.

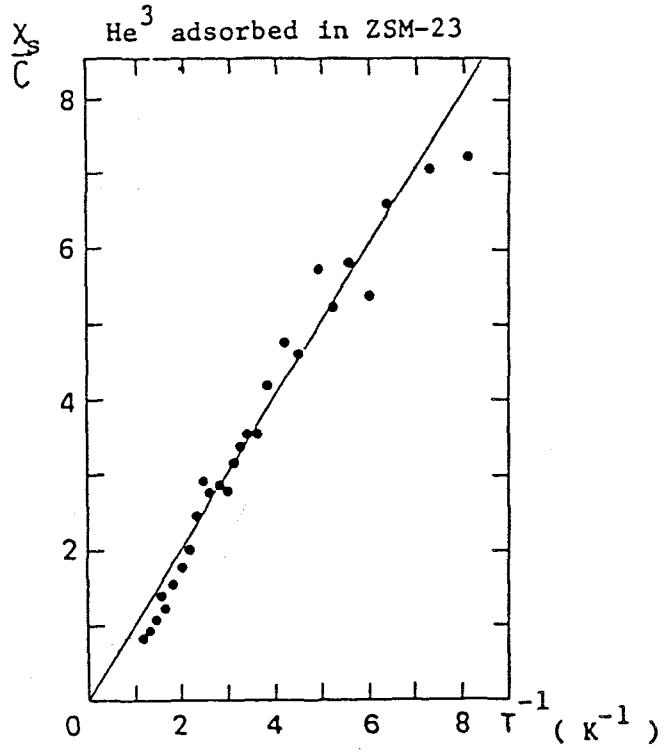

Fig. 17 Magnetic susceptibility of He^3 adsorbed in ZSM-23. Solid line is Curie's law.

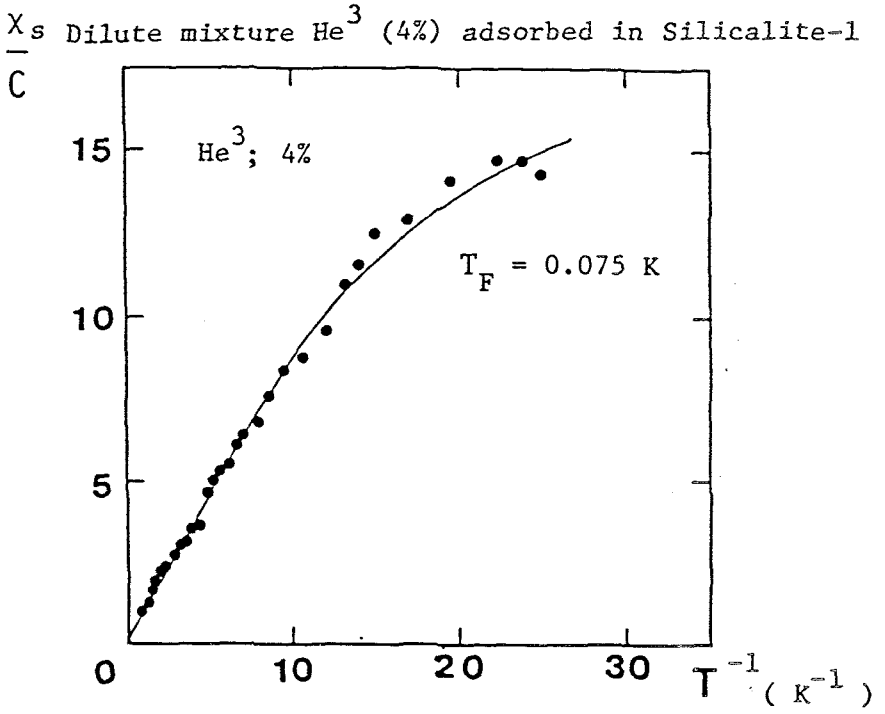

Fig. 18 Magnetic susceptibility of dilute mixture of He^3 in He^4 with concentration of 4 % adsorbed in Silicalite-1.
Solid curve is the theoretical susceptibility of liq.He^3 using T_F=0.075K

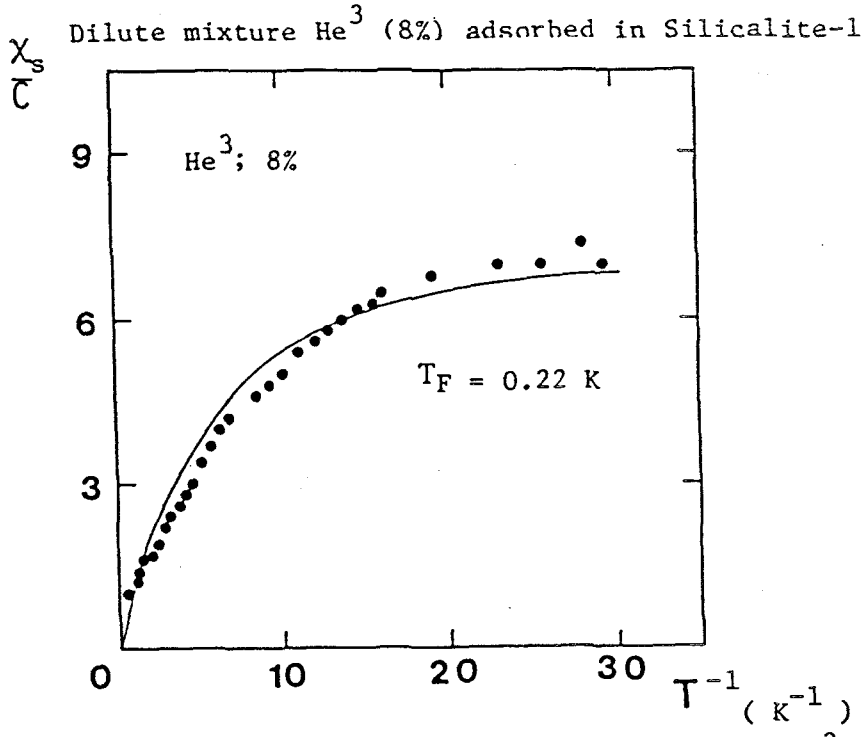

Fig. 19 Magnetic susceptibility of dilute mixture of He^3 in He^4 with concentration of 8 % adsorbed in Silicalite-1. Solid curve is the theoretical susceptibility of liq. He^3 using T_F = 0.22 K.

§ 4 Discussion

4-1 The Fermi degeneracy of He^3 in narrow channels and voids

We studied some aspects of Fermi degeneracy of He^3 adsorbed in several kinds of restricted geometry in which the kinetic exchange or the replacement among adsorbed atoms are limited in various depends.

In 3, we compared $\chi_s(T)$ obtained by NMR experiment with the susceptibility calculated by Goldstein on a Fermi liquid theory with a fitting parameter T_F. The fact that we obtained a good agreement with theory except the case of ZSM-23 has shown the adsorbed He^3 behaved like the Fermi liquid characterized by T_F, so long as the restricted geometry had the space to allow the particle exchange. The relation between χ_s and T_F in the Fermi liquid theory by Goldstein is mentioned in Appendix.

The values of obtained T_F are listed in Table 4. Restricted geometry in $AlPO_4$-5 is 1D but the channel size of 8 Å is large enough for exchange of atoms. On the other hand, Silicalite-2, Silicalite-1 and ZSM-5 have small channel size of about 5.5 Å but the 3D network enables particles to make cyclic replacement or exchange among them cross to each other. The channel structure of ferrierite is 2D and its size of space of intersecting channels enables the exchange of atoms.

In contrast with zeolites mentioned above, ZSM-23 has ideal 1D channel structure, without any 2D or 3D bridge or connectivity, whose diameter is too narrow to allow particle exchange.

Table 4

T_F of adsorbed He^3 and bulk liq.He^3

Specimen	T_F of adsorbed He^3	
	pure He^3	dilute He^3 (He^3 concentration)
ZSM-5	0.32	——
Silicalite-1	0.32	0.22 (0.08) 0.075 (0.04)
Silicalite-2	0.40	——
Ferrierite	0.30	——
$AlPO_4$-5	0.39	——
ZSM-23	(very small)	——
Bulk liq.He^3 (P= 1 atm.)	0.43	——
Bulk dilute He^3	——	0.13 (0.013) 0.30 (0.05)

(The values of T_F are estimated by Goldstein's theory.)

Experimental results show that the value of T_F decreases with the channel size and gives a measure of exchange probability. The values of T_F are estimated by Goldstein's theory based on the molecular field approach, therefore this tendency is reasonable.

Dilution of He^3 with He^4 gives an effect to reduce the value of T_F just like in the bulk liquid. This is the evidence of He^3 in high silica zeolites being degenerated Fermi fluid. Anderson et al. measured the effective mass m^* and a Landau parameter Z_0 (see Appendix) of He^3 diluted in bulk mixture for He^3 concentration of 0.013 and 0.05 at the pressure of 0.26 bar.[21] The values of T_F are estimated to be 0.13 K and 0.30 K for the concentration 0.013 and 0.05, respectively. The comparison of this result with our case in Silicalite-1 shows the concentration dependence is more effective in the Fermi degeneracy in a restricted geometry, possibly because of the additional limitation of the geometry.

4-2 Curie's law susceptibility of He^3 in ZSM-23

Now, we discuss two possibilities for the appearance of Curie's law behavior of He^3 adsorbed in ZSM-23. The result is interpreted in the following two possibilities.

(i) He^3 atoms in ZSM-23 are localized and behaves like a solid giving Curie's law susceptibility.

Or alternatively, (ii) He^3 atoms behave like fluid, but in the ideal 1D channel structure. Kinetic exchanges among He^3 particles are forbidden perfectly. This restriction dissociates

the Fermi degeneracy, and gives Curie's law susceptibility.

To distinguish these two possibilities from the examination of dynamical properties, we performed pulsed-NMR experiments of He^3 in ZSM-23 and ZSM-5 which have the same order of SiO_2/Al_2O_3 ratio and channel size with each other. The experiments about T_1 and T_2 in both samples show almost the same results on their temperature dependences as well as their absolute values. Also, the change of the spin echo signal against pulse interval is well described by the single exponential decay in both cases. The single exponential decay of the echo signal shows that χ'' line shape is of the Lorentzian which is normally associated with rapid motion of spins. Another possibility of the Lorentzian shape which is observed in bulk solid He^3 by the exchange narrowing is not the present case because of the restriction on direct exchange of He^3 atoms.

The results of T_1 and T_2 mentioned above support the idea that He^3 atoms in ZSM-5 and ZSM-23 are in the same motional state. Then we take the latter interpretation (ii) and conclude the realization of fluid like He^3 which shows Curie's law susceptibility even if He^3 atoms are in moving state.

In 1960, Girardeau treated theoretically a system of impenetrable Fermions in 1D.[22] He discussed the energy spectra and the momentum distributions of the system. But our experimental results cannot be compared with his theory because it was the spinless fermion model.

Appendix

The susceptibility χ_s of He^3 in a Fermi liquid theory

The susceptibility χ_s of an ideal Fermi gas in the low temperature limit is given by

$$\chi_s = \frac{9\,C}{2\,T_F}\left[\,1 - \frac{\pi^2}{12}\left(\frac{T}{T_F}\right)^2 + \text{------}\,\right]$$

where C is the Curie constant and T_F is the Fermi temperature.[23] C and T_F are given in the following,

$$C = \left(\frac{\gamma\hbar}{2}\right)^2\left(\frac{n}{3k_B}\right)$$

$$T_F = \frac{\hbar\,(3\pi^2 n)^{2/3}}{2k_B}$$

where n is the number of Fermi particles per unit volume and m is the mass of particles.

In a Fermi liquid theory, the susceptibility χ_s of an interacting Fermi gas of "quasiparticles" with an effective mass m^* is given by

$$\chi_s = \frac{9\,C}{2T_F^*\left(1+\frac{Z_0}{4}\right)}\left[\,1 - \frac{\pi^2}{12}\left(\frac{T}{T_F}\right)^2 + \text{------}\,\right]$$

where $T_F^* = T_F(m/m^*)$ is the Fermi temperature of the ideal gas having the mass m^*, and Z_0 is a Landau parameter which means the measure of the "molecular field" a He^3 quasiparticle sees from the surrounding medium.[24] The notation T_F which is given by Goldstein and used in this text corresponds to $T_F^*(1+Z_0/4)$. Therefore, T_F in this text contains an effective mass m^* and the "molecular field" parameter Z_0.

References

1) R.J.Rollefson : Phys. Rev. Lett. 29 (1972) 410.

2) D.C.Hickernell, D.L.Husa and J.G.Daunt : J. Low Temp. Phys. 15 (1974) 29.

3) D.C.Hickernell, E.O.McLean and O.E.Viches : Phys. Rev. Lett. 28 (1972) 789.

4) D.J.Creswell, D.F.Brewer and A.L.Thomson : Phys. Rev. Lett. 29 (1972) 1144.

5) D.F.Brewer and J.S.Rolt : Phys. Rev. Lett. 27 (1972) 1485.

6) D.F.Brewer and J.S.Rolt : Phys. Rev. Lett. 48A (1974) 141.

7) M.Shimoda, T.Mizusaki, T.Suzuki and A.Hirai : Phys. Lett. 102A (1984) 426.

8) G.Careri, M.Givra and M.Santini : Phys. Lett. 4 (1963) 61.

9) H.T.Weaver : J. Phys. Chem. Solids. 34 (1973) 421.

10) H.Kato, N.Wada, T.Ito, S.Takayanagi and T.Watanabe : J. Phys. Soc. Jpn. 55 (1986) 246.

11) G.T.Kokotailo, S.L.Lawton, D.H.Olsen and W.M.Meier : Nature 272 (1978) 437.

12) D.H.Olsen, G.T.Kototailo, S.L.Lawton and W.N.Meier : J. Phys. Chem. 85 (1981) 2238.

13) L.M.Parker : Zeolite 3 (1983) 8.

14) E.M.Flanigen, J.M.Bennett, R.W.Grose, J.P.Cohen, R.M.Kirchner and J.V.Smith : Nature 271 (1978) 512.

15) G.T.Kokotailo, P.Chu, S.L.Lawton and W.M.Meier : Nature 275 (1978) 119.

16) D.M.Bibby, N.B.Milstone, L.P.Aldridge : Nature 280 (1979)

664.

17) P.A.Vaughan : Acta Cryst. 21 (1966) 983.

18) S.T.Wilson, B.M.Lok, C.A.Messina, T.R.Cannan and E.M.Flanigen : J. Am. Chem. Soc. 104 (1982) 1146.

19) R.F.Code : Rev. Sci. Instrum. 46 (1975) 661.

20) L.Goldstein : Phys. Rev. 133 (1964) A52.

21) A.C.Anderson, D.O.Edwards, W.R.Roach, R.E.Sarwinski and J.C.Wheatly : Phys. Rev. Lett. 17 (1966) 367.

22) M.Giradeau : J. Mathematical Physics 1 (1960) 516.

23) E.C.Stoner : Phil. Mag. 25 (1938) 899.

24) L.D.Landau : Sov. Phys. JETP 3 (1957) 920, 5 (1957) 101, 8 (1959) 70.

Summary

Properties of H_2, D_2, He^4 and He^3 adsorbed in some restricted geometries such as Y zeolite, pillar intercalated montmorillonite and high silica zeolite are studied experimentally.

In search for superfluid H_2 by the supercooling in the severely restricted geometry of Y zeolite, we does not observe the transition between the solid and the liquid state as a distinct heat capacity peak. Instead, the results support the idea of the continuous transition around 10 K when the density of adsorbed H_2 is low. This is more clearly demonstrated in the case of H_2 adsorbed in the interlayer space of Al_2O_3-montmorillonite. In the 2D space, heat capacity of H_2 shows a hump around 10 K, which seems to correspond to the melting transition and shows the further supercooling comparing with the result in Vycor glass. In the case of full pore, where H_2 fill the adsorption space completely, heat capacity measurement shows that H_2 molecules behave as solid, giving Debye type or Einstein type temperature dependence over the measured temperature range. Another support for being solid state of H_2 is given by the observation of λ-type anomaly of the heat capacity in purely 2D space of $N^+(CH_3)_4$-montmorillonite. The anomaly is interpreted as the orientational ordering of 2D ortho-H_2 solid.

The properties of He^4 are also studied in the present restricted geometries. The heat capacities show similar temperature dependence to those previously observed by Tait and

Reppy in submonolayer He^4 in Vycor glass. The important result in our case is that we observed a hump around 1.7 K in the case of He^4 in a interlayer space of Al_2O_3-montmorillonite. The hump is interpreted to be due to the superfluid transition and not observed in more restricted space. The reported behaviors such as single-particle excitation and 2D Debye solid are also appeared but depend on the geometry.

We are also interested in the properties of He^3 - Fermi particle - in an extremely restricted geometry where particle exchange is not allowed anymore. This situation is expected to reveal some of characteristics of Fermi statistics. Nuclear susceptibility of He^3 in ZSM-23 which has purely 1D channel shows to obey Curie's law in the temperature range down to about 0.1 K. The result reflect not the solid like properties of the adsorbed atoms but a property deriving from the restriction of particle exchange in the used geometry. This is in contrast with other quasi 1D, 2D or 3D channel system, for which a simple Fermi liquid theory is applicable with suitable parameter T_F. General tendencies of T_F value are found in the experiment. Dilution of He^3 with He^4 is performed in the restricted geometry and concluded that the dilution effect is more pronounced than in the bulk case.

So far as magnetic properties are concerned, we are now studying molecular O_2 in restricted geometries with expectation of finding magnetic liquid there in the same mechanism of supercooling studied here.

Acknowledgments

The author would like to express his sincere thanks to Professor T. Haseda for his promoting this study and for stimulating discussions. He is indebted to Professor K. Amaya for carrying out the experiment and his continuous discussions. His thanks are due to Professor K. Takeda of Kyushu University and Professor M. Matsuura for valuable comments on this study. Thanks are also due to Dr. Y. Kitaoka and Dr. Y. Kohori for their kind help on the pulsed NMR measurement. He is grateful to Professor Y. Nagaoka of Nagoya University for stimulating discussions about the property of He^3 system in restricted geometries.

He is grateful to Professor S. Yamanaka of Hiroshima University for preparing the specimens of montmorillonites and to Dr.K. Ikawa of Tōyō Sōda Manufacturing Co. Ltd. for preparing the specimens of Y zeolite and ferrierite. He is also grateful to Dr. S. Ueda of Osaka University, Dr. O. Terasaki of Tohoku University and Dr. S. Asaoka of Chiyoda Chemical Engineering and Construction Co. Ltd. for preparing high silica zeolites and $AlPO_4$-5.

He also thanks to Mr. N. Morita and Mr. Y. Moriyasu for proceeding the heat capacity measurement and to Mr. S. Araki and Mr. T. Kouyama for proceeding the NMR measurement in the course of this study. Thanks are due to Mr. A. Kawai for his assistance in preparation of experimental apparatus.

He thanks the colleagues of Matsuura and Amaya laboratory for their helps throughout this work.